

**IZMIR UNIVERSITY OF ECONOMICS  
FACULTY OF ENGINEERING  
AEROSPACE ENGINEERING**

**Autonomous Optical and Inertial Navigation of a  
Solar-sail Propelled CubeSat Class Spacecraft  
Targeting Mars and its Moons**

Authors: Ahmet Orhun Sivaslı  
Burak Köse  
Ekin Gürhan

Supervisor: Dr. Fabrizio Pinto

“Autonomous optical and inertial navigation of a solar-sail propelled CubeSat class spacecraft targeting Mars and its moons” by Ahmet Orhun Sivaslı, Burak Köse, and Ekin Gürhan is licensed under a Creative Commons Attribution 4.0 International License, except where otherwise noted.  
<https://creativecommons.org/licenses/by/4.0>

**Attribution** - You must give appropriate credit, provide a link to the license, and indicate if changes were made. You may do so in any reasonable manner, but not in any way that suggests the licensor endorses you or your use.

<https://doi.org/10.5281/zenodo.8188984>

**We would like to thank our supervisor Dr. Fabrizio Pinto for his guidance throughout our project and Dr. Jon Giorgini from NASA JPL for his helps about Horizons System.**

# Contents

<b>1</b>	<b>Abstract</b>	<b>5</b>
	List of Symbols and Definitions	6
<b>2</b>	<b>Introduction</b>	<b>7</b>
<b>3</b>	<b>Literature Review</b>	<b>7</b>
3.1	A. Roy, “Orbital Motion” (2005)[1]	7
3.2	J. E. Riedel et al, “Autonomous Optical Navigation (AutoNav) Technology Validation Report” [2]	8
3.3	J. Meuss, Astronomical Algorithms (1998)[3]	10
3.4	F. Pinto, Elements of Optical Navigation (2018)[4]	12
	3.4.1 Inertial Navigation	13
	3.4.2 Autonomous Optical Navigation	13
	3.4.3 Autonomous Pulsar-Based Navigation	14
3.5	Karaaliler et al. , “Autonomous optical and inertial navigation of solar-sail propelled CubeSat class spacecraft during targeting missions to asteroids and minor moons. (2022)”[5]	14
3.6	E. Sahr et al “Post-Launch Characterization of the Optical Navigation Instruments For Nasa’s Lucy Mission”[6]	15
3.7	M. Vertregt, “Orientation in Space” (1956) [7]	18
<b>4</b>	<b>Methodology</b>	<b>19</b>
4.1	<b>Tools Used</b>	19
	4.1.1 Horizons System	19
	4.1.2 AstroGrav	20
	4.1.3 Stellarium	21
4.2	<b>First Trials</b>	21
4.3	<b>Direct Problem</b>	21
	4.3.1 Earth Observer	23
	4.3.2 Non-Earth Observer	32
	4.3.3 Error Calculation for the Direct Problem	32
4.4	<b>Inverse Problem</b>	33
4.5	<b>How to Choose Asteroids?</b>	37

<b>5</b>	<b>Results</b>	<b>39</b>
5.1	<b>Direct Problem Results</b>	39
5.1.1	Uppsala	39
5.1.2	Urla	62
5.1.3	Rome	82
5.1.4	Pasadena	102
5.1.5	Non-Earth Case: Ceres	122
5.2	<b>Inverse Problem Results</b>	125
5.2.1	Uppsala	127
5.2.2	Urla	133
5.2.3	Rome	139
5.2.4	Pasadena	145
5.2.5	Non-Earth Observer: Ceres	151
5.3	<b>Change in Error with Time</b>	153
5.4	<b>AstroGrav Results:</b>	155
5.5	<b>Stellarium Results:</b>	157
<b>6</b>	<b>Discussion on the Results</b>	<b>159</b>
6.1	<b>Direct Problem Results' Analysis</b>	159
6.2	<b>Inverse Problem Results' Analysis</b>	160
<b>7</b>	<b>Conclusion</b>	<b>161</b>
<b>8</b>	<b>Appendix</b>	<b>162</b>
	<b>References</b>	<b>164</b>

**FENG 498**

**Project Final Report**

**Autonomous optical and inertial navigation of a  
solar-sail propelled CubeSat class spacecraft  
targeting Mars and its moons.**

Ahmet Orhun Sivaslı<sup>1</sup>, Burak Köse<sup>1</sup>, Ekin Gürhan<sup>1</sup>

July 27, 2023

**1 Abstract**

A successful space mission depends on crucial systems and teams working together. Designing a feasible trajectory for the spacecraft that satisfies the goals of the mission, accurately conducting simulations on a digital twin to control the health and fluidity of operations, and navigating to correctly estimate the location of the spacecraft in space are just a few of the vital responsibilities that a space mission brings. In this paper, space navigation, specifically optical spacecraft navigation, is put to the test with the help of many Freeware and Free Open Source Software tools such as Wolfram Mathematica and Jupyter Notebook to see the validity of an optical navigation model. Direct and inverse problems are proposed to calculate and observe whether it is possible to accurately measure the topocentric ecliptic and celestial coordinates of 55 systematically chosen beacon asteroids of known heliocentric Cartesian coordinates. Then, going in reverse, as the inverse problem, computing the heliocentric coordinates to compare with the original known values establishes the model's reliability. By doing so, systematic errors were identified and discussed.

## List of Symbols and Definitions

**ASTAP** Astrometric Stacking Program by hnsky.org [14](#)

**AU** Astronomical Unit, 1 AU = 149 597 871 kilometers [37](#)

**AutoNav** Autonomous Navigation System [8–10](#)

**AutOpNav** Autonomous Optical Navigation System [13, 14](#)

**DS1** Deep Space 1 [8–10](#)

**DSN** Deep Space Network, is the network of spacecraft communication ground antennas which are located in the United States, Spain and Australia to support spacecraft missions to interplanetary and deep space missions. [7, 8, 15](#)

**ecliptic** The ecliptic plane refers to the planet's orbit in which the Earth revolves around the Sun. [8](#)

**FOSS** Free Open Source Software [14, 19, 21](#)

**FPA** First Point of Aries: The position where the celestial equator circle and the ecliptic circle intersection is the zero point for the right ascension. It marks the moment when the Sun enters the northern hemisphere at the start of spring (the vernal equinox). [8](#)

**GMT** Greenwich Mean Time [11](#)

**heliocentric** Heliocentric model is a model that the Sun is at the center and planets are rotating around it. [8, 41](#)

**IAU** International Astronomical Union [10](#)

**ICRF** International Celestial Reference Frame [8, 19, 20, 40](#)

**LOS** Line of Sight [14](#)

**OpNav** Optical Navigation [15, 16](#)

**RF** Reference Frame [42–121](#)

**topocentric** Topocentric model uses the celestial coordinates of a specific point on the surface of the Earth. [8, 40, 41](#)

## 2 Introduction

Given how frequently they are used today by the average person, navigation systems play a significant role in humanity. This matter will play a significant role in the immediate future and the far future, as humans still need navigation when attempting to travel to a new location. Therefore, navigation systems are employed all over the globe. For instance, navigation systems are used in cars, submarines, and commercial aircraft. Space is another discipline where navigation systems are employed. The Deep Space Network (DSN) is currently used for most spacecraft. Whether it is the 1960s satellites sent into space or the International Space Station located in orbit, use this network. However, over recent years, the amount of spacecraft launched has increased drastically, resulting in an evergrowing load on the DSN. Besides the overloading of the DSN, spacecraft that are planned to traverse long distances will eventually have problems with this system's effectiveness due to the finite speed of light. For such reasons, new navigation systems have begun to appear. One way of navigating in space is the optical navigation system. An optical navigation system can have the option to relieve the dependency on DSN and find the spacecraft's position, distance to other planets or asteroids, and angles relative to the sun all by itself with the systems onboard. This system is also being pushed to increase the independency of the spacecraft to almost a three-digit percentage by combining the propulsion system solar sail. If this system is automated in the future, it will go down in history as one of the most significant steps toward deep space travel. In this project, we have developed an automated calculation of an optical navigation model to contribute to autonomous optical navigation systems by trying to determine a theoretical spacecraft's position, which is located on Earth, by processing asteroid data obtained from NASA JPL Horizons.

## 3 Literature Review

### 3.1 A. Roy, "Orbital Motion" (2005)[1]

Navigation systems take an essential place in interplanetary missions. Navigation for space missions can be controlled with two methods and sub-methods under those two methods.

The first method is the Earth-controlled navigation system. As a sub-method of Earth-based navigation, optical tracking can be used. In this method, the spacecraft is tracked with some instruments, such as telescopes in the observatories. The major problem with this method is that as the spacecraft gets farther away from the Earth, it becomes harder to see the spacecraft. After the spacecraft travels far enough, it becomes invisible to the observer. As for the second sub-method, radar

observations are employed where [DSN](#) is predominantly used.

The second method involves applying the same methodology to a spacecraft. For example, optical navigation can be done onboard by simply assembling a camera to observe the spacecraft's environment. These systems generally use the coordinate system, which is already known and determined by many parameters, such as the positions of the star, planets, and other celestial objects at a given time. During navigation, if the perturbations due to gravitational effects, radiation, and air drag (for the Earth orbiter spacecraft) are considered, the spacecraft's orbit can be calculated for all epochs. Hence, the velocity and acceleration of the spacecraft can be calculated, too.

In space navigation, multiple coordinate systems exist, which will be discussed in the following sections. Nevertheless, keeping it simple, Roy uses J2000/[ICRF](#) to do his calculations.

Generally, the planned trajectory to reach the target differs from the actual orbit during the mission due to perturbations. The spacecraft's trajectory can be corrected for perturbations by applying maneuvers throughout the mission.

Roy's approach, which we used in our project, is based on the position and angles of the spacecraft. He keeps his approach basic for easier understanding and uses three objects with known positions. Those three objects are the spacecraft, the Sun, and a beacon. The coordinate system is assumed as an [heliocentric ecliptic](#) Cartesian system by using the First Point of Aries ([FPA](#)). Heliocentric [ecliptic](#) coordinates of the spacecraft can be calculated as below:

$$\lambda = \arctan\left(\frac{Y}{X}\right)\text{Degrees}$$
$$\beta = \arctan\left(\frac{Z}{\sqrt{X^2 + Y^2 + Z^2}}\right)\text{Degrees}$$

With these calculations, Archie Roy ends up with the [topocentric ecliptic](#) coordinates of the beacon as seen from the spacecraft. Calculating the [topocentric](#) celestial coordinates (RA and Dec) of the beacon is possible. (Meuss).

Assuming the inverse, if the [heliocentric ecliptic](#) coordinates of the spacecraft at time t are known, by using observations, the [heliocentric](#) cartesian coordinates of the spacecraft can be calculated. However, the issue with this approach is the accuracy of the calculation. Nevertheless, in pursuit of increasing the accuracy of this approach, it is possible to increase the number of beacons.

### 3.2 J. E. Riedel et al, “Autonomous Optical Navigation (AutoNav) Technology Validation Report” [2]

In the year 2000, 8th of February, J. E. Riedel and their [DS1](#) Navigation team members from both [AutoNav](#) and [RadioNav](#) teams publish a report regarding the



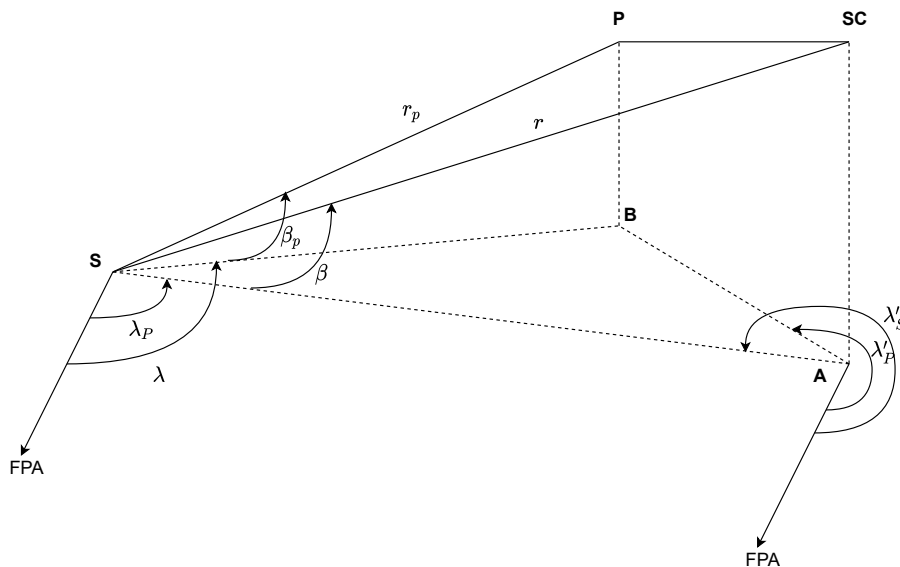


Figure 1: Roy's Model for Optical Navigation, Sketched via diagrams.net

**DS1** mission, the first mission of NASA's new millennium program. In this report, Riedel and their colleagues discuss the important **DS1** mission with a focus on its navigation system technology. In the report, they proceed to discuss the development of the navigation systems, interdependencies of the technology, ground, and flight testing, **AutoNav** difficulties in the actual mission of **DS1**, and future applications of **AutoNav** on upcoming missions. **DS1** mission was the first optically autonomous system deployed in deep space. **AutoNav** uses images of nearby celestial objects, such as asteroids, against distant celestial objects and stars to determine geometric properties through parallax. This information is then used in a dynamic filter to compute the main navigational parameters of the spacecraft, coordinates and velocity vectors, and other parameters such as the performance of the ion propulsion system (IPS) and solar radiation pressure. These calculations are done via the software onboard through a variety of functions. As for **DS1**'s case, the most essential functions of **AutoNav** were NavRT, NavExec, ImageProcessor, OD, and ManeuverPlanner. Providing vital navigation-related information to other subsystems, executing navigation-related tasks such as capturing images of asteroids, processing these images, determining the orbit through these images, and planning necessary maneuvers and corrections were the purposes of said functions, respectively. As is possible with any technology demonstration space mission, shortly after the launch of **DS1** in October 1998, **AutoNav** experienced many difficulties. Firstly, there was a significant issue with light leaking in the **DS1** imaging system, which is the lens glare through the reflection of sunlight on the spacecraft's body. This issue severely limited the camera's ability to detect

asteroids as the lens took too much light from the spacecraft’s body, rendering the asteroids less detectable. Furthermore, data gathered after the launch revealed that the camera had much worse geometric distortions of the camera field than anticipated before the launch. Even with all these difficulties combined, J. E. Riedel et al. report that while the estimated errors due to these conditions were 1000 km and 7 m/s, it was still sufficient for an interplanetary mission. Although the error was adequate, due to the unideal conditions that skewed their results, the team acted swiftly to update the software to compensate for these conditions and were able to reduce the error even more to about 250 km and 0.2 in 1999, February. Overall, much detail about [AutoNav](#) is contained within this report with technical detail. As a result of the accomplishments and issues of [DS1](#), vital data were collected for future use cases of [AutoNav](#).

### 3.3 J. Meuss, *Astronomical Algorithms* (1998)[3]

As the author indicates, this book is for researchers interested in astronomy calculations with programming languages, such as FORTRAN. All calculations were adapted to the J2000 reference frame.

Before explaining the coordinate transformations, we should look at Chapter 1 of Meuss, which is about choosing the correct quadrant of the coordinate system. It is known that when the angle of sine, cosine, tangent, or cotangent is known, we can calculate the angle just by using the inverse trigonometric function of them. As the inverse trigonometric functions have different values for the four main quadrants of the coordinate system, it may be hard to calculate the exact value of the angle. To do that, we can use different programming languages. However, most of them do not include any function to calculate them. However, the expression to calculate those angles by Meuss can be used to determine the required function for our programming language. Although it is going to be explained in the following chapters of our report, the example given by Meuss is the following:

“For example, try  $\cos 147^\circ$ . The answer is -0.8387, which reverts to  $147^\circ$  the inverse function is taken. Now try  $213^\circ$ . The answer is again -0.8387, which, when its arccosine is taken, gives  $147^\circ$ .”

Hence, the opacity occurs using inverse trigonometric functions, which must be solved to get accurate results.

It is important to note that he is not following [IAU](#) resolution but using west longitudes as positive. Longitudes are measured positively to the west because this approach can be used for different planets. This is why their central meridian increases with time during observation from the Earth.

$$\tan \lambda = \frac{\sin \alpha \cos \epsilon + \tan \delta \sin \epsilon}{\cos \alpha} \quad (1)$$

$$\sin \beta = \sin \delta \cos \epsilon - \cos \delta \sin \epsilon \sin \alpha \quad (2)$$

$$\tan \alpha = \frac{\sin \lambda \cos \epsilon - \tan \beta \sin \epsilon}{\cos \lambda} \quad (3)$$

$$\sin \delta = \sin \beta \cos \epsilon + \cos \beta \sin \epsilon \sin \lambda \quad (4)$$

The equations above explain the relationship between celestial coordinates to ecliptic coordinates where  $\epsilon$  is the obliquity of the ecliptic.

Meuss also mentions the time conventions in Chapter 10. The Universal Time (UT) is based on the rotation of the Earth. UT is used in daily life to determine work and school hours. It is also necessary to include UT when astronomical observations are done based on local hours. Most navigators generally use UT instead of GMT. However, this is not true for astronomical observations because GMT and UT differ by 12 hours. As the Earth's rotational speed slows down, UT is no longer a uniform time for astronomers. Hence, a new time scale was determined called Ephemeris Time, which had started to be called Dynamical Time which uses atomic clocks to be defined. There is a difference between Barycentric Dynamical Time (TDB) and Terrestrial Dynamical Time (TDT) by at most 0.0017 seconds because of the Sun's relativistic effect due to the Earth's motion on the orbit. As this error is negligible for practical usage, both times are called Dynamical Time or, in short "TD". The difference between TD and UT can only be calculated via observations.

$$\Delta T = TD - UT \quad (5)$$

$$t = \frac{year - 2000}{100} \quad (6)$$

Where  $\Delta T$  is in seconds and  $t$  is the time measured in centuries from the J2000.

$\Delta T$  for different year intervals can be calculated with the following equations.

For year;948,

$$\Delta T = 2177 + 497t + 44.1t^2 \quad (7)$$

For the year between 948 and 1600, and after the year 2000,

$$\Delta T = 102 + 102t + 25.3t^2 \quad (8)$$

However, to avoid discontinuity at 2000, the following correction should be added:

$$+0.37 \times (year - 2100) \quad (9)$$

So the equation above can be applied to years 2000 to 2100.

Some examples for about this formulation can be found in this book for who is interested in.

### 3.4 F. Pinto, Elements of Optical Navigation (2018)[4]

Dr. Pinto uses the approaches by Roy[1] and Meuss[3] to determine the topocentric positions of the beacon asteroids when the heliocentric Cartesian positions of the asteroids and the spacecraft are known, and he calls this method as the direct problem. Then he continues his calculations with the inverse problem, which means that the celestial coordinates of the asteroids, as seen from the spacecraft, and the ecliptic coordinates of the Sun are known by using this data to determine the spacecraft's position. He and his former student, Hazal Karaaliler, from the Izmir University of Economics, did outstanding work despite substantial errors. Dr. Pinto creates the figures below, showing the positions of asteroids (10) Hygiea and (944) Hidalgo.

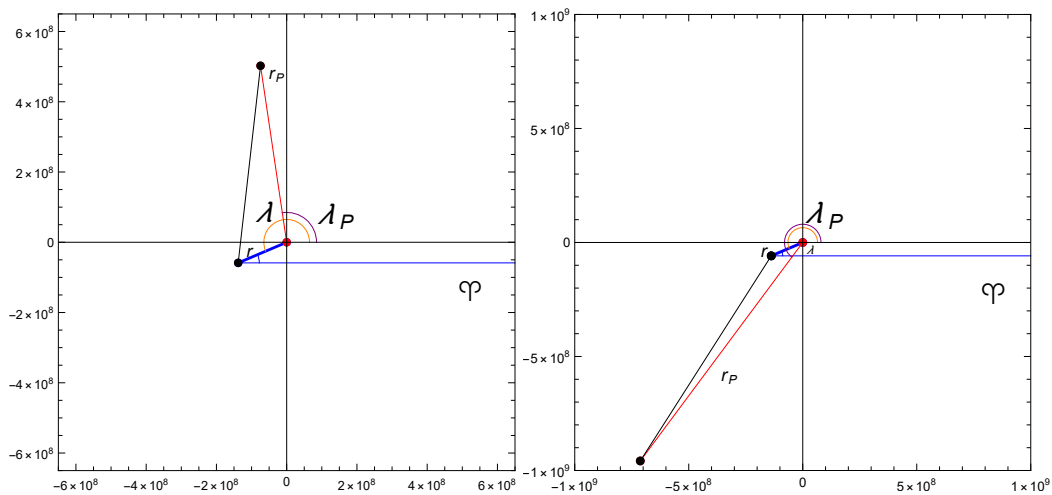


Figure 2: Hygiea (Left) and Hidalgo (Right) Asteroids

### subsection Wang et al. , “Spacecraft Autonomous Navigation Technologies Based on Multi-Source Information Fusion”[8]

Space navigation systems involve undertaking a series of tasks, including identifying a spacecraft's path in space and determining its current position, speed, and distance from Earth.

Three different systems belong to this navigation systems category: inertial navigation, autonomous optical navigation, and autonomous navigation based on pulsars.

### 3.4.1 Inertial Navigation

Inertial navigation uses the inertia of the spacecraft for measurement. Thanks to the measuring instruments, the spacecraft can find the speed and position of the spacecraft. The inertial navigation system has a mechanical system. It has the advantages such as low or no energy requirement during measurements, obtaining a high percentage of accurate measurements, and the fact that these systems are very resistant to being damaged. For this reason, an inertial navigation system is used not only in space-related situations but also in the aviation sector. The most significant disadvantage of this system is that since the inertial navigation system is a mechanical system, researchers can say that the mechanisms used at a certain time expire and become obsolete, but even here, due to the development of technology, these periods have increased for decades.

#### Gyroscope

A gyroscope is, in essence, a machine that uses momentum conservation to determine direction. Two groups can be made up of this mechanism. These are known as gyroscopes, which feature a classical mechanism and are constructed in compliance with current physics laws.

#### Accelerometer

In contrast, the accelerometer features a spring system that lets us determine the object's acceleration from the forces acting on the springs and its vibration.

### 3.4.2 Autonomous Optical Navigation

The Autonomous Optical Navigation system was developed in the 1960s for deep-space research. Researchers applied the integration of this system to the tasks. Since an [AutOpNav](#) is not mechanical but instead based on an electronic system, because the system contains a computer system, sensors, or a camera system, and these systems are a much more open issue in terms of development, the desire to be used in deep space missions is also increasing. Moreover, thanks to these systems, a vital security net has been gained for extending a spacecraft's survival probability and mission life on a deep space mission.

The working principle of the [AutOpNav](#) is to identify the celestial bodies seen primarily following the information received (stars, asteroids, or planets in the solar system) and to determine the movements, distances, velocities of the celestial bodies found and identified on the pictures taken after this identification. After

such operations, the [AutOpNav](#) is a fundamental system that finds the spacecraft's speed and position.

### 3.4.3 Autonomous Pulsar-Based Navigation

The purpose of this autonomous system is to determine the position unit vector of the pulsars using very long basic interferometry in a barycentric celestial reference system based on the X-rays emitted by pulsars in fast space and the standard arrival time of the X-ray pulse. To compare them with the pulsar, the [LOS](#) direction and the actual arrival time are measured by an X-ray detector on the deep space probe, and a suitable filtering algorithm is used to obtain navigational information such as spacecraft position, speed, and time.

### 3.5 Karaaliler et al. , “Autonomous optical and inertial navigation of solar-sail propelled CubeSat class spacecraft during targeting missions to asteroids and minor moons. (2022)”[5]

Hazal Karaaliler and her team, in the academic year of 2021-2022, aimed to prove the concept of the optical navigation model as mentioned in section (3.1). However, to achieve such a feat, her team had to start from the very beginning by describing the astrophotographic requirements to extract the astrometric data.

In order to optically navigate in space, imaging equipment is essential. Theoretically, a simple camera onboard shall efficiently measure astrometric data in space. As with any measuring tool, calibration of the equipment is a must. This is exactly where Hazal Karaaliler and her team start by gathering calibration frames which are: Dark, Bias, and Flat-Field Frames. It is very important that in order to average out the expected noise in the camera's sensor, each calibration frame has to be taken multiple times; the more, the better. These calibration images are then fed into a series of software which are all either [FOSS](#) or freeware. First, DeepSkyStacker is used to stack and create "Master Frames," including "Master Light Frame." An additional alignment and stacking of these frames are done to create the final "Science Frame." Once a calibrated image is obtained, it is possible to start photometric and astrometric calculations with the help of another [FOSS](#), [ASTAP](#). Alongside [ASTAP](#), Astrometry.net, an astronomical image astrometric calibration and analysis web service, is used to double-check the accuracy of the center pixel coordinate of the science frame. Applying necessary adjustments via [ASTAP](#), they were able to utilize the blinking method to detect and obtain the first approximation of the asteroid pixel coordinates. Additionally, they also used the blinking method to create an MPC-80 file to feed into the FindOrb application to find orbit. At this point, Hazal Karaaliler and her team decided to increase the accuracy of their measurements of asteroids by analyzing the subpixels of asteroids

and applying Point Spread Function to remedy the stretching and blur occurring due to the limitations of the imaging equipment. Thus, Hazal Karaaliler and her team obtained a close approximation of data captured by the imaging equipment on Urla, Izmir, and finalized their work by applying the navigation model on certain large asteroids.

For our case, their work is invaluable to us as our team decided to pick up the same [OpNav](#) model where they, our predecessors, stopped. Their work laid the groundwork and allowed our team, and their successors, to focus on automating the process of navigational calculations by assuming position, allowing the user to integrate as many asteroids as desired, measure and investigate many error possibilities within the navigation model to reduce the error levels as much as possible. Thanks to their work, it was possible to understand the process of obtaining coordinates from amateur astrophotography hardware and freely available software.

### **3.6 E. Sahr et al “Post-Launch Characterization of the Optical Navigation Instruments For Nasa’s Lucy Mission”[6]**

The Lucy spacecraft was launched in October 2021, and its purpose is to explore the asteroids in the Trojan regions located on Jupiter’s surface; the mission’s duration is specified as 12 years. These Trojan regions are called “L4” and “L5”. The spacecraft is estimated to arrive in the L4 region in June 2027, and until November 2028, it is planned to study asteroids by passing near five different asteroids in this region. As the spacecraft leaves the L4 Trojan region after a planned five-year flight to the L5 region, the mission will be considered successful as enough data will be gathered by studying the asteroids. The Lucy spacecraft would normally require much fuel to complete this long-term, long-distance mission. On such mission, if a spacecraft were to travel through deep space, it was decided that utilizing the Earth’s gravitational force would be worthwhile. In order to go to the desired regions, the orbit must be adjusted as such, and the Lucy spacecraft will do this by getting very close to the Earth. By doing so, the spacecraft will complete its journey without carrying too much fuel onboard, thanks to this maneuver. Nevertheless, an additional engine located at the bottom of Lucy was added to the spacecraft to avoid the Earth’s crowded orbit, and it is planned to be fired to prevent Lucy from colliding with satellites as it enters the Earth’s orbit. Lucy will fly near those asteroids during the mission to get quality results. Furthermore, Lucy, which uses the [DSN](#) as usual, is also planned to use [OpNav](#) as a navigation system for precise spacecraft navigation. Since a cutting-edge sensitive navigation system is required to ensure the close flight of the spacecraft, detailed visual measurements will be obtained as optical navigation systems require an imaging system.

The Lucy spacecraft uses tools such as cameras and antennas for many different purposes. On the spacecraft, two cameras exist which are planned to be used for [OpNav](#). These are “L’LORRI”, which will be used for long-range reconnaissance, and “TTCAM,” with two thermal cameras. [OpNav](#) will be used when the spacecraft approaches each Trojan region, and thus factors such as the position and speed of the orbit will be analyzed and reconstructed again. As with every system, there are some errors before using this navigation system, and one of the most important issues is ensuring that these potential errors are eliminated before using this system. The geometric distortions found in the shooting of these images will be corrected, and the photometric values of the photos will be edited and characterized on the Instrument Marking Platform (IPP) located on Lucy.

### **IPP-Gimbal-Angle-Based Instrument Marking Simulator**

In the characterization of the “L’LORRI” and “TTCAM” cameras for navigation, significant difficulties were encountered in meeting the IPP requirements. This characterization was made to cover improving aspects such as stray light sensitivity and pointing stability. However, the adjustment system required to ensure that all other requirements are met has been found to be very problematic, and an IPP-Gimbal Angle-Based Tool Marking Simulator has been developed to detect these problems.



## Equipment of the L'LORRI [9]

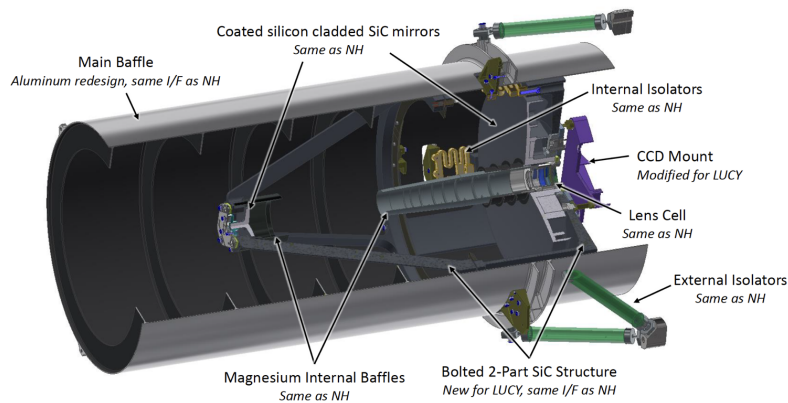


Figure 3: L'LORRI's Equipments

This camera is the most sensitive camera on the Lucy spacecraft. It is called "eagle eyes." This panchromatic camera utilizes the Ritchey-Chrétien telescope, similar to the one employed by the Hubble telescope. The hyperbolic secondary mirror in this telescope reflects light that first travels down the tube and is reflected by the hyperbolic primary mirror. The secondary mirror focuses the light before passing through a gap in the primary mirror. It then moves through several lenses in L'LORRI's case. A charge-connected device, a photosensitive device used in place of film in digital cameras, is utilized to record the image.

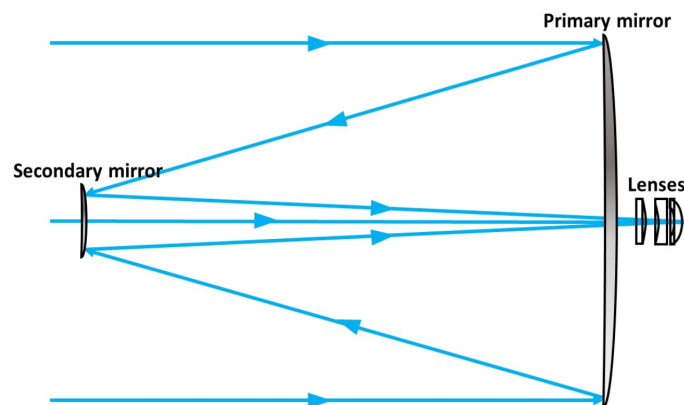


Figure 4: L'LORRI's Equipments

One of L'LORRI's objectives is to create distinct photographs of the Trojan asteroids, despite being quite dark. L'LORRI will be able to see craters with a

diameter of 70 m (i.e., 14 m per pixel) from a distance of 1000 km. Researchers will be able to grasp the Trojan asteroids' surface geology better thanks to L'LORRI's fine-grained imagery.

### 3.7 M. Vertregt, "Orientation in Space" (1956) [7]

The orientation in space should be based on different principles from orientation on the Earth because some orientation systems used on the Earth are not applicable in space. For example, on Earth, there are different bodies and shapes that a navigator could use to determine his position and velocity, hence its acceleration. However, in space, there is generally a piece of light and planets, stars, and different celestial bodies. If they are so far from the spacecraft, it is hard to determine their position in space. However, if the reference system is drawn based on the Earth, which has the Vernal Equinox point and celestial equator, then the angles of Right Ascension and Declination can be determined. However, there are better ways to do that than this because the Vernal Equinox point shifts about 50.3" or more per seventy years. It is also known that the Earth's orbit is precessing. Then the positions of the stars change continuously. The Earth's orbit can be chosen as a reference plane, neglecting the perturbations. The obliquity of the Earth is also not constant but decreases 0.47" per year.

The same approach with Roy([1]) works here and continues with the determination of the orbit. By taking the bearings of the reference body and taking the Gaussian Problem, the orbit can be determined if the orbital elements are known, and the orbit is Keplerian. However, as there are perturbations that should be considered, such as the effect of other bodies, the orbit is no longer Keplerian.

## 4 Methodology

Two main methods were used for this project: “Direct Problem” and “Inverse Problem”. Although these methods will be explained more in detail later, for replication purposes, start method was chosen as the relatively inaccurate method that was also chosen in both the papers called “Elements of Optical Navigation” by Pinto (3.4) and “Autonomous optical and inertial navigation of solar-sail propelled CubeSat class spacecraft during targeting missions to asteroids and minor moons” by Karaaliler (3.5).

The reader needs to know about the FOSS tools that were used throughout this project.

### 4.1 Tools Used

#### 4.1.1 Horizons System

Horizons System is an online tool that NASA JPL developed. In this app, the user can create outputs to observe:

- the ecliptic longitude and the latitude of the target body
- the ecliptic cartesian coordinates of the target body

and more...

Horizons uses ICRF as a reference frame. For the Earth observer, the atmospheric effect is optional. The user can also choose the time form and time type, discussed in earlier sections of the report. In this project, settings used are always as below:

- When Observing the Heliocentric Ecliptic Coordinates:
  - Ephemeris Type: Observer Table
  - Target Body: Any Celestial Object
  - Observer Location: @Sun
  - Time: Time - Type: UT
  - Table Settings: Options 2, 18 are checked.
  - ... Reference Frame: ICRF
  - ... Angle format: Decimal Degrees, Extra Precision: On
  - ... CSV Format

- When Observing the Heliocentric Cartesian Coordinates:
  - Ephemeris Type: Vector Table
  - Target Body: Any Celestial Object
  - Observer Location: @Sun
  - Time: Time - Type: UT
  - Table Settings: Output Quantities: 1 with XYZ uncertainties
  - ... Reference Frame: [ICRF](#)
  - ... Reference Plane: ecliptic x-y plane derived from reference frame
  - ... (standard obliquity, inertial)
  - ... Vector Correction: Apparent States
  - ... CSV Format
- When Observing the Topocentric Ecliptic and Celestial Coordinates:
  - Ephemeris Type: Observer Table
  - Target Body: Any Celestial Object
  - Observer Location: @ Any Celestial Object
  - Time: Time - Type: UT
  - Table Settings: Options 2, 18, 31 are checked.
  - ... Reference Frame: [ICRF](#)
  - ... Angle format: Decimal Degrees, Extra Precision: On
  - ... CSV Format

For more information, please check the Appendix [\(8\)](#)

#### 4.1.2 AstroGrav

AstroGrav is a software that calculates the gravitational interactions and forces between all celestial bodies in the Solar System. For our project, it is used to see the orbital motion of asteroids and planets in the Solar System. The effects of radiation pressure and general relativity can be considered for calculations with this tool. For more information, see Appendix [8](#).

### 4.1.3 Stellarium

Stellarium is a [FOSS](#) tool that can be used on a computer. It is capable of showing the sky with stars, planets, and asteroids on it. In this tool, users can also choose the observer location of any celestial object and the target body. Once the target body is selected, Stellarium can show its data on the left side of the screen. (See [Appendix 8](#)).

This article includes figures that are created with both Stellarium and Astro-Grav.([Sec 5.4](#) and [5.5](#)) All required data will be imported from Horizons App to do this project.

## 4.2 First Trials

This project was started by the reference of the papers mentioned above. The main problem for those papers was that they did not consider the quadrant calculations due to Mathematica's syntax (Please see the discussion done in [3.3](#) about choosing the correct quadrant.). However, the inverse trigonometric functions are correctly designed in FORTRAN, not Mathematica Language. As this project is based on Mathematica, adding and determining extra conditions per quadrant was necessary to correct these issues.

Another problem we faced was an unexplained error between Horizons' data and our calculations for topocentric ecliptic coordinates of asteroids. This issue will be clarified in a following section.

## 4.3 Direct Problem

Initially, F. Pinto used these methods in [Elements of Optical Navigation 3.4](#). Going by the same approach, the direct problem was the first method used in this research when the project began. The direct problem method states that when the following parameters are known:

- Heliocentric Cartesian Coordinates of the Asteroids and the Spacecraft

What were trying to find is:

- Topocentric Ecliptic Coordinates of the Asteroids
- Topocentric Celestial Coordinates of the Asteroids

This method can be explained with the following diagrams.

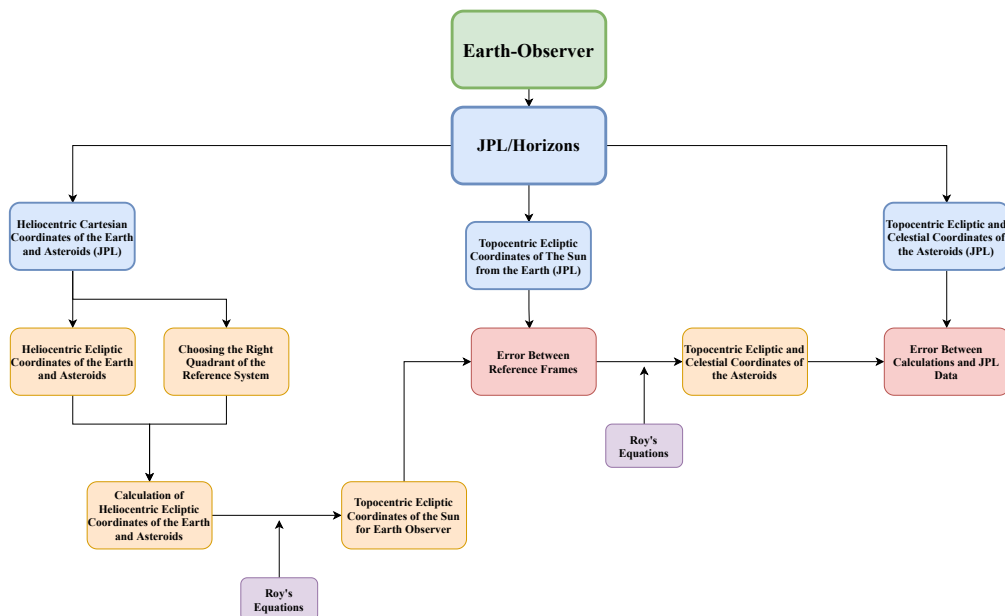


Figure 5: Roadmap for the Direct Problem for the Earth Observer

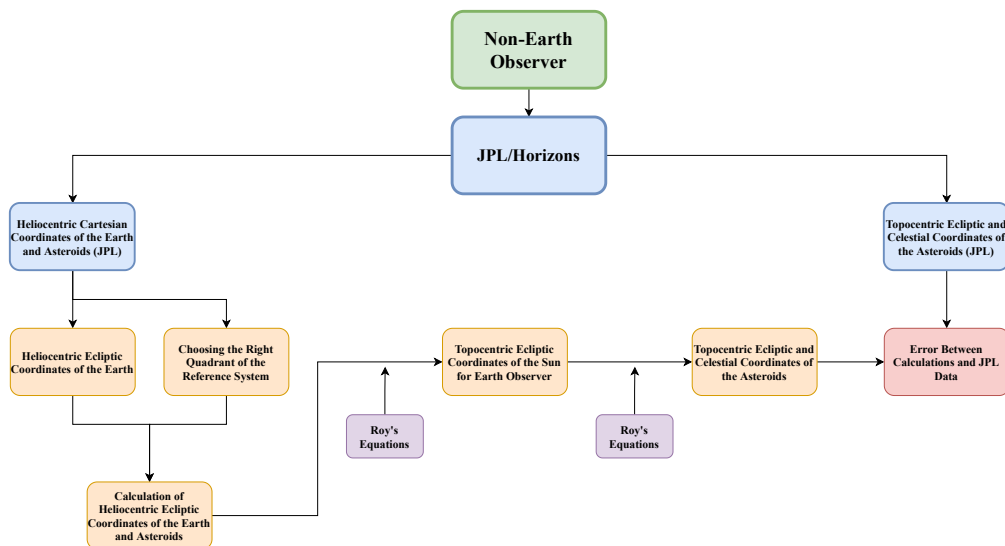


Figure 6: Roadmap for the Direct Problem for the Non-Earth Observer

In both methods, JPL / Horizons website was used as a source for our data. From Horizons, the parameters required input data for the direct problem can be determined. All the user needs is to determine from where they would like to

observe the beacon asteroid. If the Earth observer is chosen, some errors because of the different reference systems should be taken into account.

### 4.3.1 Earth Observer

For the Earth observer case, we should get the following data as our input from Horizons (See Figure 5):

- Heliocentric Cartesian Coordinates of the Earth and The Asteroids
- Topocentric Ecliptic Coordinates of the Sun from the Earth
- Topocentric Ecliptic Coordinates of the Asteroids from the Earth
- Topocentric Celestial Coordinates of the Asteroids from the Earth

As the heliocentric cartesian coordinates of the Earth and the asteroids are known, it is possible to calculate their heliocentric ecliptic coordinates by choosing the correct quadrant of the reference system.

$$\lambda = \arctan\left(\frac{Y}{X}\right) \text{ Degrees} \quad (10)$$

$$\beta = \arctan\left(\frac{Z}{X^2 + Y^2 + Z^2}\right) \text{ Degrees} \quad (11)$$

Where  $X^2 + Y^2 + Z^2$  is the distance of the Earth or asteroids from the Sun.

### Choosing The Correct Quadrant

The correction for quadrants should be done because the longitude should not be harmful by its definition. However, the formulas above may give the results in negative sign. Remember that calculation of the longitude is based on the X and Y coordinates of the object.

The formulations for four main quadrants in our reference frame can be calculated as below:

- For the First Quadrant (+,+)

$$\lambda = \arctan\left(\frac{Y}{X}\right) \text{ Degrees} \quad (12)$$

- For the Second Quadrant (-,+)

$$\lambda = \arctan\left(\frac{Y}{X}\right) + 180 \text{ Degrees} \quad (13)$$

- For the Third Quadrant (-,-)

$$\lambda = \arctan\left(\frac{Y}{X}\right) + 180 \text{ Degrees} \quad (14)$$

- For the Fourth Quadrant (+,-)

$$\lambda = \arctan\left(\frac{Y}{X}\right) + 360 \text{ Degrees} \quad (15)$$

This approach can be easily seen with the following diagrams.



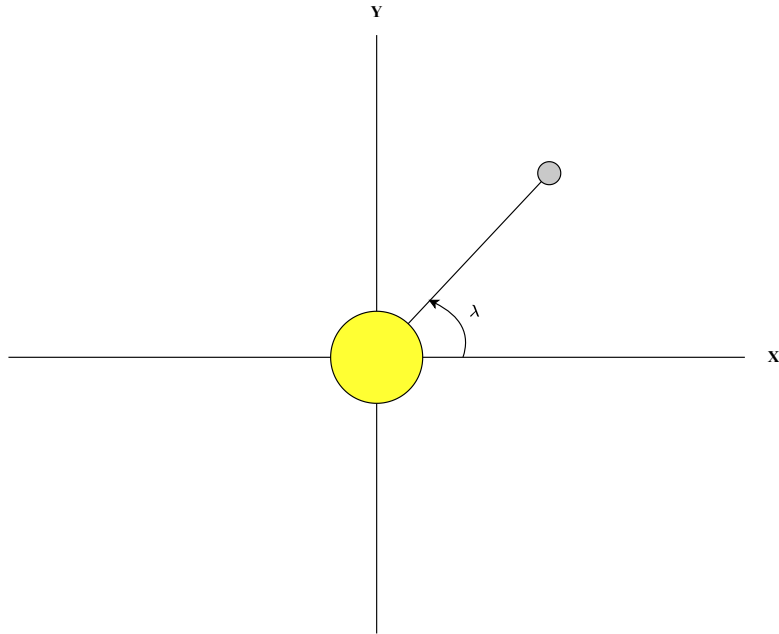


Figure 7: Mathematica gives us  $\lambda$ , what we need is  $\lambda_{Corrected}$ ,  $\lambda_{Corrected} = \lambda$

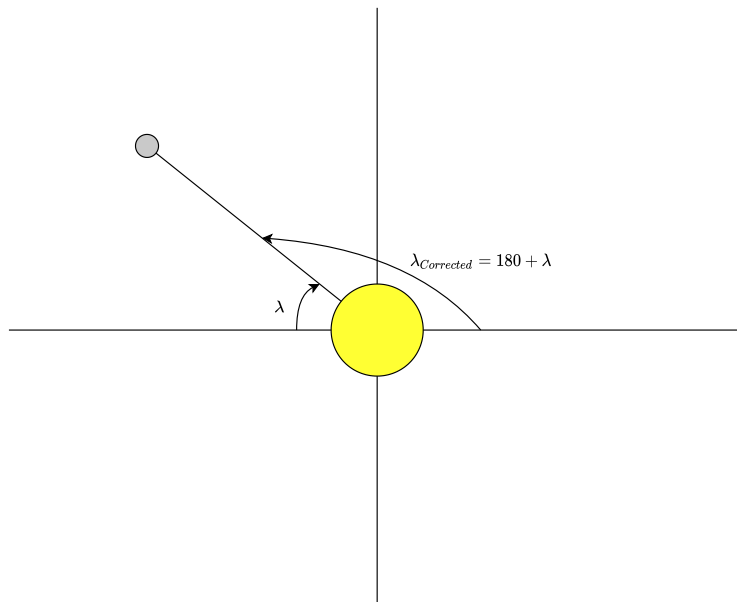


Figure 8: Mathematica gives us  $\lambda$ , what we need is  $\lambda_{Corrected}$ ,  $\lambda_{Corrected} = \lambda + 180$

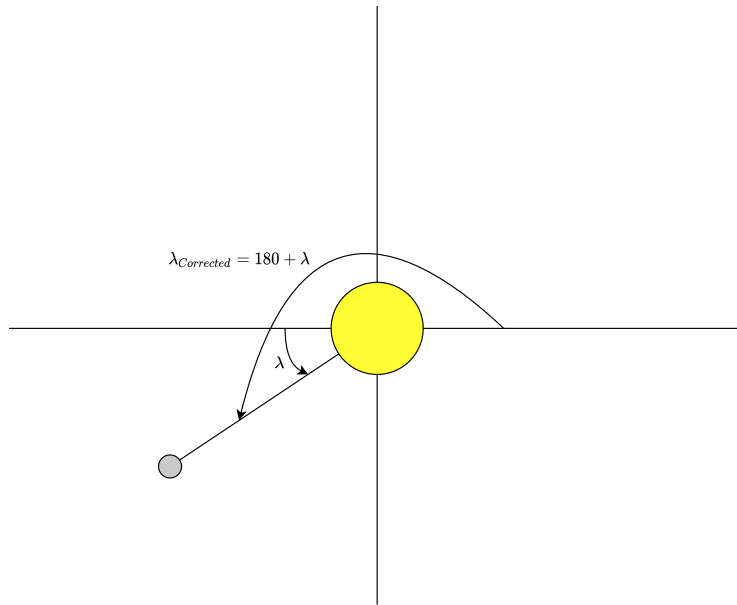


Figure 9: Mathematica gives us  $\lambda$ , what we need is  $\lambda_{Corrected}$

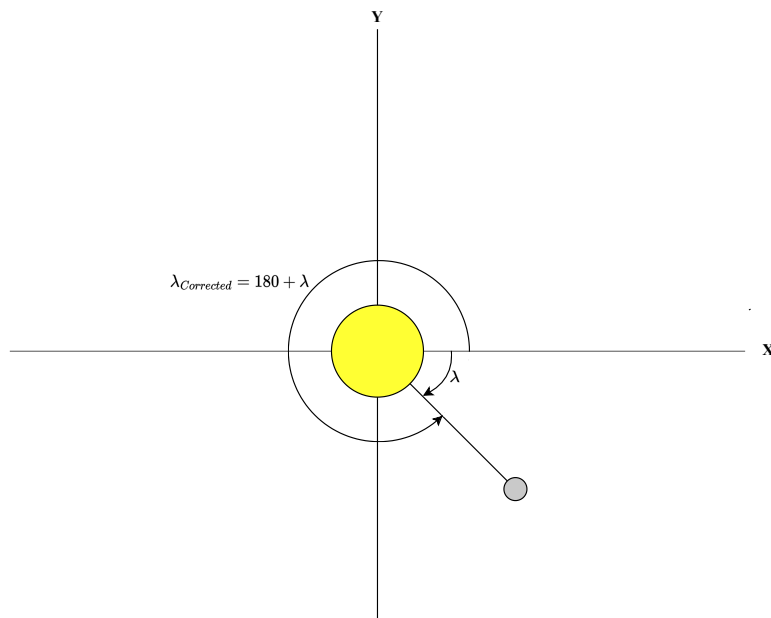


Figure 10: Mathematica gives us  $\lambda$ , what we need is  $\lambda_{Corrected}$

## Topocentric Ecliptic Coordinates of the Sun

After calculating the heliocentric ecliptic coordinates of the Earth and asteroids, Roy's approach can be applied to calculate topocentric ecliptic coordinates of the Sun for Earth observer ( $\lambda'_S$ ) and  $\beta'_S$ . This is:

$$\lambda'_S = \lambda - 180 \quad (16)$$

$$\beta'_S = -\beta \quad (17)$$

When  $\lambda'_S$  is calculated, quadrants which is in the Earth Centered model should be taken into account.

In Earth observer case, the topocentric ecliptic coordinates of the Sun for the Earth observer should be imported from Horizons case. The value found from Horizons and calculated above will differ from each other date by date. This is because when the observer is the Earth, Horizons uses on-date J2000 reference frame rather than the initial J2000 reference frame. When the observer is an object that is non-Earth, this will give the coordinates of the body on J2000 reference frame. The error between on-date reference frame and J2000 reference frame can be calculated with the following equations.

Let us assume that the topocentric ecliptic longitude of the Sun for Earth observer from Horizons is determined as  $\lambda'_{S,Hor}$ . The difference between  $\lambda'_S$  and  $\lambda'_{S,Hor}$  will give the error between on-date reference frame and J2000 reference frame.

$$\text{error} = |\lambda'_{S,Hor} - \lambda'_S|$$

Please notice that quadrants take important place during calculation of the topocentric longitude of the Sun, again.

## Topocentric Ecliptic Coordinates of the Asteroids

As the topocentric ecliptic coordinates of the Sun is known now, the next step is to find topocentric ecliptic coordinates of the asteroids. This can be calculated with Roy's approach which is

$$r = r_P \frac{\cos \beta_P \sin (\lambda_P - \lambda'_P)}{\cos \beta \sin (\lambda'_P - \lambda'_S)} \quad (18)$$

Where  $r$  is the Earth's distance from the Sun and  $r_P$  is the asteroid's distance from the Sun.  $\beta$  was previously determined above (See Eq 11). By solving this equation to find the topocentric ecliptic longitude of the asteroid ( $\lambda'_P$ ), we have,

$$\lambda'_P = \text{error} + \arctan \frac{r \cos \beta \sin \lambda'_S + r_P \cos \beta_P \sin \lambda_P}{r \cos \beta \cos \lambda'_S + r_P \cos \beta_P \cos \lambda_P} \quad (19)$$

Please notice that, quadrants should be taken into account for this condition, too.

The distance between the Earth and the asteroid  $r_{VP}$  can be also calculated as,

$$r_{VP} = \sqrt{(X_P - X)^2 + (Y_P - Y)^2 + (Z_P - Z)^2} \quad (20)$$

Hence, the topocentric ecliptic latitude of any asteroid can be calculated with,

$$\beta'_P = \arcsin \frac{Z_P - Z}{r_{VP}} \quad (21)$$

## Topocentric Celestial Coordinates of the Asteroids

Now, our system is ready to calculate the topocentric celestial coordinates of the asteroids when the observer is the Earth. The topocentric celestial coordinates, right ascension ( $\alpha$ ) and declination ( $\delta$ ), can be calculated with the following formulations which were already given by Meuss (See 3.3):

$$\tan \alpha = \frac{\sin \lambda \cos \epsilon - \tan \beta \sin \epsilon}{\cos \lambda} \quad (22)$$

Hence,

$$\alpha = \arctan \frac{\sin \lambda \cos \epsilon - \tan \beta \sin \epsilon}{\cos \lambda} \quad (23)$$

$$\sin \delta = \sin \beta \cos \epsilon + \cos \beta \sin \epsilon \sin \lambda \quad (24)$$

Then,

$$\delta = \arcsin(\sin \beta \cos \epsilon + \cos \beta \sin \epsilon \sin \lambda) \quad (25)$$

where the obliquity of the ecliptic is

$$\epsilon = 23.4393^\circ$$

However, as you may have noticed that the arctan could be a problem for us which is about the choosing the correct quadrant again. Same approach done during calculation of the heliocentric longitude  $\lambda$  can be applied to this case as the diagrams below explain. It is important to note that both the  $\alpha$  and  $\delta$  are in Degrees. To be more realistic, right ascension should be written in hours. This can be done with

$$\alpha_{Hours} = \alpha \times \frac{24}{360} \quad (26)$$

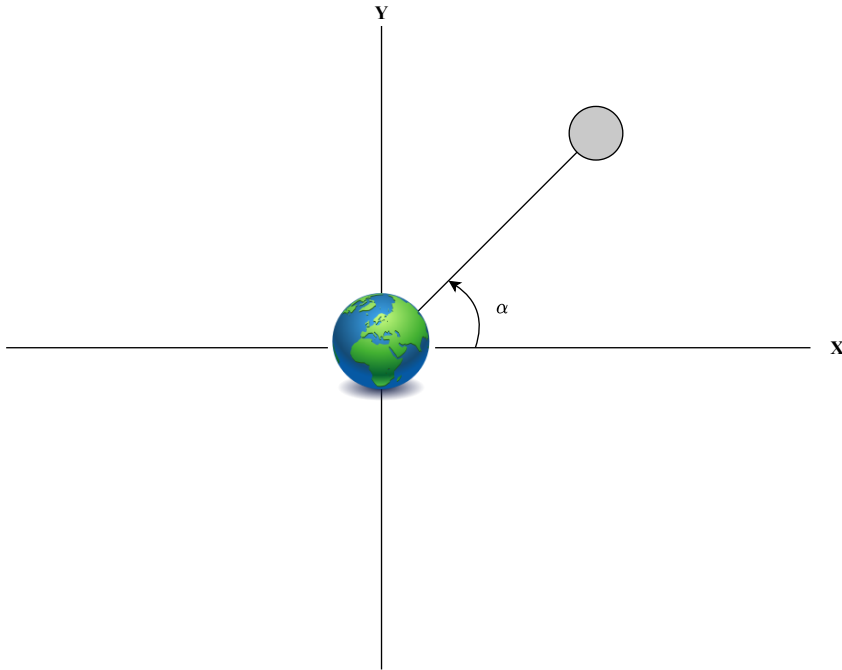


Figure 11: Mathematica gives us  $\alpha$ , what we need is  $\alpha_{Corrected}$

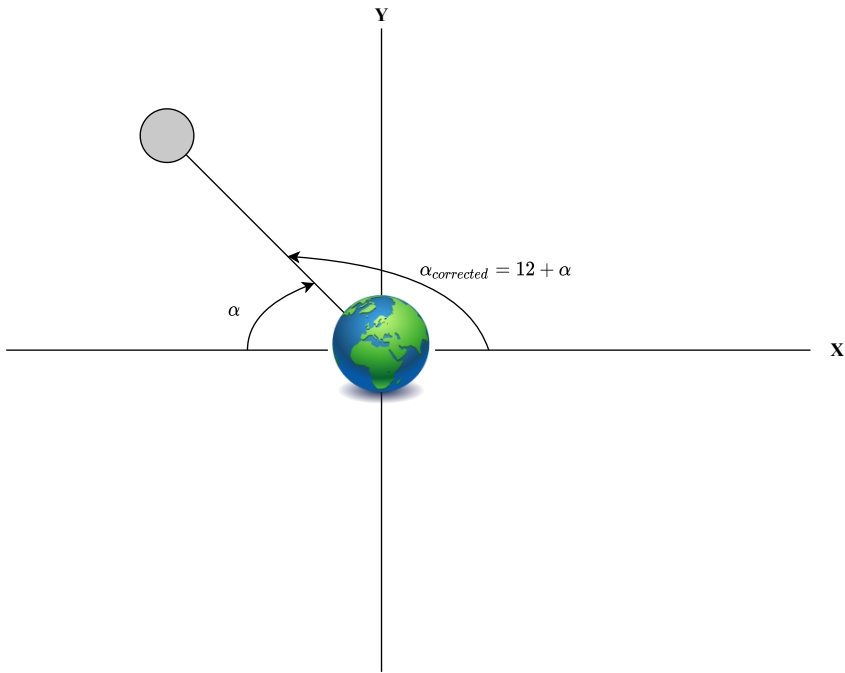


Figure 12: Mathematica gives us  $\alpha$ , what we need is  $\alpha_{Corrected}$

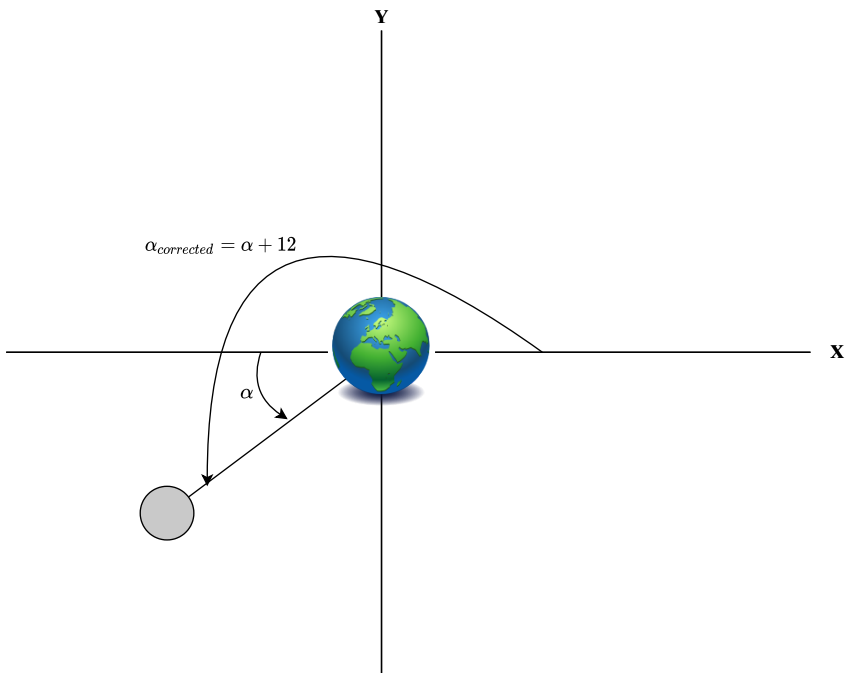


Figure 13: Mathematica gives us  $\alpha$ , what we need is  $\alpha_{Corrected}$

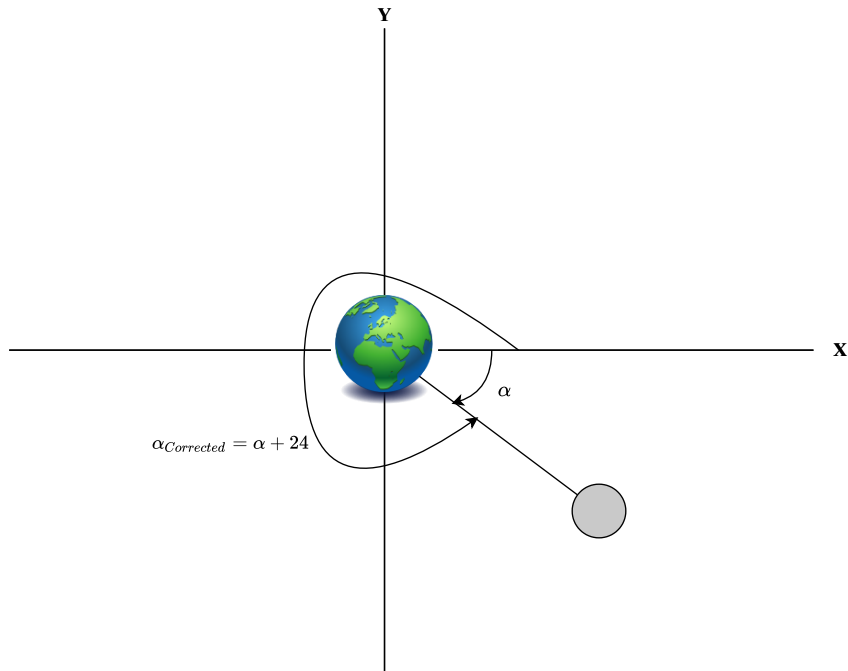


Figure 14: Mathematica gives us  $\alpha$ , what we need is  $\alpha_{Corrected}$

The main method that is used here is that when the reference frame and the body is fixed at any given time or epoch, the bodies on that reference frame are also fixed. If the J2000 Reference Frame is transformed to the Earth Centered Reference Frame. Hence, the center of the reference system, the Earth, can measure the right angle of the longitude and the latitude of the asteroids as observed. As the Right Ascension can be 24 hours at maximum, the calculated  $\alpha$  should be corrected such as,

- If the asteroid is in the first quadrant of the Earth Centered J2000 Reference System:

$$\alpha = \alpha \text{ (h)} \quad (27)$$

- If the asteroid is in the second quadrant of the Earth Centered J2000 Reference System:

$$\alpha = \alpha + 12 \text{ (h)} \quad (28)$$

- If the asteroid is in the third quadrant of the Earth Centered J2000 Reference System:

$$\alpha = \alpha + 12 \text{ (h)} \quad (29)$$

- If the asteroid is in the fourth quadrant of the Earth Centered J2000 Reference System:

$$\alpha = \alpha + 24 \text{ (h)} \quad (30)$$

### 4.3.2 Non-Earth Observer

In section 4.3.1, the source of the error was explained as the discrepancy between the reference frames that chosen bodies use. Horizons uses the J2000 Inertial Reference Frame for non-Earth observers. In this case, Roy's treatment about the apparent longitude of the Sun for an observer, which is explained in equation 16 above will be true. Hence, error calculation for different reference frames will not be needed.

### Topocentric Ecliptic and Celestial Coordinates of the Asteroids

With the reference of information above, the topocentric ecliptic longitudes of the asteroids ( $\lambda'_p$ ) can be calculated with Roy's approach again. (See Eq 18 and 19). Equation 19 will differ as below:

$$\lambda'_p = \arctan \frac{r \cos \beta \sin \lambda'_s + r_p \cos \beta_p \sin \lambda_p}{r \cos \beta \cos \lambda'_s + r_p \cos \beta_p \cos \lambda_p} \quad (31)$$

The issue of quadrants for Mathematica should also be taken into account for this calculations, too. As the topocentric ecliptic longitudes and latitudes of asteroids are calculated, the topocentric celestial coordinates of the asteroids can be calculated as same as done in 4.3.1. After conversion from degrees to hours for Right Ascension is done, next step is to calculate error between calculations and JPL values as explained in Figures 5 and 6

### 4.3.3 Error Calculation for the Direct Problem

In this part, in order to prove the reliability of the calculations the error between Horizons' data and our calculations must be calculated. Remembering the source we trust is Horizons, this can be done with the following formulation for every error will be get.

$$\text{error} = \text{Horizons} - \text{Calculations} \quad (32)$$

At the end of the process, errors for

- Topocentric Ecliptic Coordinates of the Asteroids



- Topocentric Celestial Coordinates of the Asteroids

can be calculated with respect to other parameters such as the distance between the observer and the beacon asteroid. Generally, the error for the longitude which is less than  $0.001^\circ = 3''$  is acceptable for optical navigation.

#### 4.4 Inverse Problem

Having giving a detailed expression about the Direct Problem, Inverse Problem can be explained. The Inverse Problem can be stated as when

- the Heliocentric Ecliptic Cartesian Coordinates of the Asteroids

are known and other parameters that could be determined via observations from the spacecraft such as

- the Topocentric Celestial Coordinates of the Asteroids
- the Topocentric Ecliptic Coordinates of the Sun

determination of the

- the Topocentric Ecliptic Coordinates of the Spacecraft

so that

- the Heliocentric Ecliptic Cartesian Coordinates of the Spacecraft

The figure below explains what Inverse Problem means clearly.

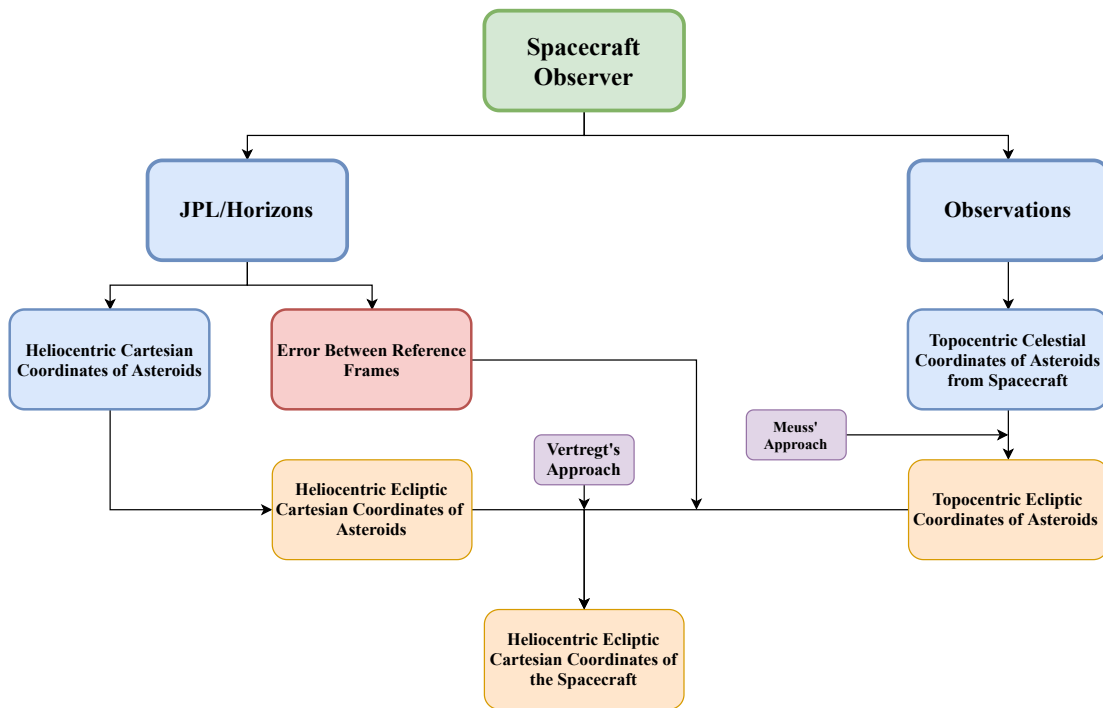


Figure 15: Roadmap for the Inverse Problem

In our project, as the beacons cannot be observed from anywhere rather than the Earth in space (We cannot do that.), it is decided to test the position of the observer when the observer is in different positions on the Earth at first. It is not the only reason why the Earth is chosen as a initial observer location for tests but it is required to have realistic photos taken with CCD camera that would include additional errors to this project. Also, by using this method, as the position of the observer (Somewhere on the Earth) is also known the error in the position of the observer can be calculated (With respect to the Horizons data and the data will be given by the Group-3 of this project.).

So, our approach is really simple. If the position of the Sun and another beacon object on the sky, could you determine your position with respect to the Sun? To understand this better, review the items above and see the figure below.

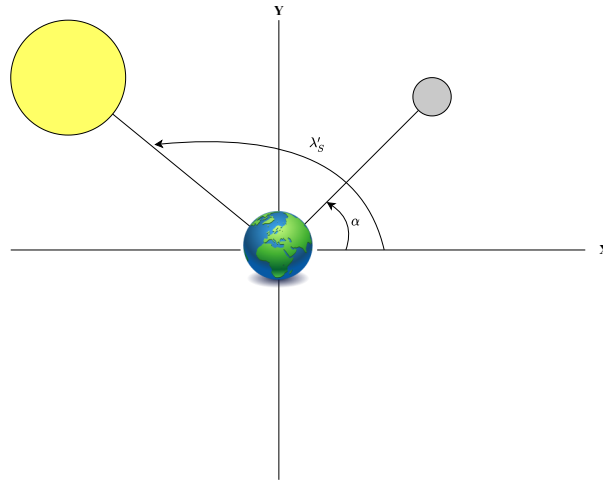


Figure 16: Example Figure For the Inverse Problem

Then the answer to the question is, yes.

### **Observation Based Topocentric Celestial Coordinates of Asteroids from Spacecraft**

As the photographs of the asteroids could not be taken because of the air conditions, it is needed to continue this process by using the data were created in the Direct Problem in section 4.3.1. However, any researcher could use his observational data to test this.

### **Observation Based Topocentric Ecliptic Coordinates of Asteroids from Spacecraft**

The topocentric celestial coordinates of the asteroids are known and by using Meuss' Approach as explained in 4.3.1 and the topocentric ecliptic coordinates of asteroids ( $\lambda'_p$  and  $\beta'_p$ ) can be obtained by solving the equations 23 and 25 for them. This gives:

$$\lambda'_p = \arctan \frac{\sin \alpha \cos \epsilon + \tan \delta \sin \epsilon}{\cos \alpha} \quad (33)$$

and

$$\beta'_p = \arcsin (\sin \delta \cos \epsilon - \cos \delta \sin \epsilon \sin \alpha) \quad (34)$$

Remember that the issue of the on-date J2000 Reference Frame should be calculated for all the Earth observer cases. This error should be included to the observed topocentric ecliptic coordinates of the asteroids during its calculation.

It is important to note that, the topocentric ecliptic coordinates of the Sun ( $\lambda'_S$ ,  $\beta'_S$ ) should be observed during observation.

## Heliocentric Cartesian Coordinates of The Spacecraft

When the topocentric ecliptic coordinates of the asteroids and the Sun are known, the spacecraft's distance from the Sun can be calculated by using the equation

$$r = r_P \frac{\cos \beta_P \sin (\lambda_P - \lambda'_P)}{\cos \beta \sin (\lambda'_P - \lambda'_S)} \quad (35)$$

where  $\beta_P$  is the heliocentric ecliptic latitude of the asteroid and  $\beta = -\beta'_S$  which states heliocentric ecliptic latitude of the spacecraft. Note that asteroids' heliocentric ecliptic longitudes and latitudes are also known.

In the Direct Problem 4.3,  $r$  was given as:

$$r = \sqrt{X^2 + Y^2 + Z^2} \quad (36)$$

In the Inverse Problem, the heliocentric ecliptic longitude of the spacecraft can be calculated from the following equation:

$$\lambda = \lambda'_S - 180 \quad (37)$$

where  $\lambda'_S$  was calculated via observations.

In F. Pinto's Elements of Optical Navigation, there is a way to convert cartesian coordinates to ecliptic coordinates such as done in the Direct Problem case (10). Now, same equations should be used with its familiar ones.

$$x = r \cos \beta \cos \lambda \quad (38)$$

$$y = r \cos \beta \sin \lambda \quad (39)$$

$$z = r \sin \beta \quad (40)$$

So, the Inverse Problem is solved now. If you would like to test it, try to use Earth observer cases at first and then the error between the calculated ones and Horizons' data could be obtained.

## 4.5 How to Choose Asteroids?

Optical space navigation requires pre-determined beacon celestial objects which are then utilized for trigonometric calculations to find the location of the spacecraft. As a proof of concept, our team intends to use the pictures of asteroids that are taken from earth to find the location of the camera located on earth. To achieve this we have to filter the suitable asteroids as some asteroids are too small, too faint or too far to photograph. Luckily, there are reputable asteroid databases for us to choose from to filter, such as The Minor Planet Physical Properties Catalogue (MP3C), maintained by Observatoire de la Côte d'Azur, which will be the source of this example. Link for the MP3C is available in the Appendix 8.

As can be seen from the "Documentation" tab of the website of MP3C, this database has many parameters that are specific to each asteroid. We can use these parameters to our advantage to filter out unwanted asteroids to focus on gathering a list of asteroids. We shall arbitrarily yet scientifically reduce the number of asteroids from hundreds of thousands to only a handful of suitable ones.

### **Asteroid Diameter:**

As a first step to filtering the viable asteroids to use for optical navigation, we must address the elephant in the room: size of the asteroid. Asteroids vastly differ in size, some are only a few meters in diameter while some are as big as dwarf planets. According to MP3C database, diameter (D) is measured in km.

We shall only consider asteroids that are larger than 20 kilometers in diameter to eliminate smaller bodies. This filtering reduces our minor body count which is the same as our output's row count from 1,169,173 to 2,293.

### **Semimajor Axis:**

Following similar procedure, Semi-major axis (a) is measured in AU, denotes the heliocentric semi-major axis distance of the asteroid's orbit. We have to use this filter because many asteroids are located in the Kuiper Belt as opposed to the Asteroid Belt. Asteroid Belt lies between Mars and Jupiter, which is perfect for our mission. Additionally, while it may be possible, Kuiper Belt objects are much much further away, existing mainly beyond Neptune, making them unreasonable to use as beacons. Thus, Our celestial object should lie between Mars and Jupiter.

We shall limit the orbit of the minor bodies between 1.5 and 5 AU. This may be filtered down more if it is found that the asteroids located in the inner part of the belt are much easier to work with.

This filtering reduced our output's row count from 2,293 to 2,162.

### **Eccentricity:**

Eccentricity ( $e$ ) is an orbital property that determines how elliptic the orbit is. It can only range from 0 to 1 as any value above 1 would not define an orbit while 0 is a perfect circle.

We shall limit our eccentricity to 0.5 to filter out highly elliptic objects. These objects are not the best for our use case as they could have a comet-like orbit such as 3552 Don Quixote. This only eliminates a few asteroids.

### **Inclination:**

Inclination of an orbit refers to how tilted the orbit plane is compared to the reference plane. If an orbit is too inclined, such as Pallas, the asteroid may end up being out of the frame of the photograph. Thus, making that asteroid inconsistent.

We shall limit our inclination to be less than 20 degrees.

### **Absolute Magnitude:**

Absolute Magnitude is the measurement of how visible an object in the sky is if it were to be 10 parsecs away. This will be the step where we get rid of many asteroids as we cannot do any navigation if the asteroid is too faint to be picked up by our equipment. For astrophotography, even though apparent magnitude is what matters at the end of the day, absolute magnitude gives us a very good idea if our apparent magnitude would be below 13, which is the limit of our equipment.

Objects with absolute magnitude values lower than 7.4 tend to have apparent magnitudes better than 13. We shall use this value for now as it eliminates the asteroid count down to a handful, 55 in total (See Appendix 8). This can be increased on the following studies, as suggested before.

## 5 Results

Tests are done by using the methods which are explained above. Those tests are performed with respect to mainly two different parameters:

- Date - Time:

2037 January 13, 03:18:17 UT

2037 April 13, 03:18:17 UT

2037 July 13, 03:18:17 UT

2037 October 13, 03:18:17 UT

2037 November 13, 03:18:17 UT

- Observer Location:

Uppsala Astronomical Observatory, Uppsala, Sweden

Mount Wilson Observatory, Pasadena, California, United States

Collegio Romano Observatory, Rome, Italy

Urla, Izmir, Türkiye

Dates above are chosen in order to see the effect of the change in the Earth's reference frame. Different locations on the Earth are chosen in order to see how it affects the calculations. Note that, the refraction model on Horizons is chosen as "no refraction (airless)" when tests are performed.

### 5.1 Direct Problem Results

#### 5.1.1 Uppsala

In this case, the observer location is chosen as Uppsala, Sweden. To solve the direct problem, as stated above (See 4.3), the heliocentric cartesian coordinates of the observer should be known.

However, for the Earth observers, which we mean that the observer is on the surface of the Earth, it is not possible to determine its heliocentric cartesian position directly. Hence, it is possible to do it by using the following method.

## Requesting The Heliocentric Cartesian Coordinates of the Observatories

- When Observing the Heliocentric Cartesian Coordinates:
  - Ephemeris Type: Vector Table
  - Target Body: Sun
  - Observer Location: → Choose a method → Type: Observatories
  - Time: Time - Type: UT
  - Table Settings: Output Quantities: 1 with XYZ uncertainties
  - ... Reference Frame: [ICRF](#)
  - ... Reference Plane: ecliptic x-y plane derived from reference frame
  - ... (standard obliquity, inertial)
  - ... Vector Correction: Apparent States
  - ... CSV Format

With this method, it is possible to directly get the “inverse” heliocentric cartesian coordinates of the observer. For example if the “inverse” heliocentric cartesian coordinates of the observer is given as (X,Y,Z), the heliocentric cartesian coordinates of the observer is (-X,-Y,-Z). This approach will be always used on the following tests.

### Example for Direct Problem

By knowing the definition of the direct problem and the methodology explained above will be followed to solve it. The question is, what are the [topocentric](#) celestial coordinates of the asteroid (1) Ceres when it is observed from the Uppsala Observatory on the epoch 2037 April 13, 03:18:17 UT?

The Heliocentric Coordinates of the Uppsala Observatory from Horizons:

$$X_{Upp} = -1.380477801635898 \times 10^8 \text{ km,}$$

$$Y_{Upp} = -5.866790214272577 \times 10^7 \text{ km,}$$

$$Z_{Upp} = 1.243088926630840 \times 10^4 \text{ km,}$$

The distance of Uppsala from the Sun is:

$$r = 3.91785 \times 10^8$$

The Heliocentric Coordinates of the Uppsala Observatory from Horizons:

$$X_{Ceres} = -3.57411 \times 10^8 \text{ km,}$$



$$Y_{Ceres} = -1.48438 \times 10^8 \text{ km},$$

$$Z_{Ceres} = 6.09816 \times 10^8 \text{ km},$$

The distance of (1) Ceres from the Sun is:

$$r_P = 2.44737 \times 10^8$$

Hence the **heliocentric** ecliptic coordinates of the Uppsala Observatory with choosing the right quadrants Mathematica Language can be found as:

$$\lambda = 203.025^\circ,$$

$$\beta = 0.00474834^\circ,$$

Let's calculate the error caused by different reference frames used in Horizons for different cases (See 4.3.1).

Importing topocentric ecliptic coordinates of the Sun:

$$\lambda'_{S,Hor} = 23.5412222^\circ,$$

$$\lambda'_S = 23.0246^\circ,$$

$$\beta'_S = -0.00474834^\circ$$

$$\text{error} = 0.516575^\circ$$

Hence the **heliocentric** ecliptic coordinates of the asteroid (1) Ceres with choosing the right quadrants Mathematica Language can be found as:

$$\lambda_P = 202.554^\circ,$$

$$\beta_P = 8.95454^\circ,$$

As the required parameters to calculate **topocentric** ecliptic coordinates of (1) Ceres are known, they can be calculated as (From Eq 19 and 21):

$$\lambda'_P = 202.773^\circ,$$

$$\beta'_P = 14.4255^\circ$$

The topocentric celestial coordinates can be given by 23 and 25:

$$\alpha = 13.7592 \text{ h},$$

$$\delta = 4.55692^\circ$$

Errors for both **topocentric** ecliptic coordinates and topocentric celestial coordinates:

$$e_{\lambda'_P} = 0.00561557^\circ,$$

$$e_{\beta'_P} = -0.00247184^\circ,$$

$$e_\alpha = 0.000248232 \text{ h},$$

$$e_\delta = -0.00157496^\circ$$

As explained in Roy (3.1), the accuracy will increase as the number of beacons increased.

Solving an example, the results for 55 chosen asteroids for different locations and dates are figurized below. Yellow disk represents the Sun in the center and blue disk is the Earth, others are asteroids.

2037 January 13, 03:18:17 UT

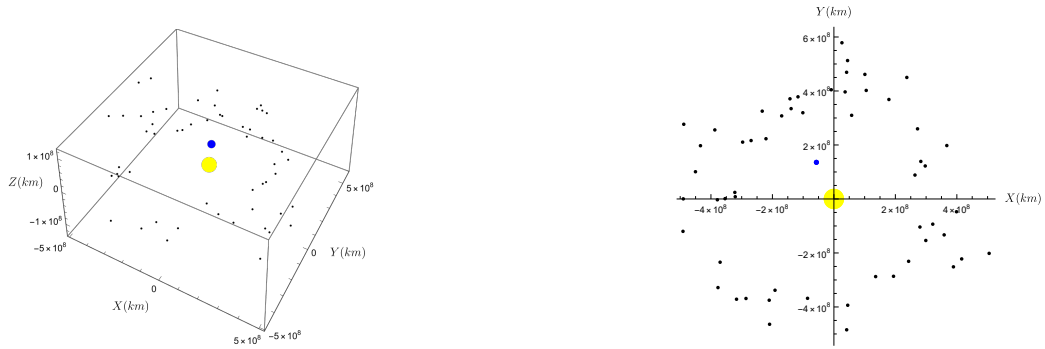


Figure 17: 3D Model of the System Created with Mathematica and Its XY Plane



Figure 18: The Distribution of Error in  $\lambda'_p$  of Asteroids with Respect to Their Distance From the Sun, Error of the RF is not included on the left - included on the right.

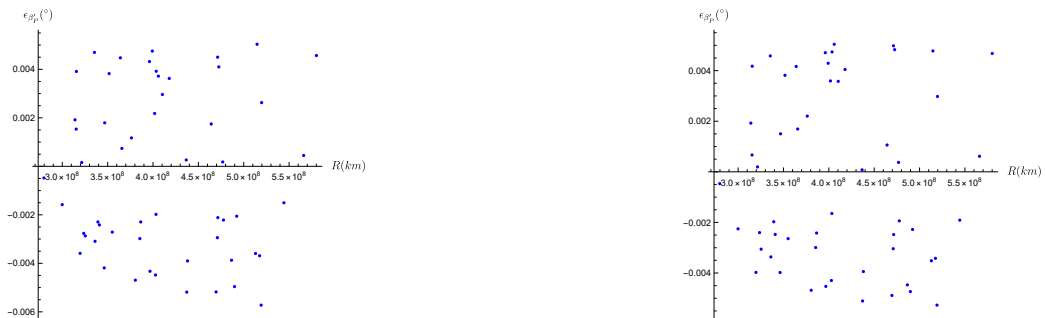


Figure 19: The Distribution of Error in  $\beta'_p$  of Asteroids with Respect to Their Distance From the Sun, Error of the RF is not included on the left - included on the right.

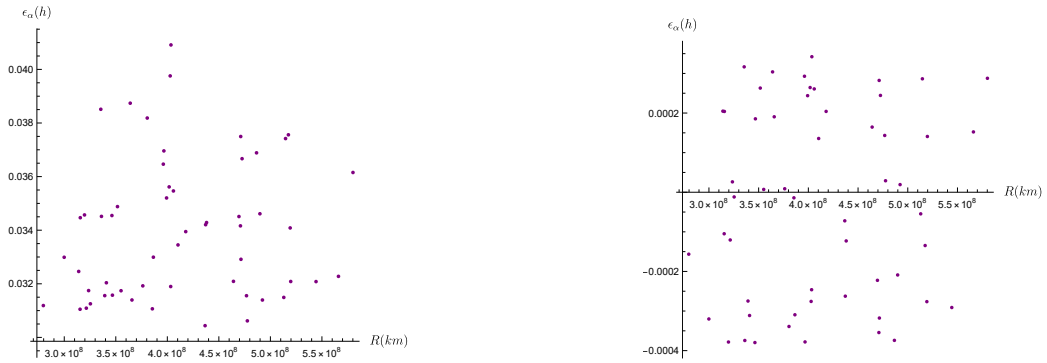


Figure 20: The Distribution of  $\alpha$  Error of Asteroids with Respect to Their Distance From the Sun, Error of the RF is not included on the left - included on the right.

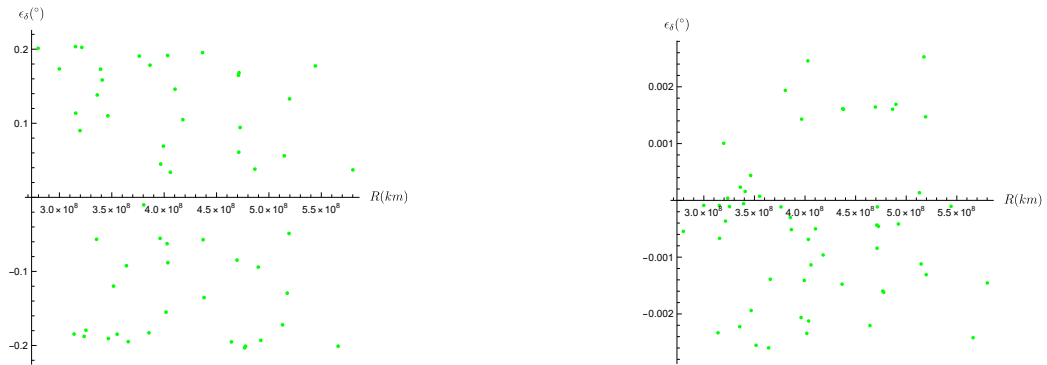


Figure 21: The Distribution of  $\delta$  Error of Asteroids with Respect to Their Distance From the Sun, Error of the RF is not included on the left - included on the right.

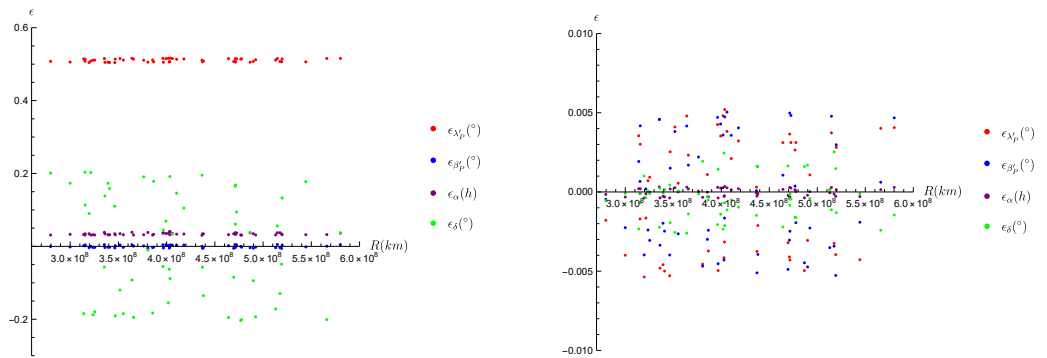


Figure 22: The Distribution of all Errors of Asteroids with Respect to Their Distance From the Sun, Error of the RF is not included on the left - included on the right.

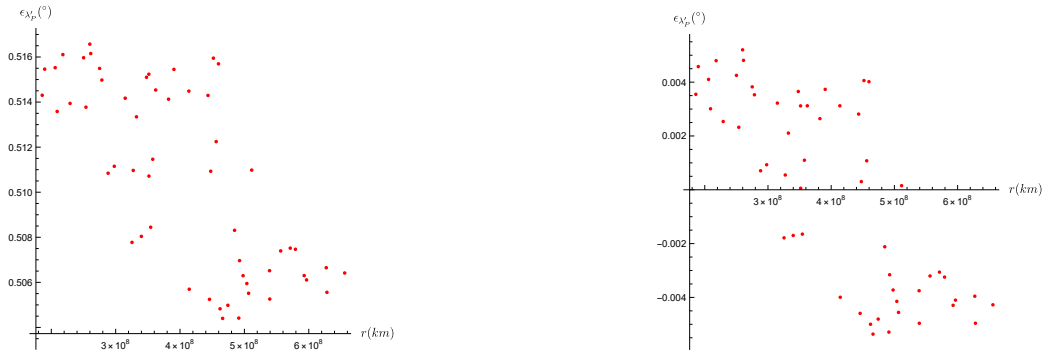


Figure 23: The Distribution of Error in  $\lambda'_p$  of Asteroids with Respect to Their Distance From the Earth, Error of the RF is not included on the left - included on the right.

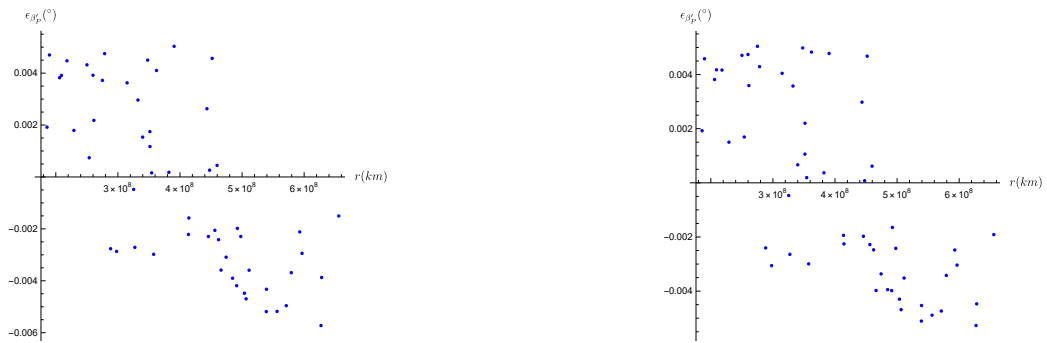


Figure 24: The Distribution of Error in  $\beta'_p$  of Asteroids with Respect to Their Distance From the Earth, Error of the RF is not included on the left - included on the right.

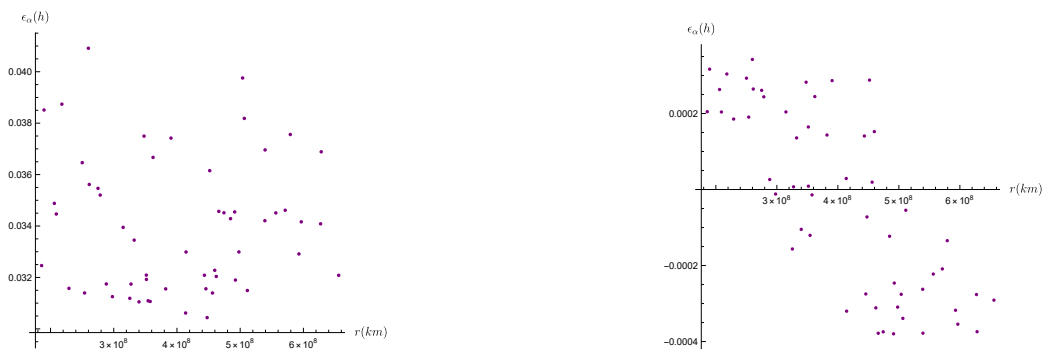


Figure 25: The Distribution of Error in  $\alpha$  of Asteroids with Respect to Their Distance From the Earth, Error of the RF is not included on the left - included on the right.

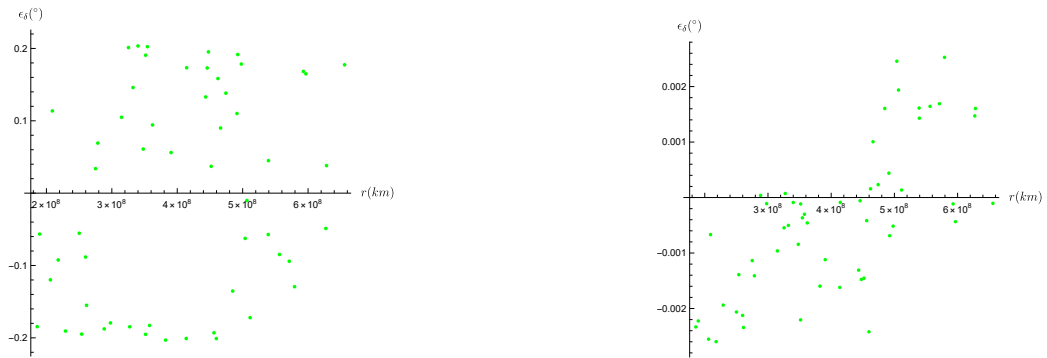


Figure 26: The Distribution of Error in  $\delta$  of Asteroids with Respect to Their Distance From the Earth, Error of the RF is not included on the left - included on the right.

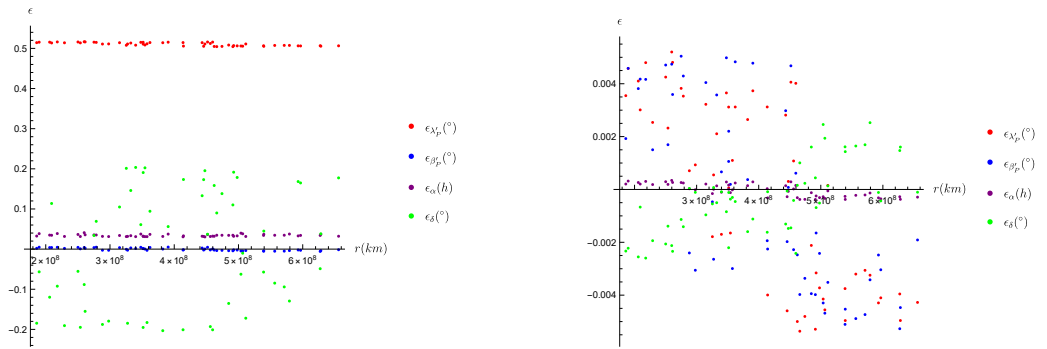


Figure 27: The Distribution of All Errors of Asteroids with Respect to Their Distance From the Earth, Error of the RF is not included on the left - included on the right.

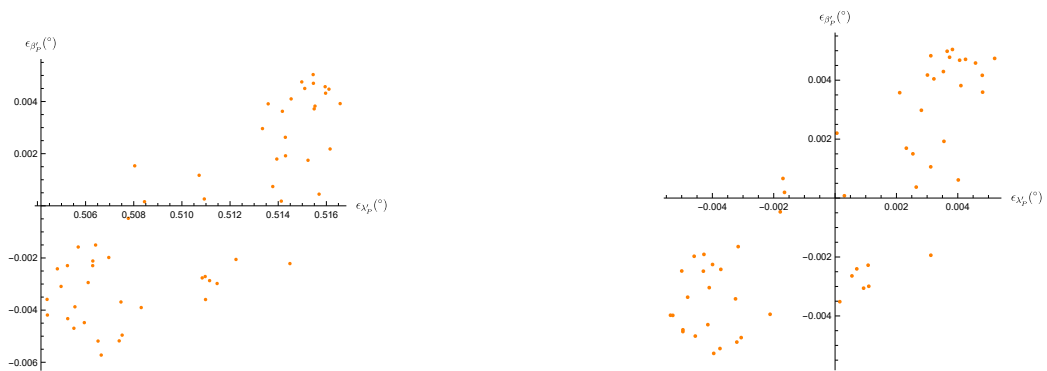


Figure 28: The Distribution of Error in  $\lambda'_p$  vs  $\beta'_p$ , Error of the RF is not included on the left - included on the right.

2037 April 13, 03:18:17 UT



Figure 29: 3D Model of the System Created with Mathematica and Its XY Plane



Figure 30: The Distribution of  $\lambda'_p$  Error of Asteroids with Respect to Their Distance From the Sun, Error of the RF is not included on the left - included on the right.



Figure 31: The Distribution of  $\beta'_p$  Error of Asteroids with Respect to Their Distance From the Sun, Error of the RF is not included on the left - included on the right.

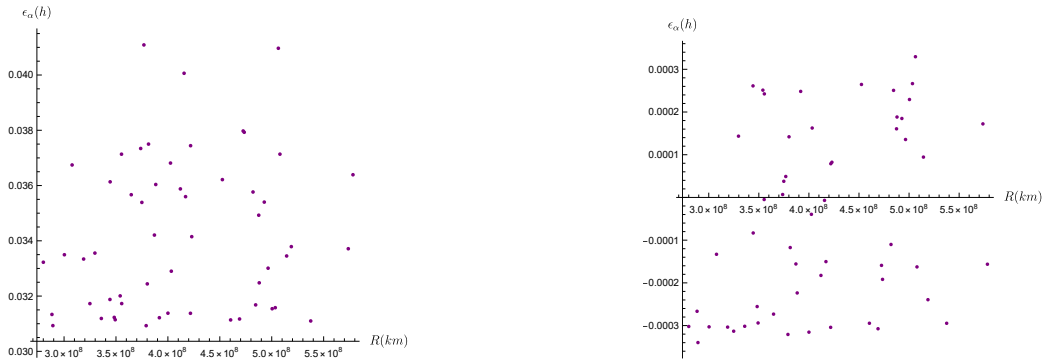


Figure 32: The Distribution of  $\alpha$  Error of Asteroids with Respect to Their Distance From the Sun, Error of the RF is not included on the left - included on the right.

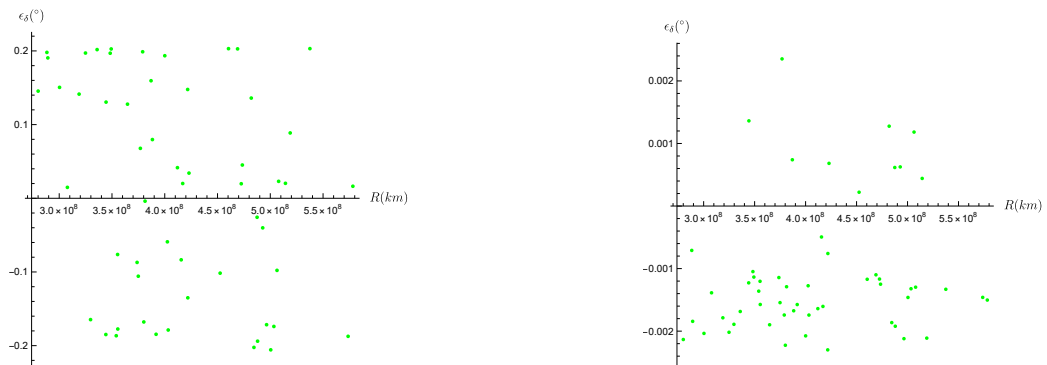


Figure 33: The Error of  $\delta$  of Asteroids with Respect to Their Distance From the Sun, Error of the RF is not included on the left - included on the right.

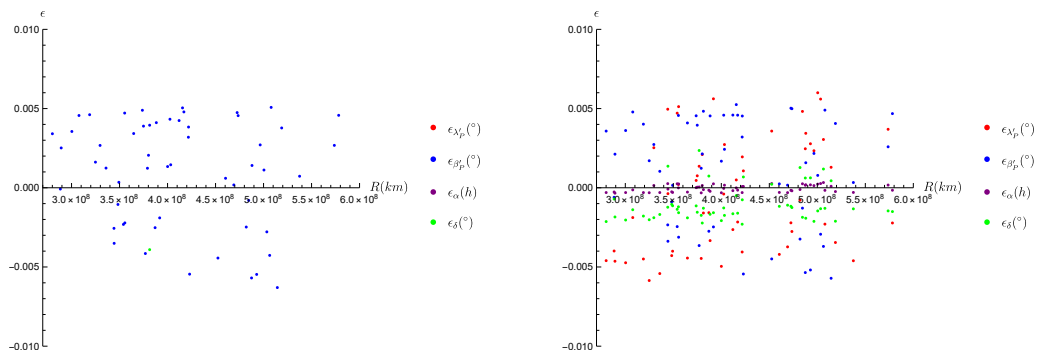


Figure 34: The Distribution of all Errors of Asteroids with Respect to Their Distance From the Sun, Error of the RF is not included on the left - included on the right.



Figure 35: The Error Distribution of  $\lambda'_p$  of Asteroids with Respect to Their Distance From the Spacecraft, Error of the RF is not included on the left - included on the right.

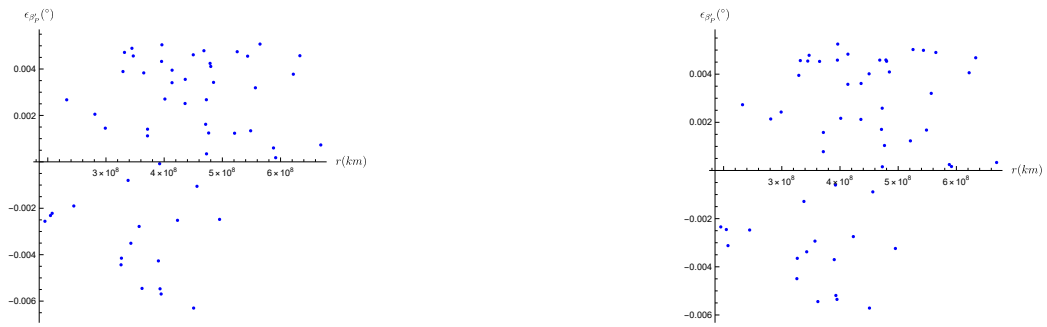


Figure 36: The Error Distribution of  $\beta'_p$  of Asteroids with Respect to Their Distance From the Spacecraft, Error of the RF is not included on the left - included on the right.



Figure 37: The Error Distribution of  $\alpha$  of Asteroids with Respect to Their Distance From the Spacecraft, Error of the RF is not included on the left - included on the right.





Figure 38: The Error Distribution of  $\delta$  of Asteroids with Respect to Their Distance From the Spacecraft, Error of the RF is not included on the left - included on the right.

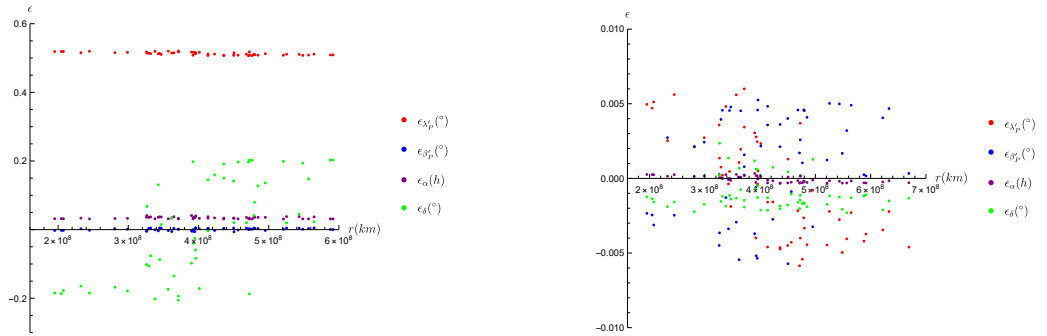


Figure 39: The Distribution of all errors of Asteroids with Respect to Their Distance From the Spacecraft, Error of the RF is not included on the left - included on the right.



Figure 40: The Error Distribution of  $\lambda'_p$  vs  $\beta'_p$ , Error of the RF is not included on the left - included on the right.

2037 July 13, 03:18:17 UT

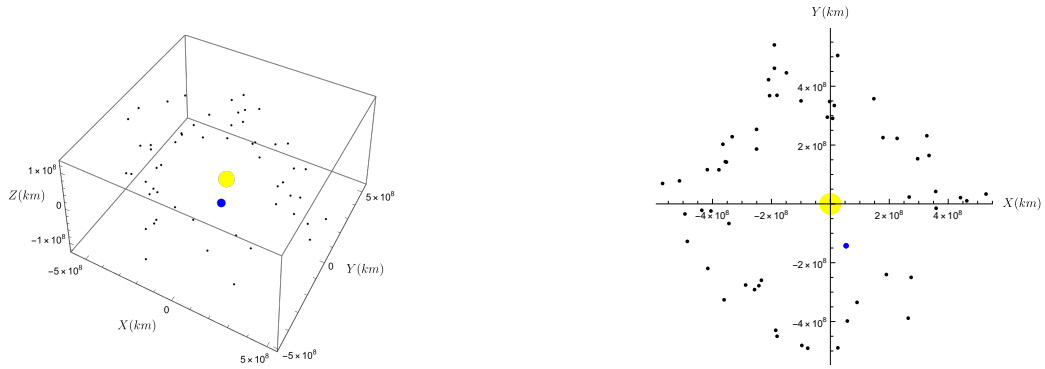


Figure 41: 3D Model of the System Created with Mathematica and Its XY Plane

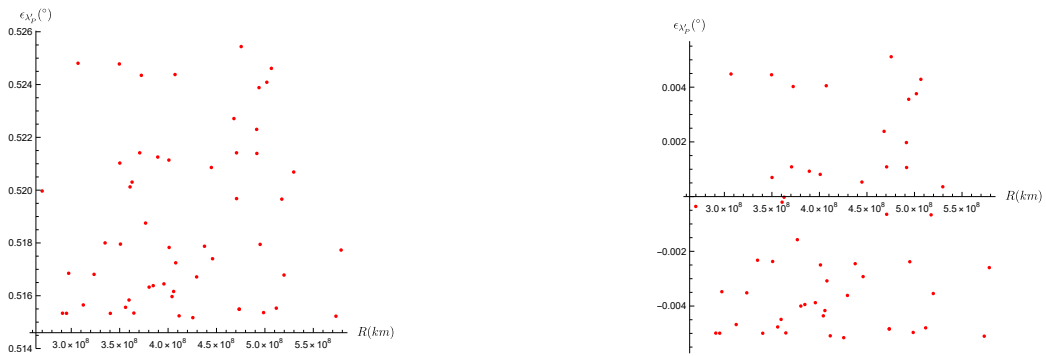


Figure 42: The Distribution of  $\lambda'_p$  Error of Asteroids with Respect to Their Distance From the Sun, Error of the RF is not included on the left - included on the right.

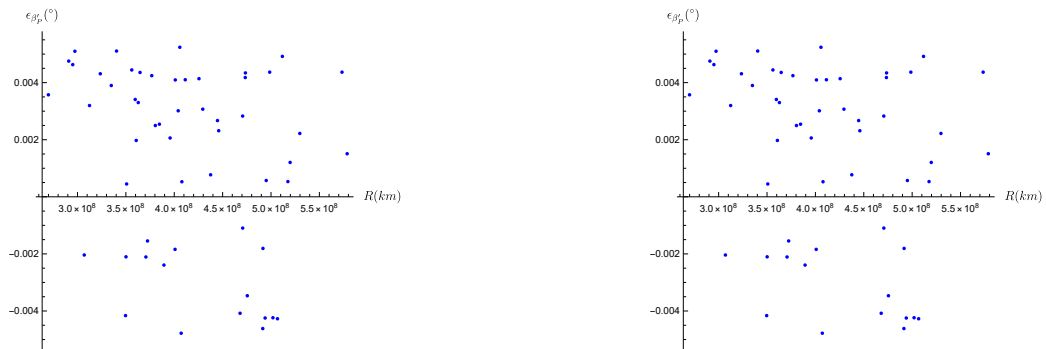


Figure 43: The Distribution of  $\beta'_p$  Error of Asteroids with Respect to Their Distance From the Sun, Error of the RF is not included on the left - included on the right.

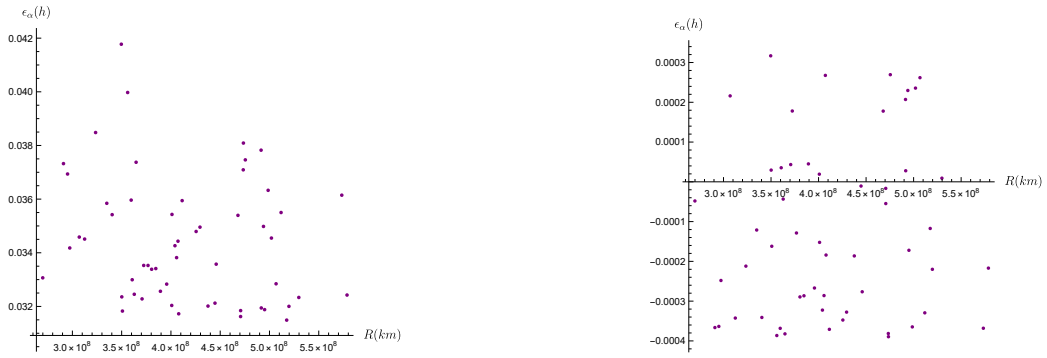


Figure 44: The Distribution of  $\alpha$  Error of Asteroids with Respect to Their Distance From the Sun, Error of the RF is not included on the left - included on the right.

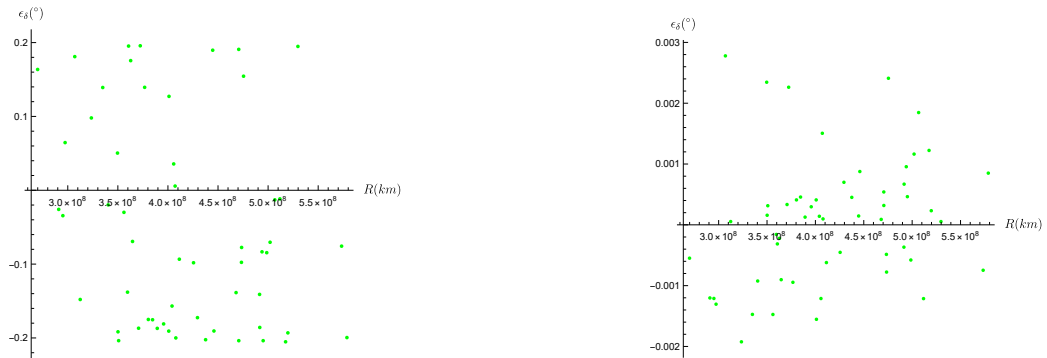


Figure 45: The Distribution of  $\delta$  Error of Asteroids with Respect to Their Distance From the Sun, Error of the RF is not included on the left - included on the right.

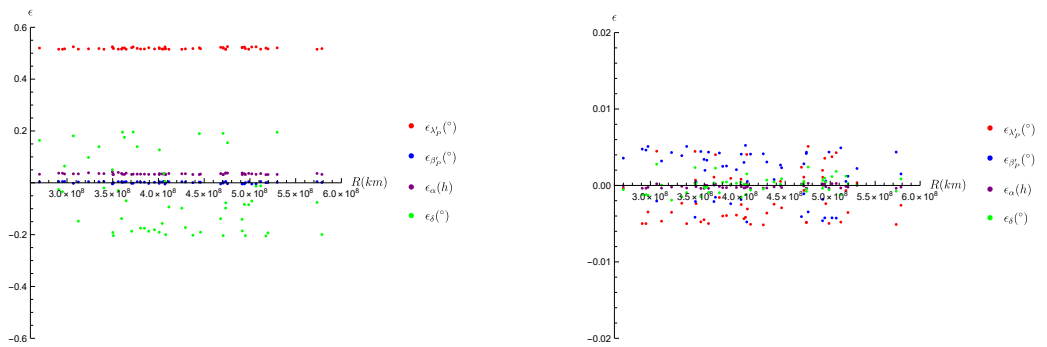


Figure 46: The Distribution of all Errors of Asteroids with Respect to Their Distance From the Sun, Error of the RF is not included on the left - included on the right.



Figure 47: The Error Distribution of  $\lambda'_p$  of Asteroids with Respect to Their Distance From the Spacecraft, Error of the RF is not included on the left - included on the right.

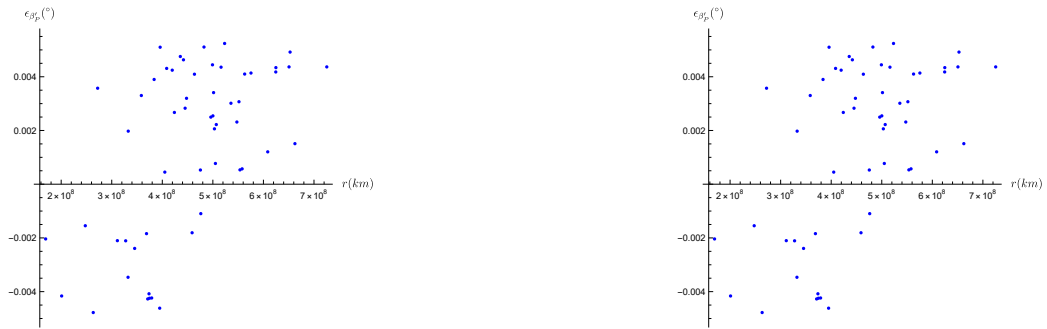


Figure 48: The Error Distribution of  $\beta'_p$  of Asteroids with Respect to Their Distance From the Spacecraft, Error of the RF is not included on the left - included on the right.

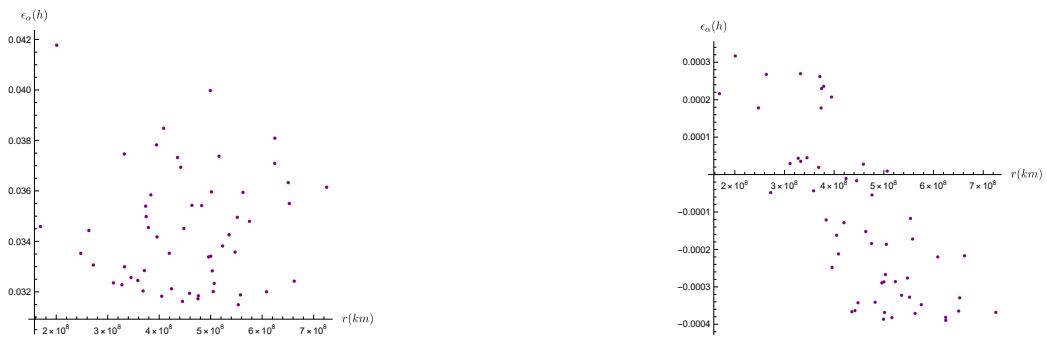


Figure 49: The Error Distribution of  $\alpha$  of Asteroids with Respect to Their Distance From the Spacecraft, Error of the RF is not included on the left - included on the right.

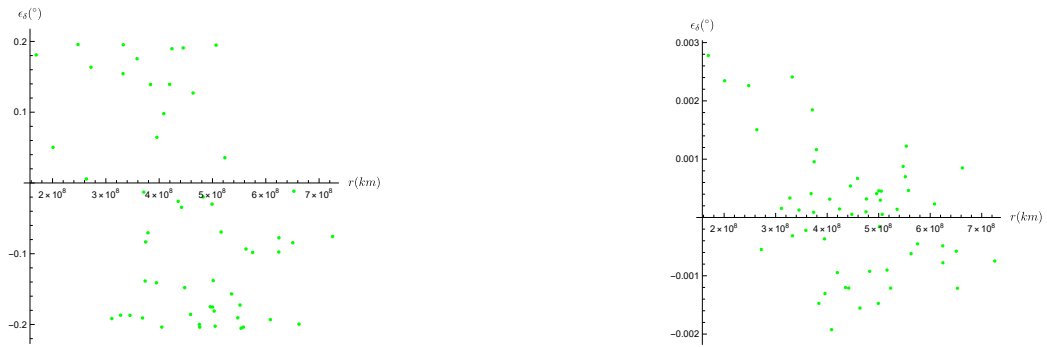


Figure 50: The Error Distribution of  $\delta$  of Asteroids with Respect to Their Distance From the Spacecraft, Error of the RF is not included on the left - included on the right.

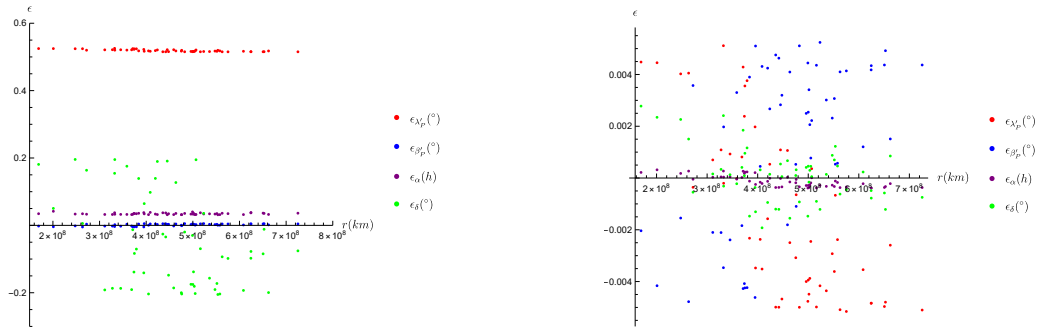


Figure 51: The Distribution of All Errors of Asteroids with Respect to Their Distance From the Spacecraft, Error of the RF is not included on the left - included on the right.



Figure 52: The Error Distribution of  $\lambda'_p$  vs  $\beta'_p$ , Error of the RF is not included on the left - included on the right.

2037 October 13, 03:18:17 UT

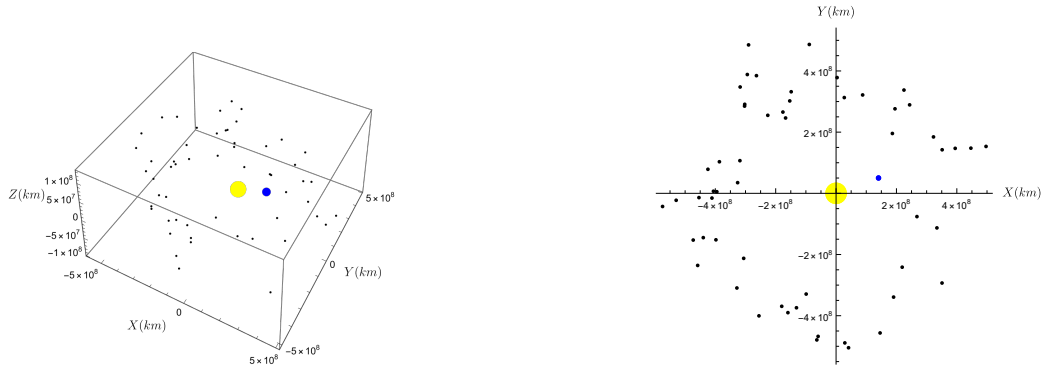


Figure 53: 3D Model of the System Created with Mathematica and Its XY Plane

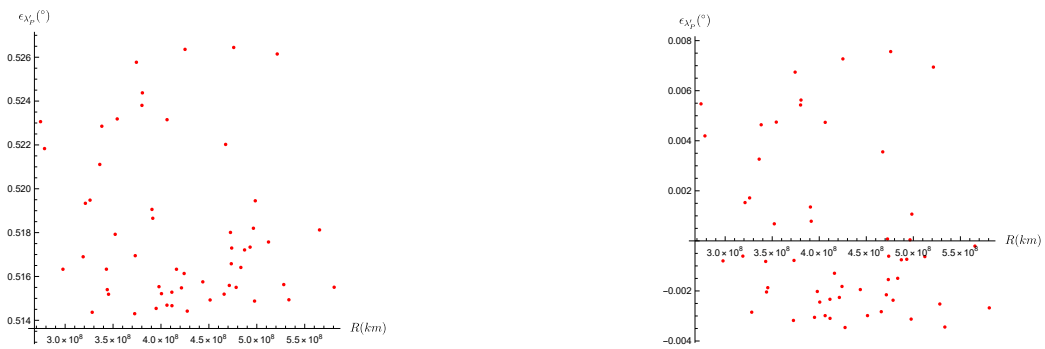


Figure 54: The Distribution of  $\lambda'_p$  Error of Asteroids with Respect to Their Distance From the Sun, Error of the RF is not included on the left - included on the right.



Figure 55: The Distribution of  $\beta'_p$  Error of Asteroids with Respect to Their Distance From the Sun, Error of the RF is not included on the left - included on the right.

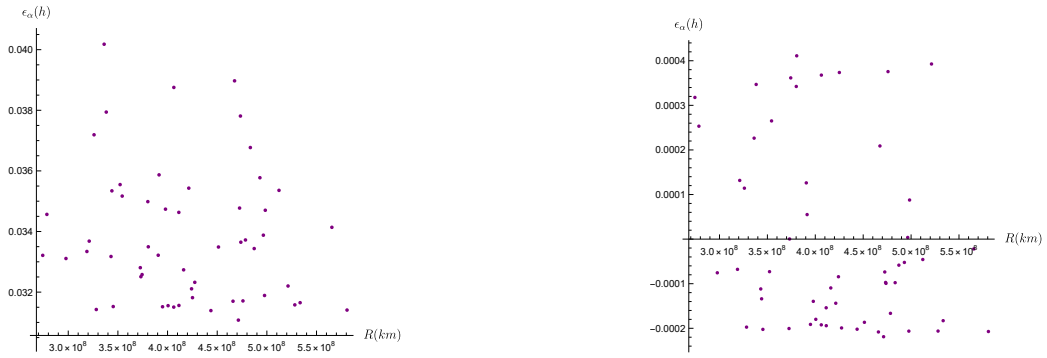


Figure 56: The Distribution of  $\alpha$  Error of Asteroids with Respect to Their Distance From the Sun, Error of the RF is not included on the left - included on the right.

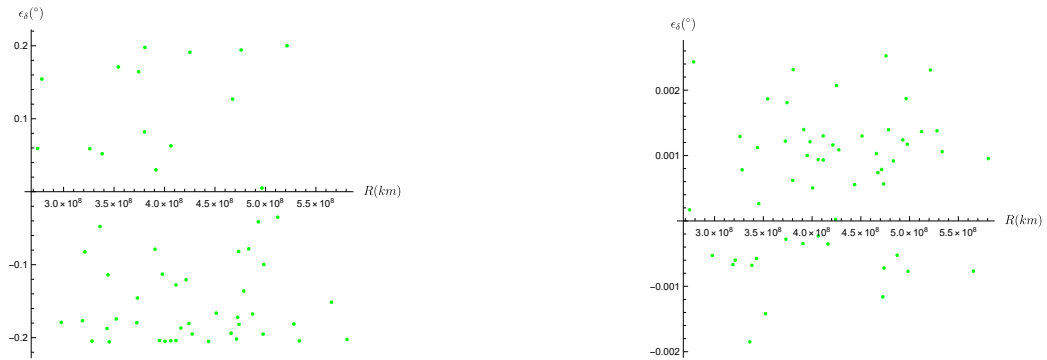


Figure 57: The Distribution of  $\delta$  Error of Asteroids with Respect to Their Distance From the Sun, Error of the RF is not included on the left - included on the right.

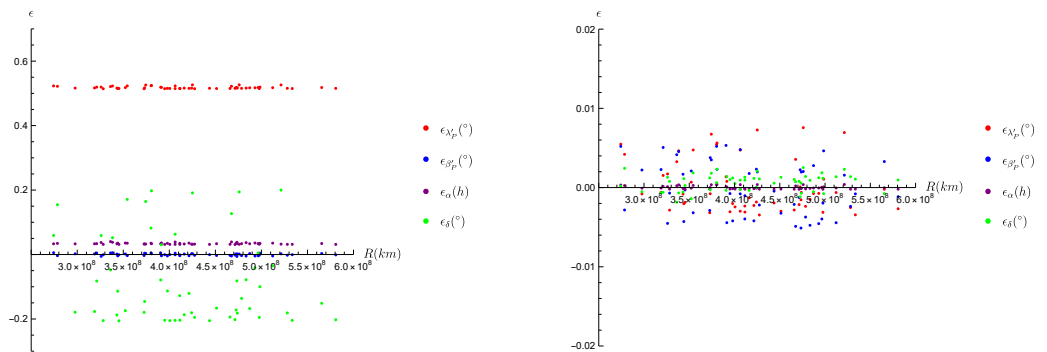


Figure 58: The Distribution of all Errors of Asteroids with Respect to Their Distance From the Sun, Error of the RF is not included on the left - included on the right.

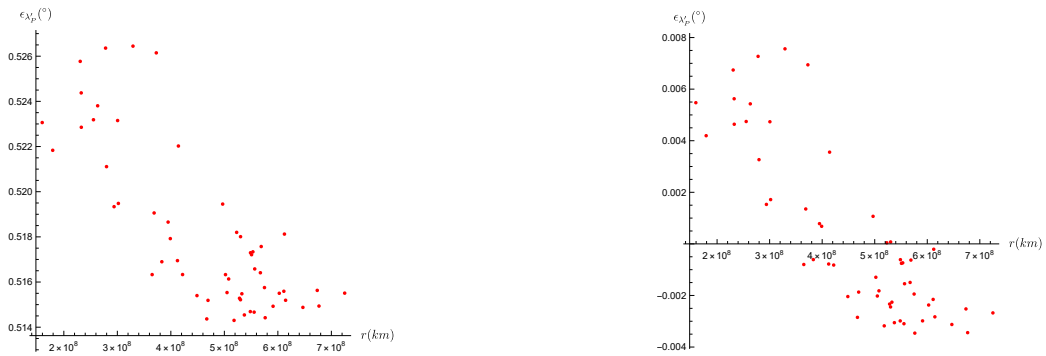


Figure 59: The Error Distribution of  $\lambda'_p$  of Asteroids with Respect to Their Distance From the Spacecraft, Error of the **RF** is not included on the left - included on the right.



Figure 60: The Distribution of Error in  $\beta'_p$  of Asteroids with Respect to Their Distance From the Spacecraft, Error of the **RF** is not included on the left - included on the right.

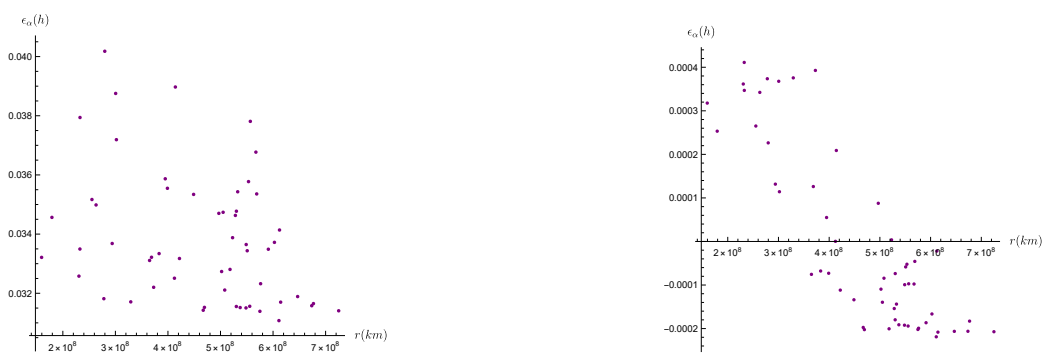


Figure 61: The Distribution of Error in  $\alpha$  of Asteroids with Respect to Their Distance From the Spacecraft, Error of the **RF** is not included on the left - included on the right.



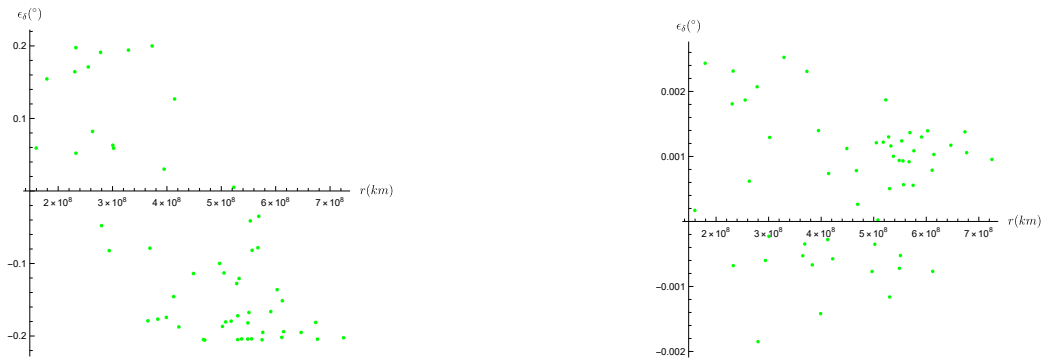


Figure 62: The Distribution of Error in  $\delta$  of Asteroids with Respect to Their Distance From the Spacecraft, Error of the RF is not included on the left - included on the right.

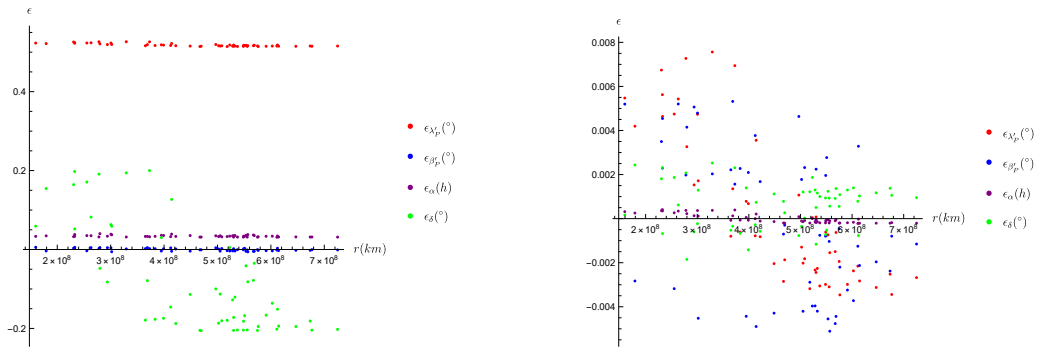


Figure 63: The Distribution of All Errors of Asteroids with Respect to Their Distance From the Spacecraft, Error of the RF is not included on the left - included on the right.



Figure 64: The Error Distribution of  $\lambda'_p$  vs  $\beta'_p$ , Error of the RF is not included on the left - included on the right.

2037 November 13, 03:18:17 UT

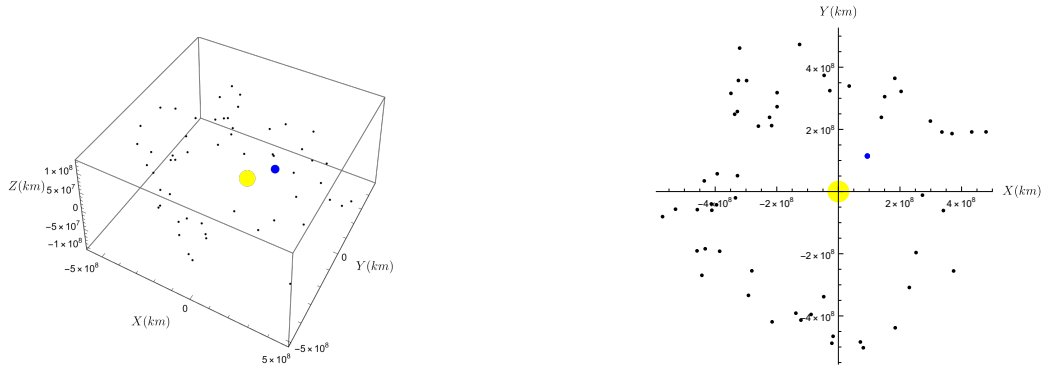


Figure 65: 3D Model of the System Created with Mathematica and Its XY Plane

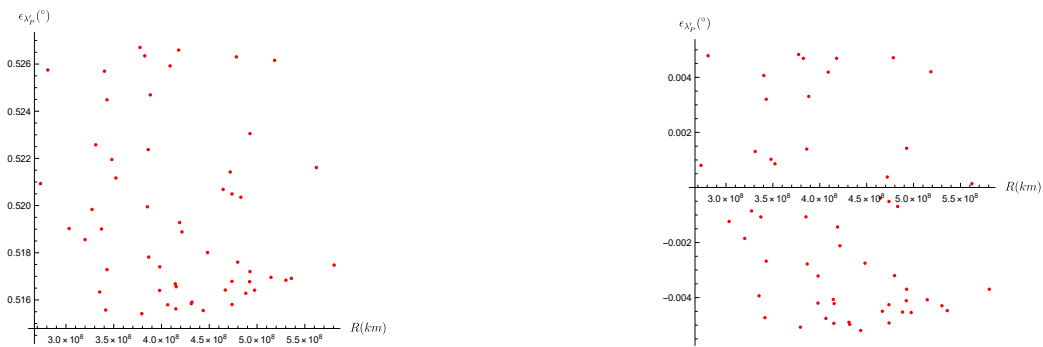


Figure 66: The Distribution of  $\lambda'_p$  Error of Asteroids with Respect to Their Distance From the Sun, Error of the **RF** is not included on the left - included on the right.



Figure 67: The Distribution of  $\beta'_p$  Error of Asteroids with Respect to Their Distance From the Sun, Error of the **RF** is not included on the left - included on the right.

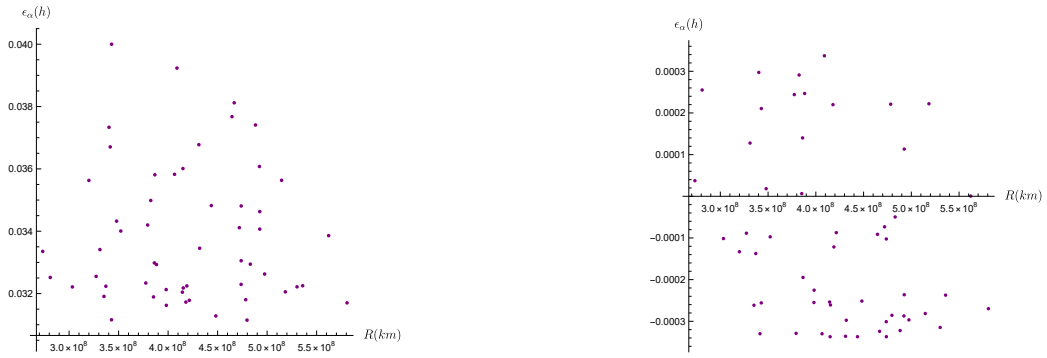


Figure 68: The Distribution of  $\alpha$  Error of Asteroids with Respect to Their Distance From the Sun, Error of the RF is not included on the left - included on the right.

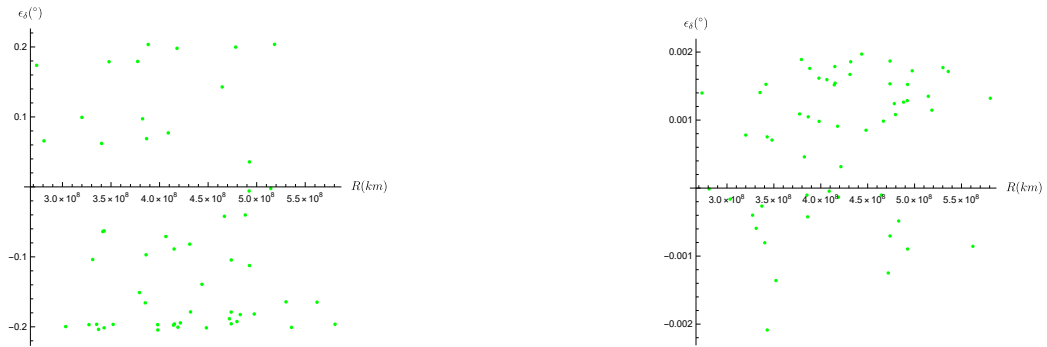


Figure 69: The Distribution of  $\delta$  Error of Asteroids with Respect to Their Distance From the Sun, Error of the RF is not included on the left - included on the right.

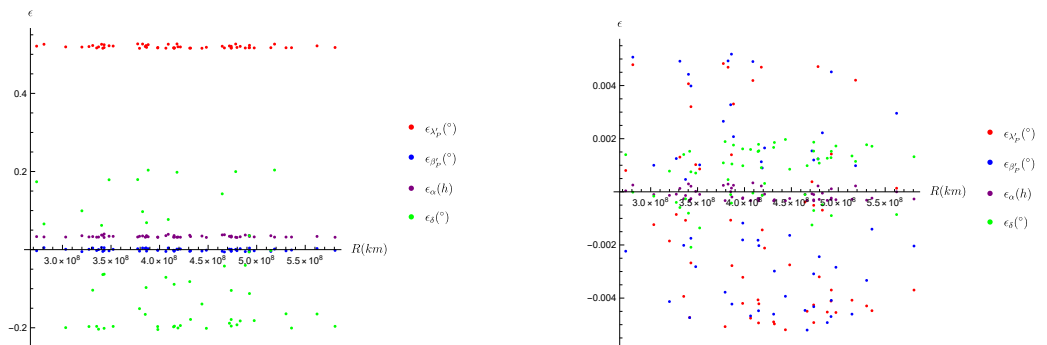


Figure 70: The Distribution of all Errors of Asteroids with Respect to Their Distance From the Sun, Error of the RF is not included on the left - included on the right.

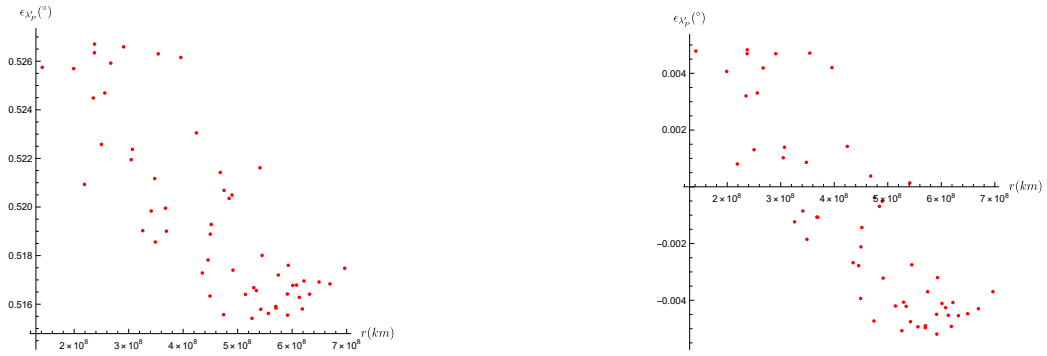


Figure 71: The Error Distribution of  $\lambda'_p$  of Asteroids with Respect to Their Distance From the Spacecraft, Error of the RF is not included on the left - included on the right.

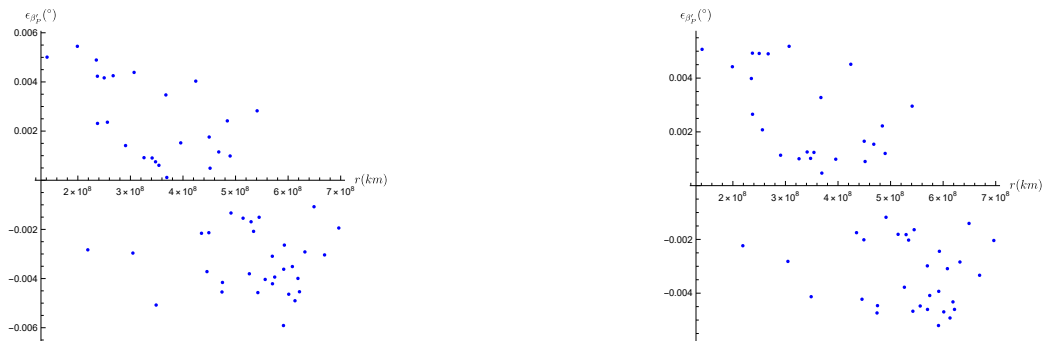


Figure 72: The Distribution of Error in  $\beta'_p$  of Asteroids with Respect to Their Distance From the Spacecraft, Error of the RF is not included on the left - included on the right.

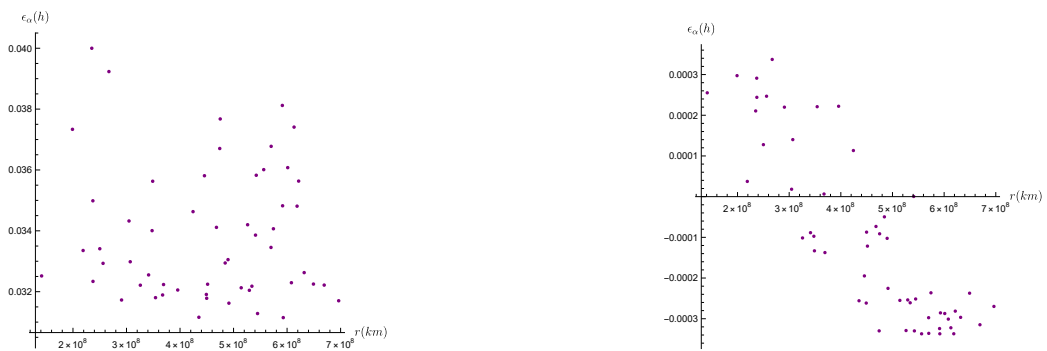


Figure 73: The Distribution of Error in  $\alpha$  of Asteroids with Respect to Their Distance From the Spacecraft, Error of the RF is not included on the left - included on the right.

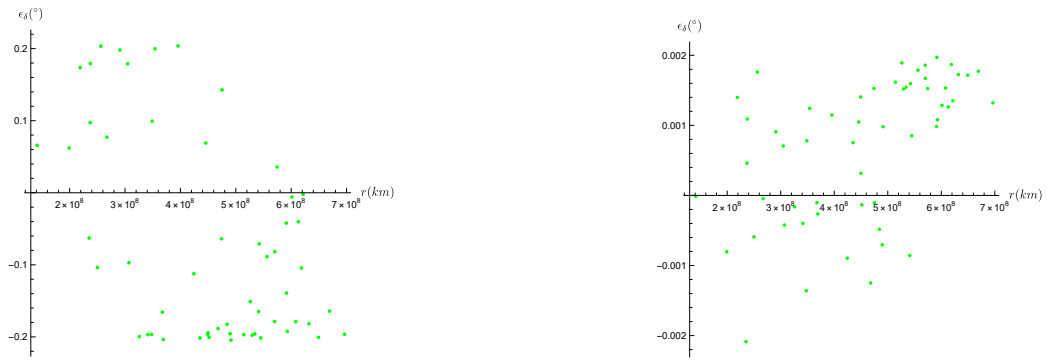


Figure 74: The Distribution of Error in  $\delta$  of Asteroids with Respect to Their Distance From the Spacecraft, Error of the RF is not included on the left - included on the right.

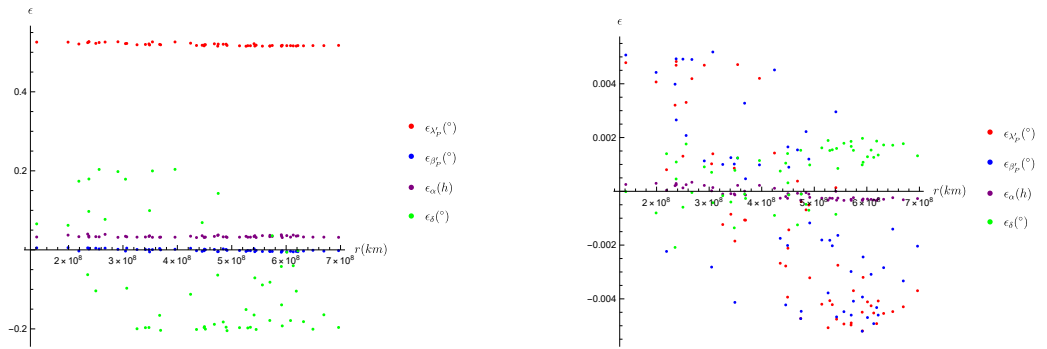


Figure 75: The Distribution of All Errors of Asteroids with Respect to Their Distance From the Spacecraft, Error of the RF is not included on the left - included on the right.

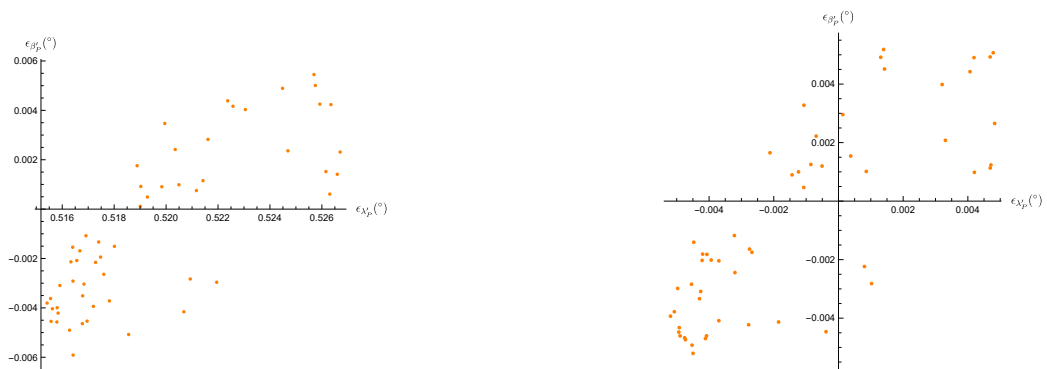


Figure 76: The Error Distribution of  $\lambda'_p$  vs  $\beta'_p$ , Error of the RF is not included on the left - included on the right.

### 5.1.2 Urla

2037 January 13, 03:18:17 UT

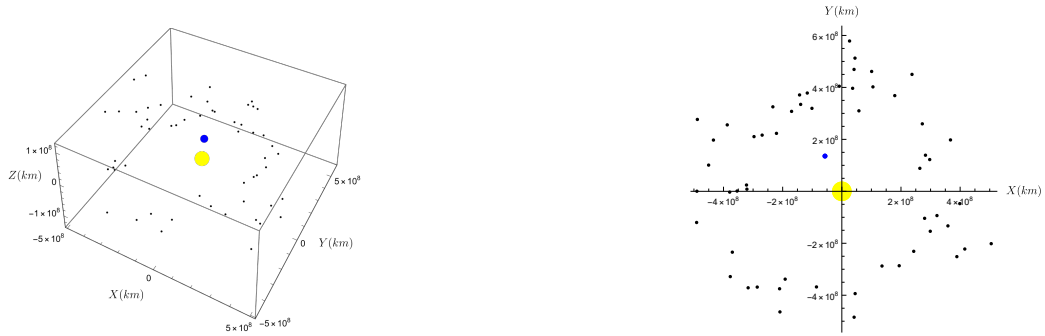


Figure 77: 3D Model of the System Created with Mathematica and Its XY Plane



Figure 78: The Distribution of Error in  $\lambda'_p$  of Asteroids with Respect to Their Distance From the Sun, Error of the RF is not included on the left - included on the right.



Figure 79: The Distribution of  $\beta'_p$  Error of Asteroids with Respect to Their Distance From the Sun, Error of the RF is not included on the left - included on the right.

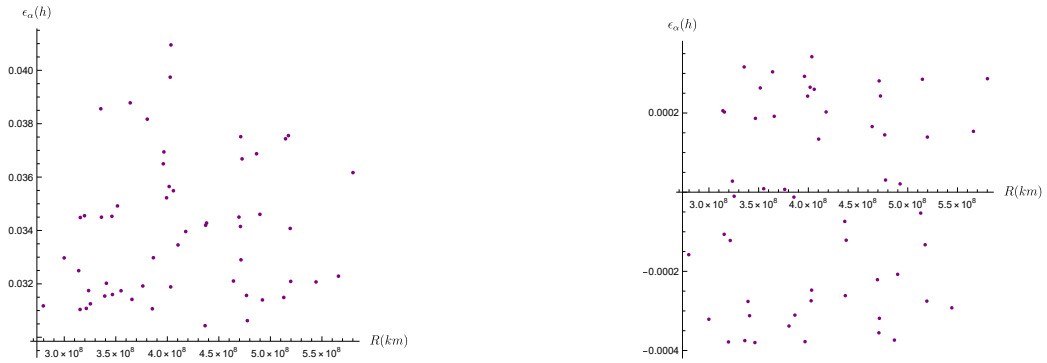


Figure 80: The Distribution of  $\alpha$  Error of Asteroids with Respect to Their Distance From the Sun, Error of the RF is not included on the left - included on the right.

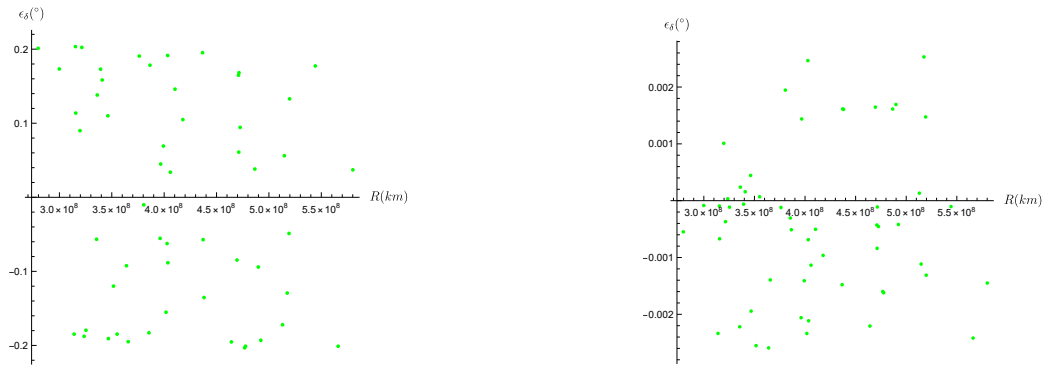


Figure 81: The Distribution of  $\delta$  Error of Asteroids with Respect to Their Distance From the Sun, Error of the RF is not included on the left - included on the right.

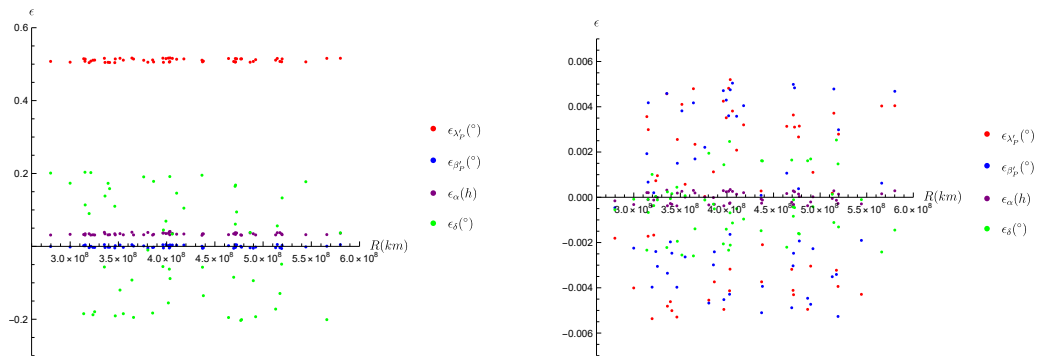


Figure 82: The Distribution of all Errors of Asteroids with Respect to Their Distance From the Sun, Error of the RF is not included on the left - included on the right.

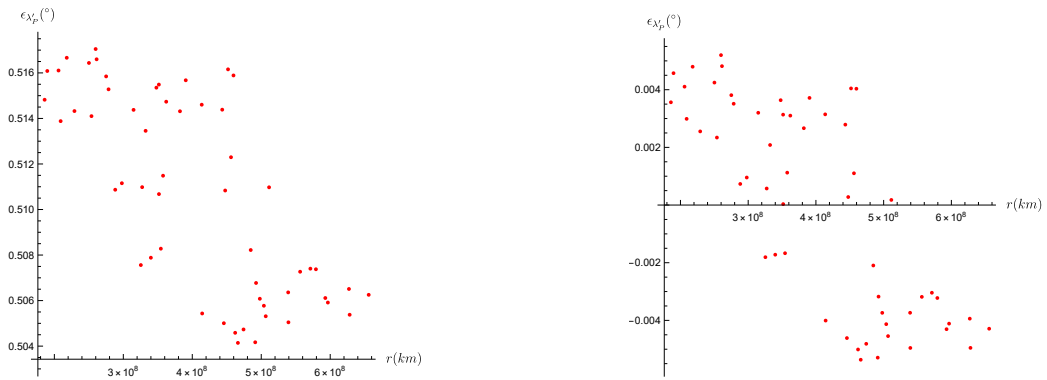


Figure 83: The Error Distribution of  $\lambda'_p$  of Asteroids with Respect to Their Distance From the Earth, Error of the RF is not included on the left - included on the right.

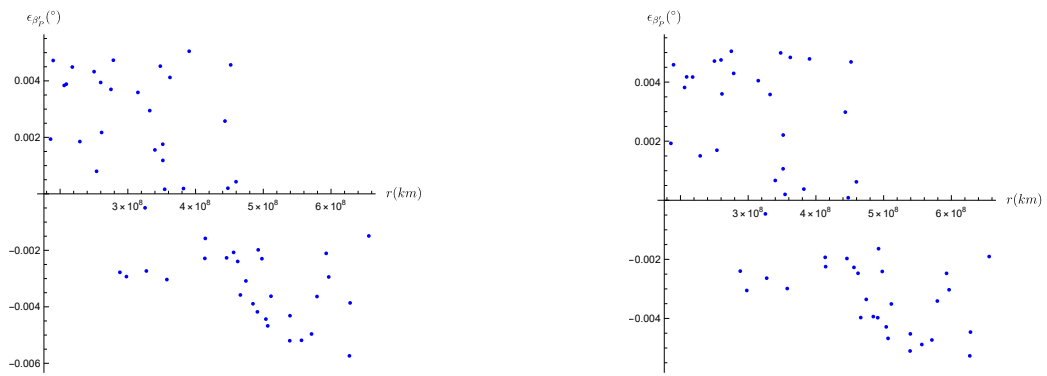


Figure 84: The Error Distribution of  $\beta'_p$  of Asteroids with Respect to Their Distance From the Earth, Error of the RF is not included on the left - included on the right.

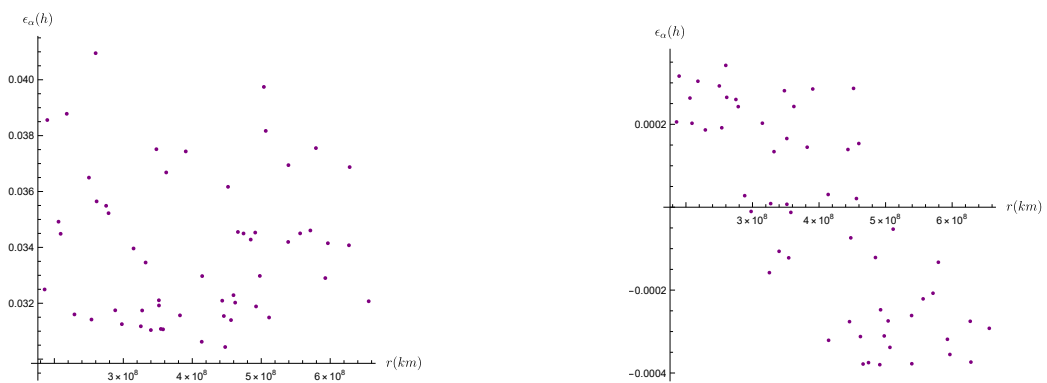


Figure 85: The Error Distribution of  $\alpha$  of Asteroids with Respect to Their Distance From the Earth, Error of the RF is not included on the left - included on the right.



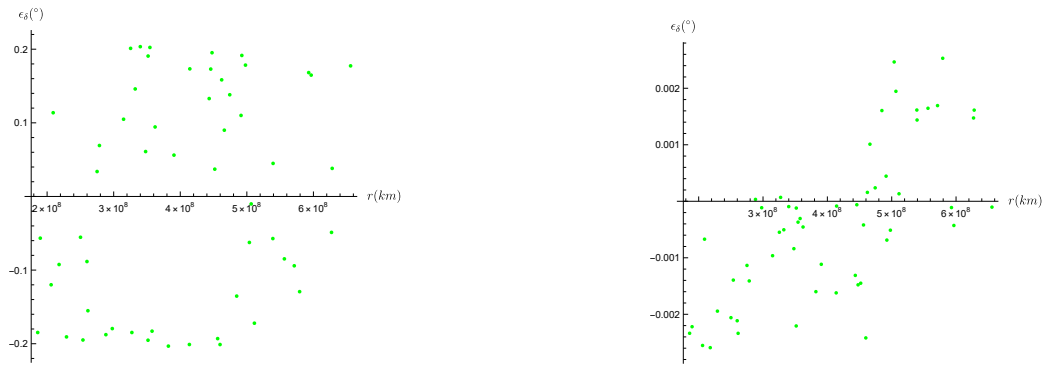


Figure 86: The Error Distribution of  $\delta$  of Asteroids with Respect to Their Distance From the Earth, Error of the RF is not included on the left - included on the right.

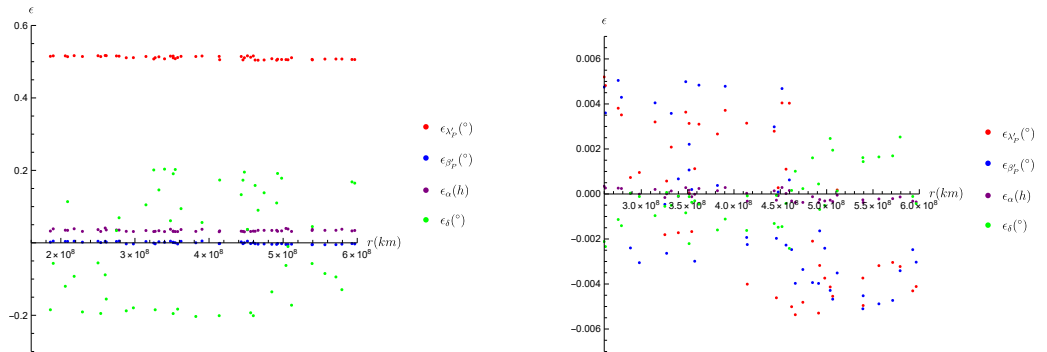


Figure 87: The Distribution of All Errors of Asteroids with Respect to Their Distance From the Earth, Error of the RF is not included on the left - included on the right.

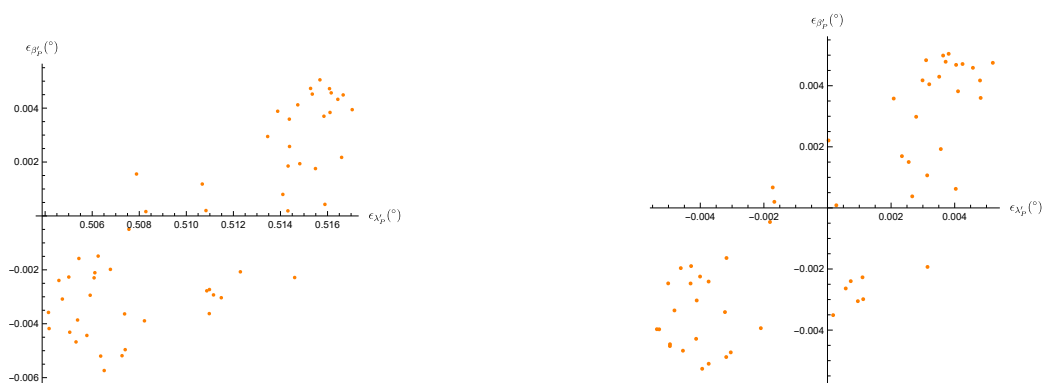


Figure 88: The Error Distribution of  $\lambda'_p$  vs  $\beta'_p$ , Error of the RF is not included on the left - included on the right.

2037 April 13, 03:18:17 UT

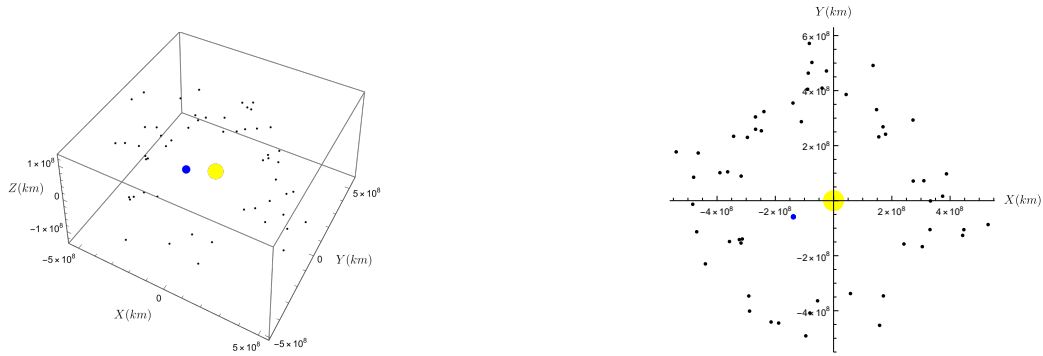


Figure 89: 3D Model of the System Created with Mathematica and Its XY Plane



Figure 90: The Distribution of  $\lambda'_p$  Error of Asteroids with Respect to Their Distance From the Sun, Error of the RF is not included on the left - included on the right.

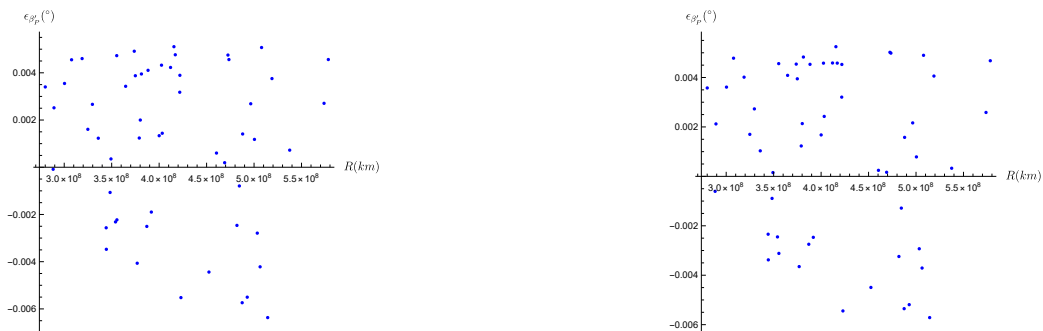


Figure 91: The Distribution of  $\beta'_p$  Error of Asteroids with Respect to Their Distance From the Sun, Error of the RF is not included on the left - included on the right.

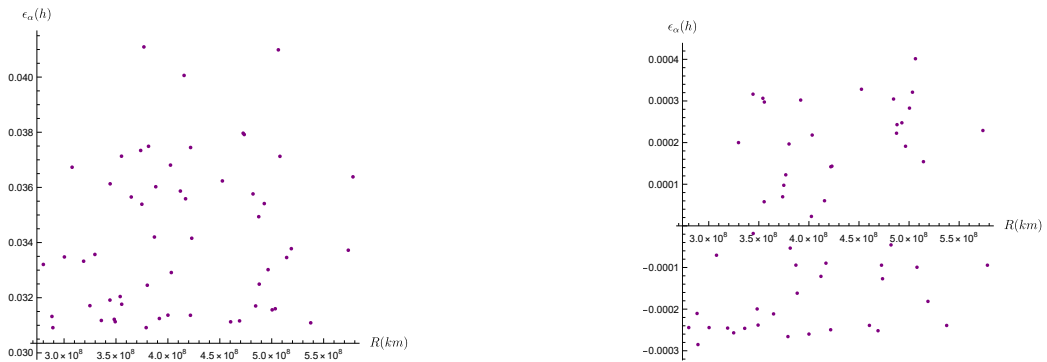


Figure 92: The Distribution of  $\alpha$  Error of Asteroids with Respect to Their Distance From the Sun, Error of the RF is not included on the left - included on the right.

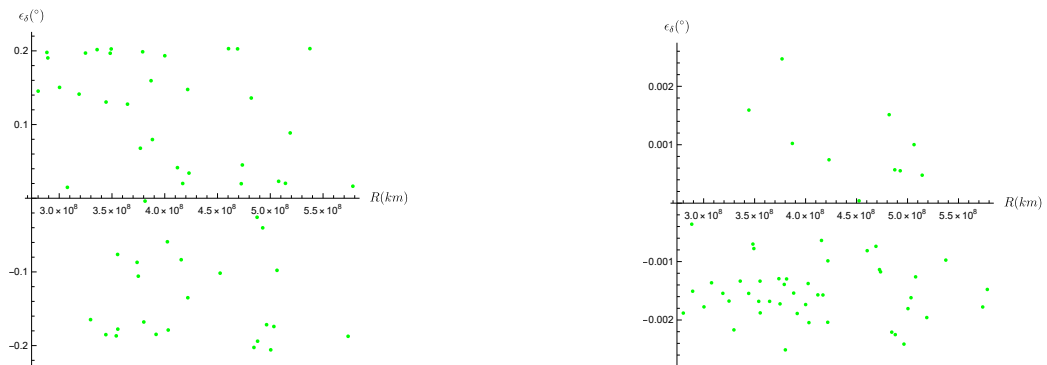


Figure 93: The Distribution of  $\delta$  Error of Asteroids with Respect to Their Distance From the Sun, Error of the RF is not included on the left - included on the right.

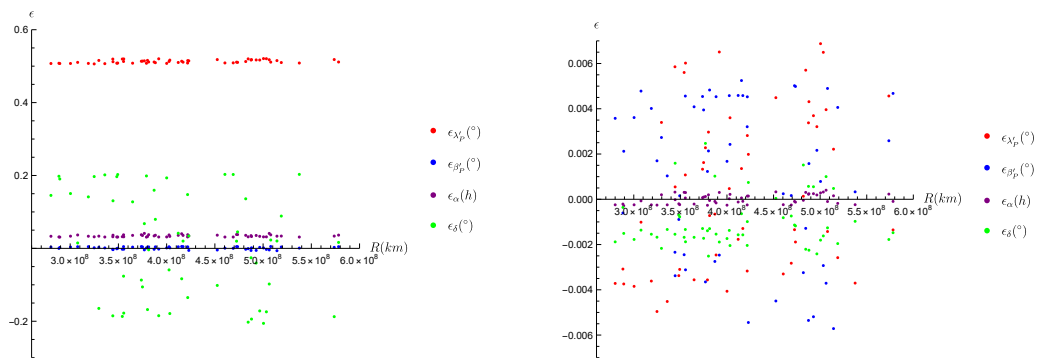


Figure 94: The Distribution of all Errors of Asteroids with Respect to Their Distance From the Sun, Error of the RF is not included on the left - included on the right.



Figure 95: The Error Distribution of  $\lambda'_p$  of Asteroids with Respect to Their Distance From the Spacecraft, Error of the RF is not included on the left - included on the right.



Figure 96: The Error Distribution of  $\beta'_p$  of Asteroids with Respect to Their Distance From the Spacecraft, Error of the RF is not included on the left - included on the right.



Figure 97: The Error Distribution of  $\alpha$  of Asteroids with Respect to Their Distance From the Spacecraft, Error of the RF is not included on the left - included on the right.

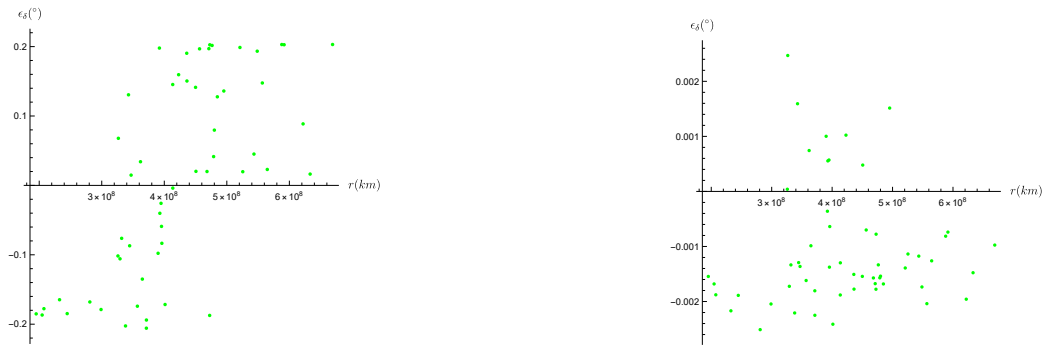


Figure 98: The Error Distribution of  $\delta$  of Asteroids with Respect to Their Distance From the Spacecraft, Error of the RF is not included on the left - included on the right.

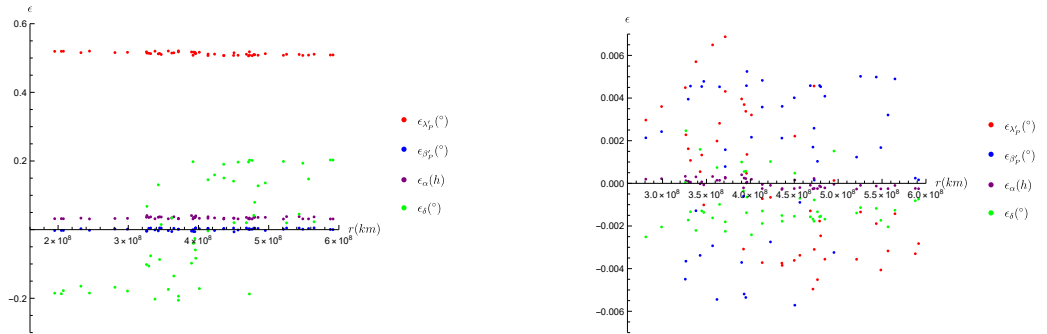


Figure 99: The Distribution of all errors of Asteroids with Respect to Their Distance From the Spacecraft, Error of the RF is not included on the left - included on the right.

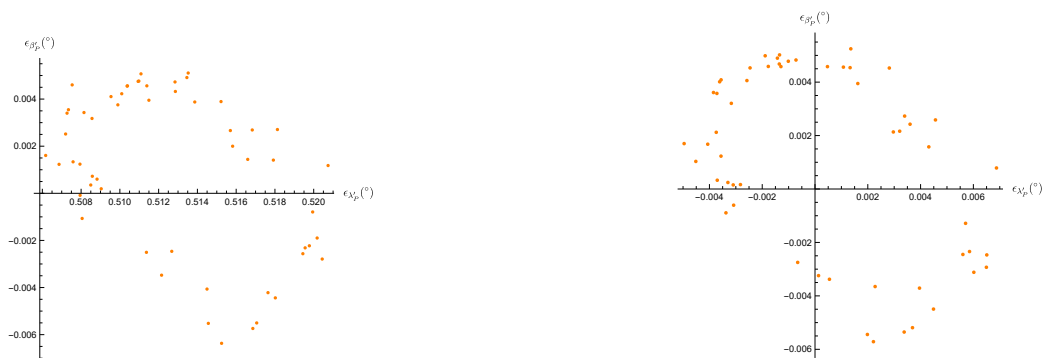


Figure 100: The Error Distribution of  $\lambda'_P$  vs  $\beta'_P$ , Error of the RF is not included on the left - included on the right.

2037 July 13, 03:18:17 UT

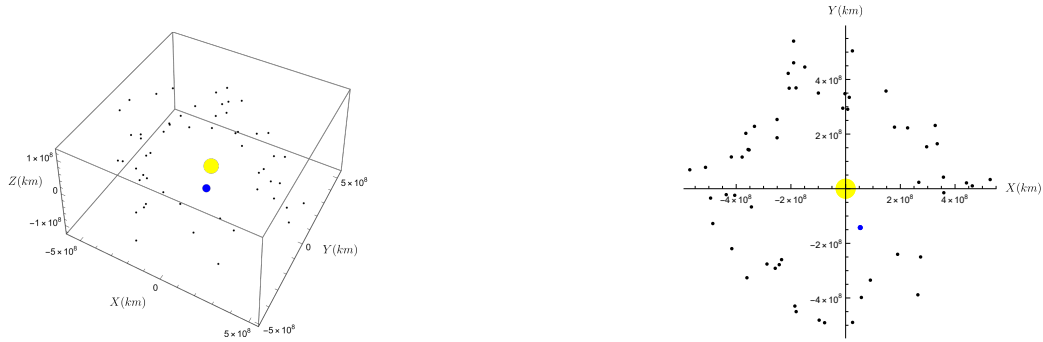


Figure 101: 3D Model of the System Created with Mathematica and Its XY Plane



Figure 102: The Distribution of  $\lambda'_p$  Error of Asteroids with Respect to Their Distance From the Sun, Error of the RF is not included on the left - included on the right.

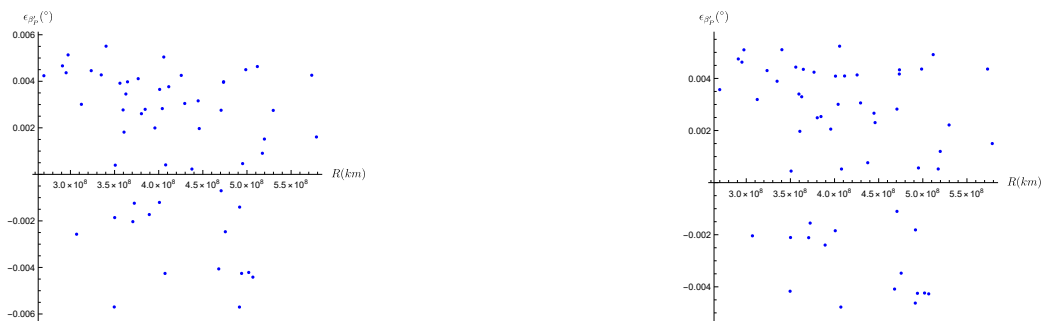


Figure 103: The Distribution of  $\beta'_p$  Error of Asteroids with Respect to Their Distance From the Sun, Error of the RF is not included on the left - included on the right.

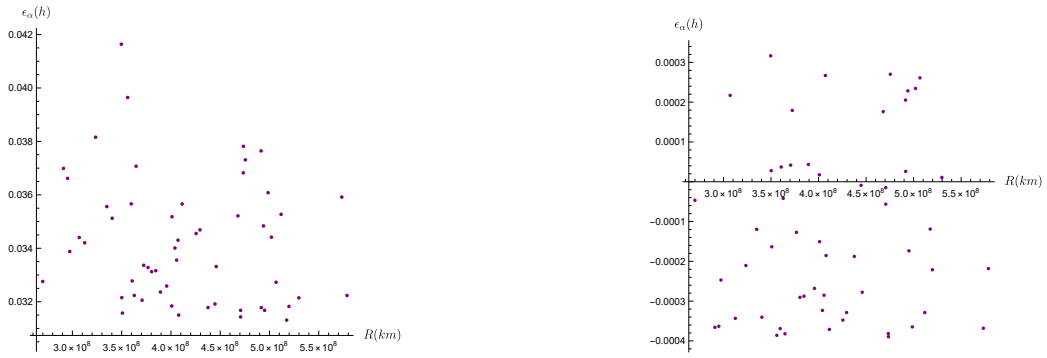


Figure 104: The Distribution of  $\alpha$  Error of Asteroids with Respect to Their Distance From the Sun, Error of the RF is not included on the left - included on the right.

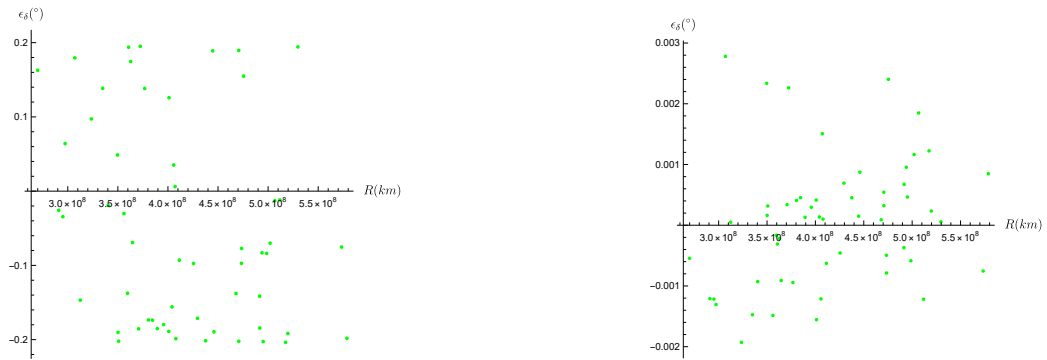


Figure 105: The Distribution of  $\delta$  Error of Asteroids with Respect to Their Distance From the Sun, Error of the RF is not included on the left - included on the right.

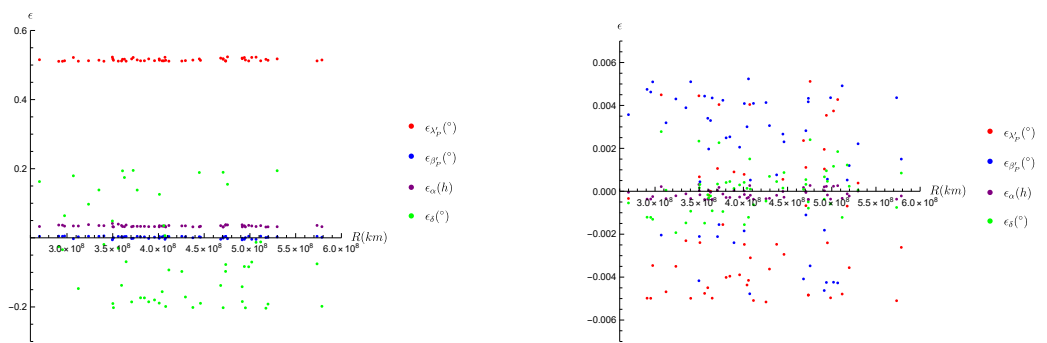


Figure 106: The Distribution of all Errors of Asteroids with Respect to Their Distance From the Sun, Error of the RF is not included on the left - included on the right.



Figure 107: The Error Distribution of  $\lambda'_p$  of Asteroids with Respect to Their Distance From the Spacecraft, Error of the RF is not included on the left - included on the right.



Figure 108: The Error Distribution of  $\beta'_p$  of Asteroids with Respect to Their Distance From the Spacecraft, Error of the RF is not included on the left - included on the right.

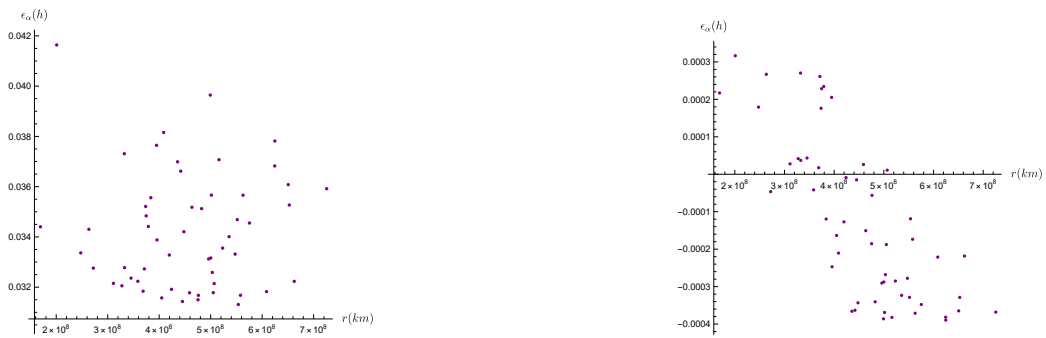


Figure 109: The Error Distribution of  $\alpha$  of Asteroids with Respect to Their Distance From the Spacecraft, Error of the RF is not included on the left - included on the right.



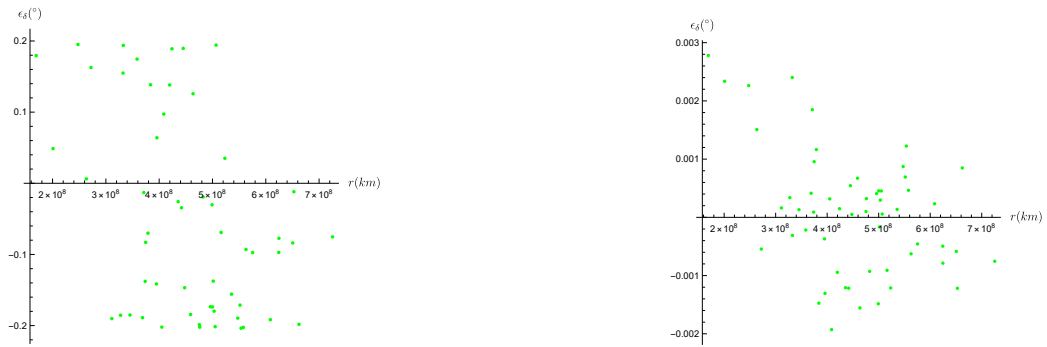


Figure 110: The Error Distribution of  $\delta$  of Asteroids with Respect to Their Distance From the Spacecraft, Error of the RF is not included on the left - included on the right.

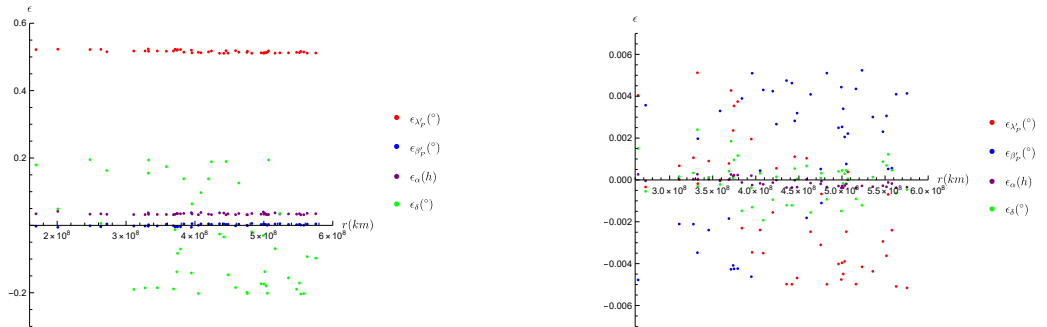


Figure 111: The Distribution of All Errors of Asteroids with Respect to Their Distance From the Spacecraft, Error of the RF is not included on the left - included on the right.

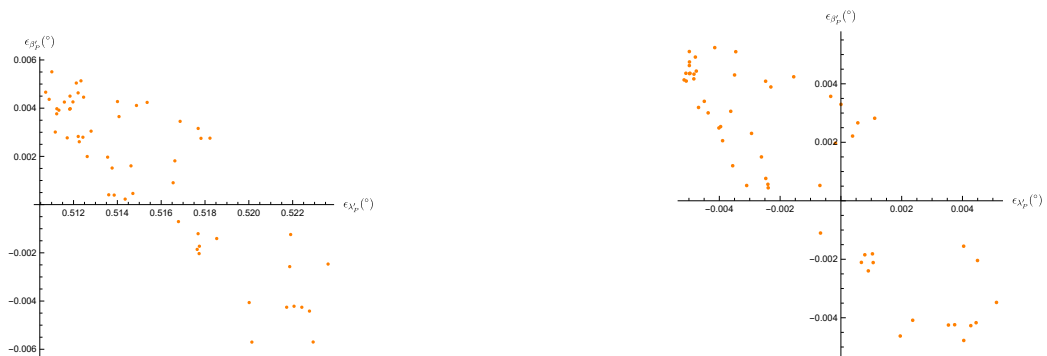


Figure 112: The Error Distribution of  $\lambda'_p$  vs  $\beta'_p$ , Error of the RF is not included on the left - included on the right.

2037 October 13, 03:18:17 UT

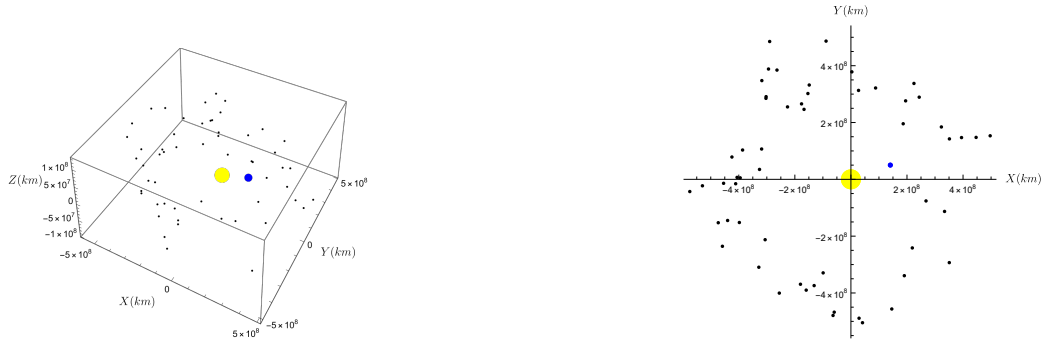


Figure 113: 3D Model of the System Created with Mathematica and Its XY Plane



Figure 114: The Distribution of  $\lambda'_p$  Error of Asteroids with Respect to Their Distance From the Sun, Error of the RF is not included on the left - included on the right.

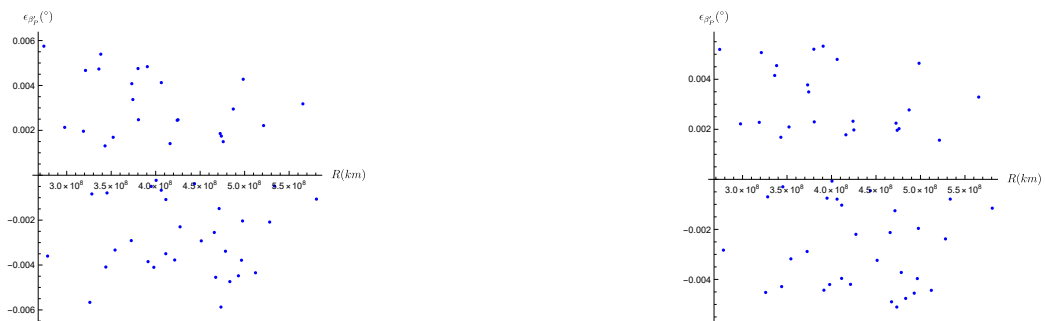


Figure 115: The Distribution of  $\beta'_p$  Error of Asteroids with Respect to Their Distance From the Sun, Error of the RF is not included on the left - included on the right.

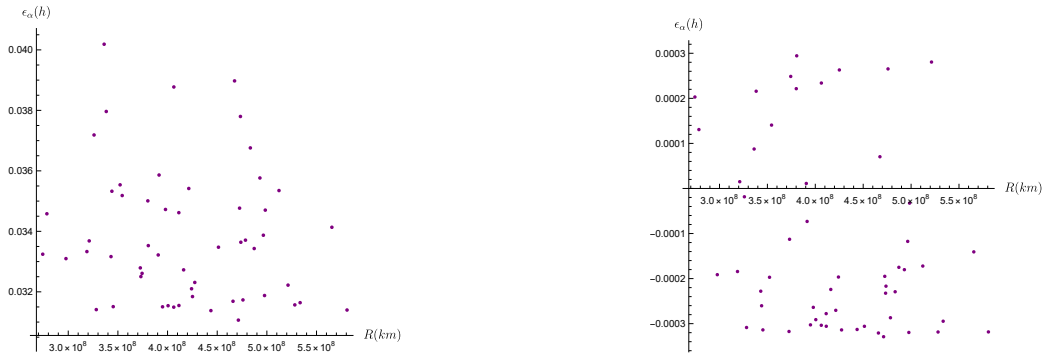


Figure 116: The Distribution of  $\alpha$  Error of Asteroids with Respect to Their Distance From the Sun, Error of the RF is not included on the left - included on the right.

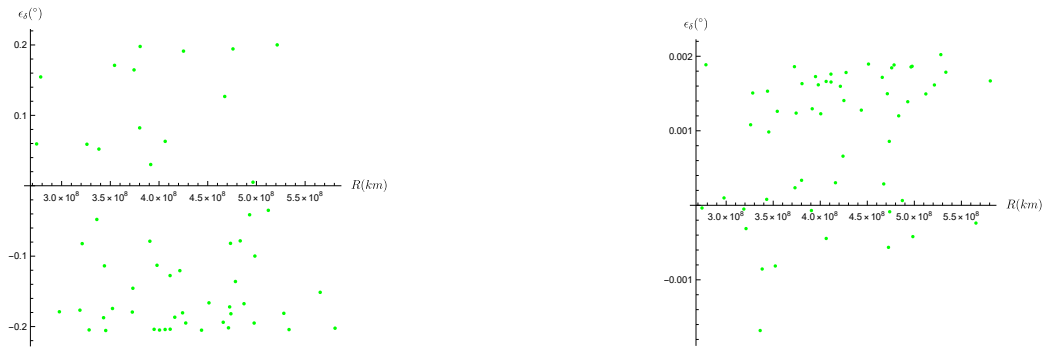


Figure 117: The Distribution of  $\delta$  Error of Asteroids with Respect to Their Distance From the Sun, Error of the RF is not included on the left - included on the right.

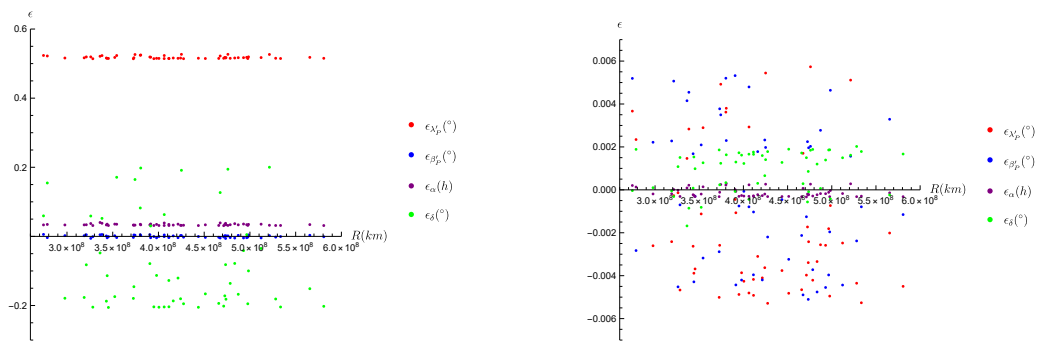


Figure 118: The Distribution of all Errors of Asteroids with Respect to Their Distance From the Sun, Error of the RF is not included on the left - included on the right.

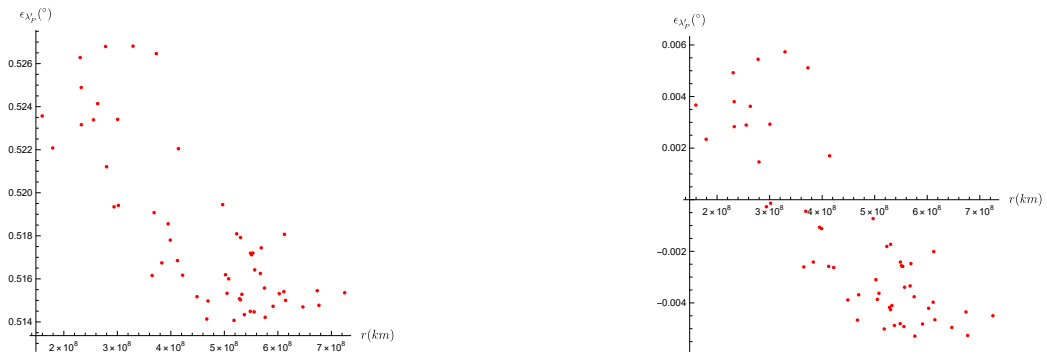


Figure 119: The Error Distribution of  $\lambda'_p$  of Asteroids with Respect to Their Distance From the Spacecraft, Error of the RF is not included on the left - included on the right.

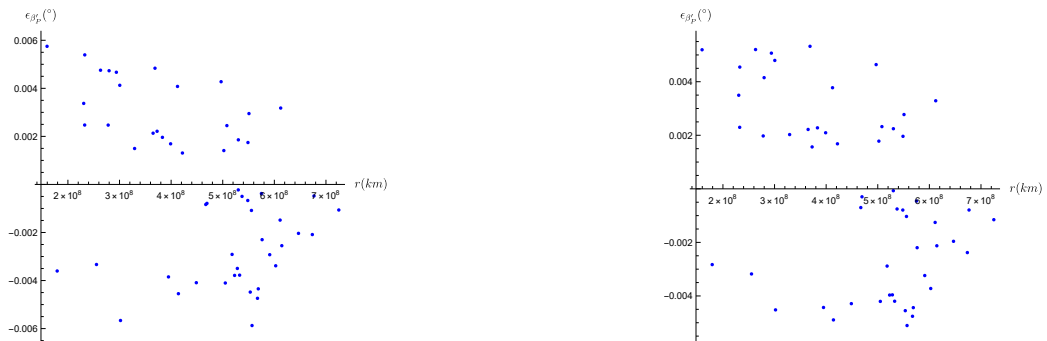


Figure 120: The Distribution of Error in  $\beta'_p$  of Asteroids with Respect to Their Distance From the Spacecraft, Error of the RF is not included on the left - included on the right.

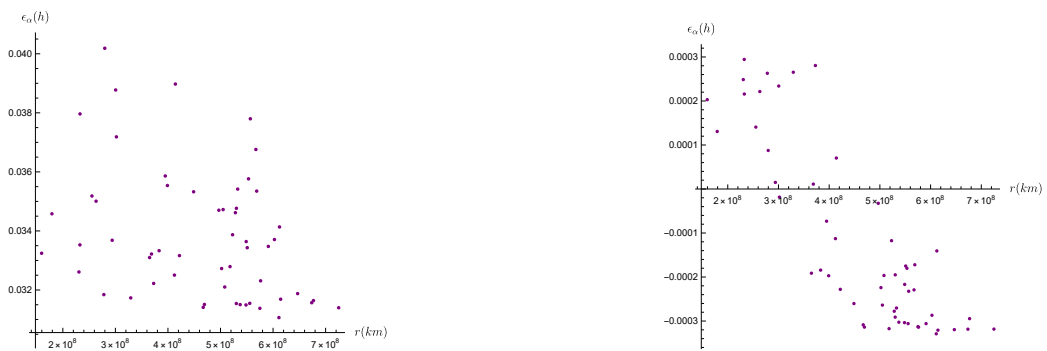


Figure 121: The Distribution of Error in  $\alpha$  of Asteroids with Respect to Their Distance From the Spacecraft, Error of the RF is not included on the left - included on the right.

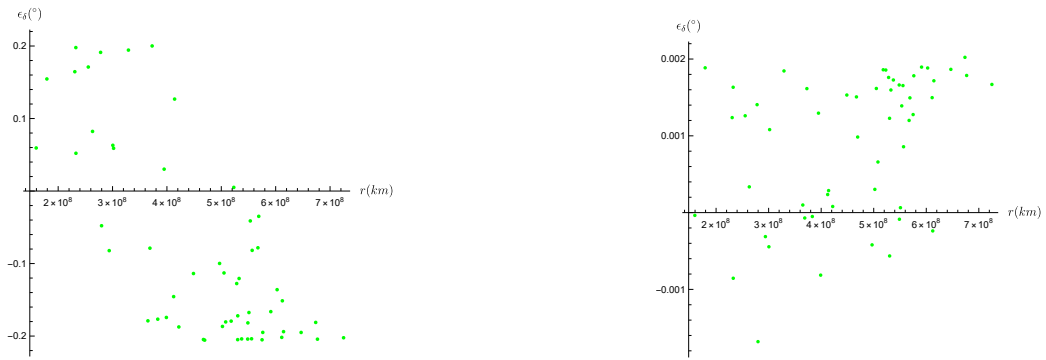


Figure 122: The Distribution of Error in  $\delta$  of Asteroids with Respect to Their Distance From the Spacecraft, Error of the RF is not included on the left - included on the right.

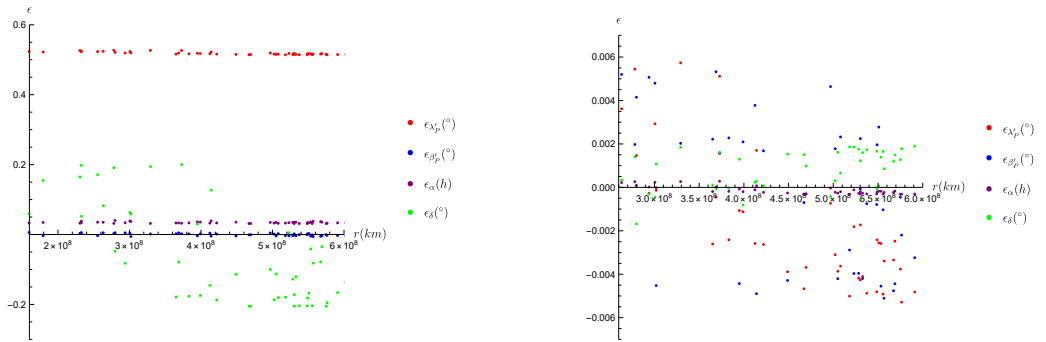


Figure 123: The Distribution of All Errors of Asteroids with Respect to Their Distance From the Spacecraft, Error of the RF is not included on the left - included on the right.

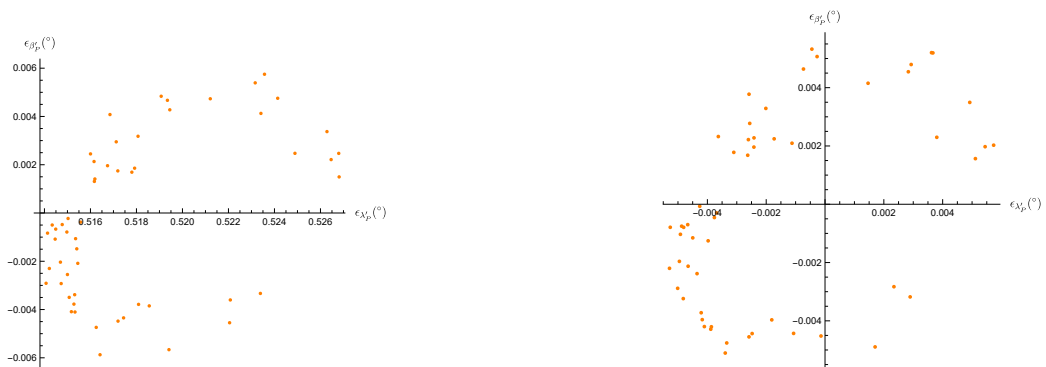


Figure 124: The Error Distribution of  $\lambda'_p$  vs  $\beta'_p$ , Error of the RF is not included on the left - included on the right.

2037 November 13, 03:18:17 UT

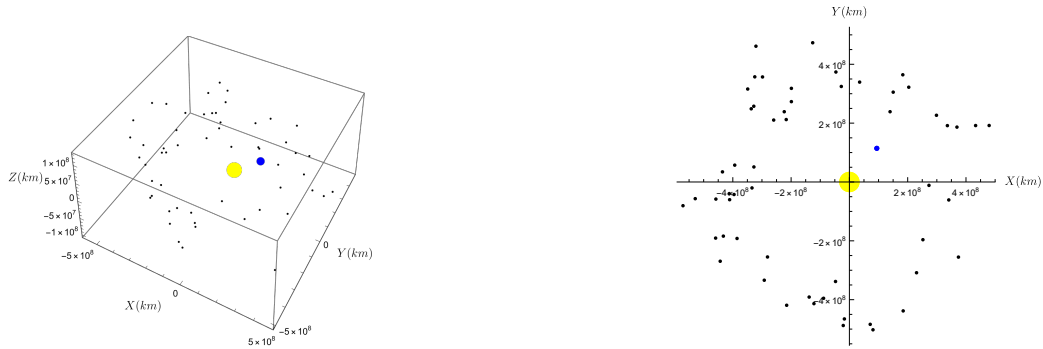


Figure 125: 3D Model of the System Created with Mathematica and Its XY Plane



Figure 126: The Distribution of  $\lambda'_p$  Error of Asteroids with Respect to Their Distance From the Sun, Error of the RF is not included on the left - included on the right.

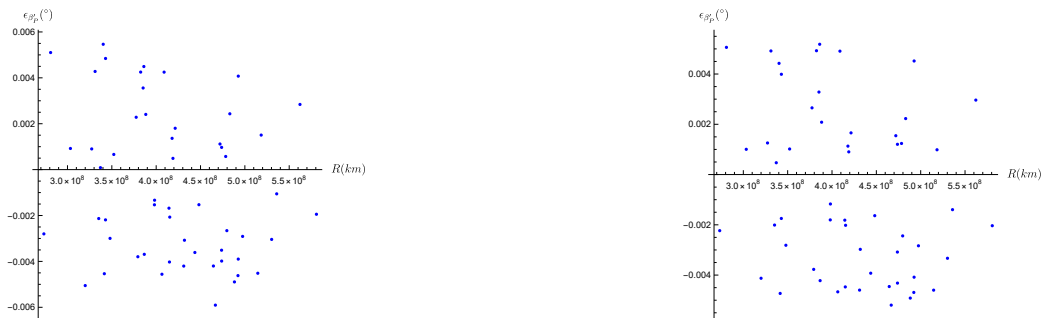


Figure 127: The Distribution of  $\beta'_p$  Error of Asteroids with Respect to Their Distance From the Sun, Error of the RF is not included on the left - included on the right.

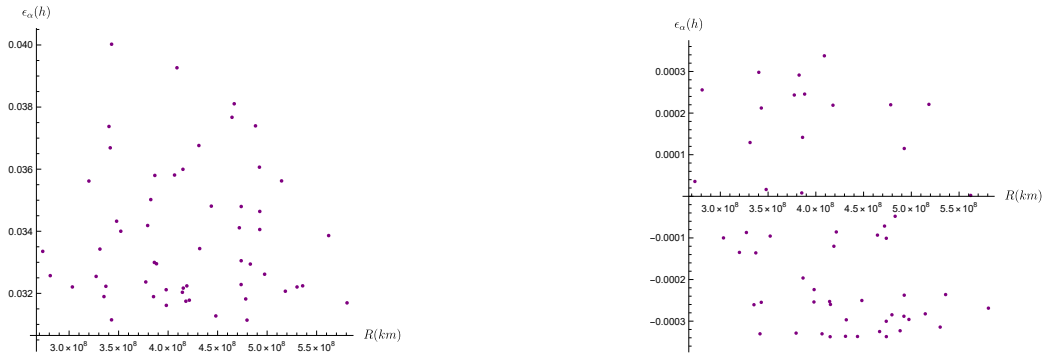


Figure 128: The Distribution of  $\alpha$  Error of Asteroids with Respect to Their Distance From the Sun, Error of the RF is not included on the left - included on the right.

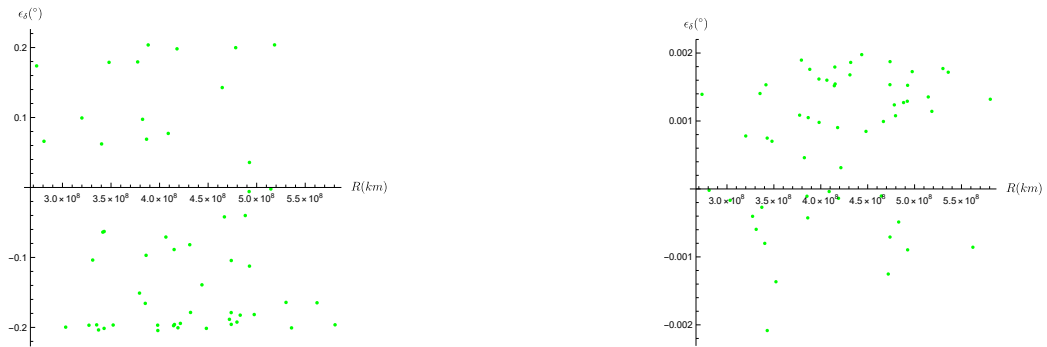


Figure 129: The Distribution of  $\delta$  Error of Asteroids with Respect to Their Distance From the Sun, Error of the RF is not included on the left - included on the right.

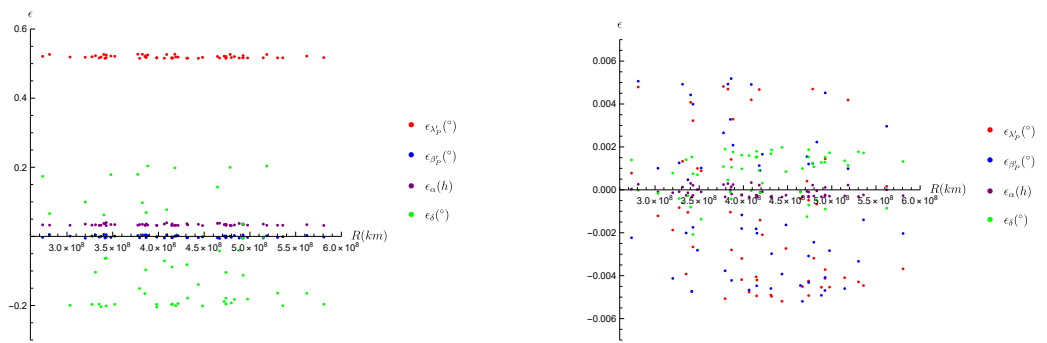


Figure 130: The Distribution of all Errors of Asteroids with Respect to Their Distance From the Sun, Error of the RF is not included on the left - included on the right.

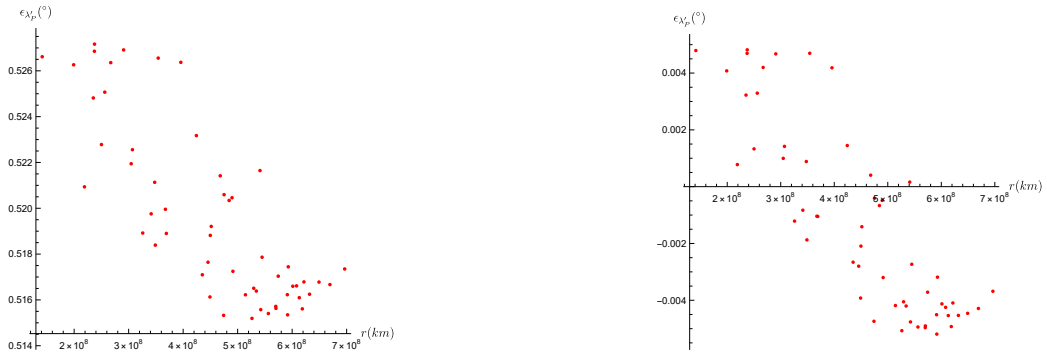


Figure 131: The Error Distribution of  $\lambda'_p$  of Asteroids with Respect to Their Distance From the Spacecraft, Error of the RF is not included on the left - included on the right.



Figure 132: The Distribution of Error in  $\beta'_p$  of Asteroids with Respect to Their Distance From the Spacecraft, Error of the RF is not included on the left - included on the right.

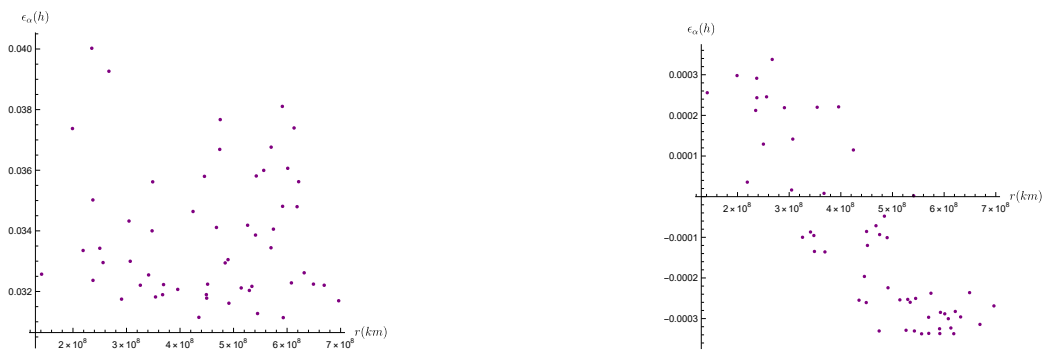


Figure 133: The Distribution of Error in  $\alpha$  of Asteroids with Respect to Their Distance From the Spacecraft, Error of the RF is not included on the left - included on the right.



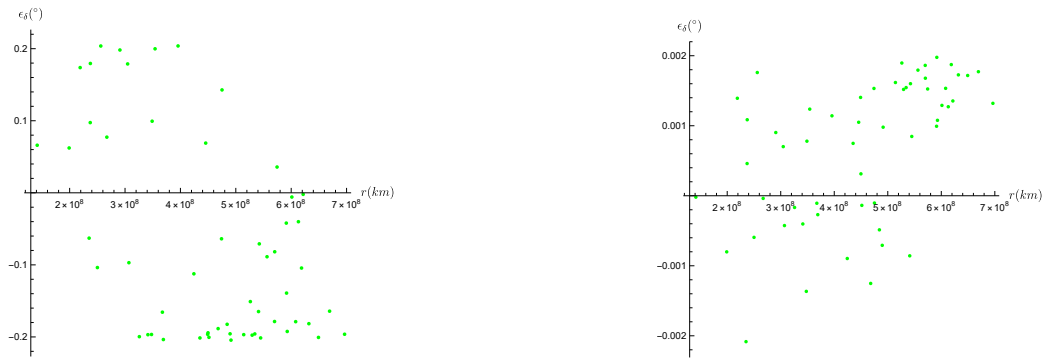


Figure 134: The Distribution of Error in  $\delta$  of Asteroids with Respect to Their Distance From the Spacecraft, Error of the RF is not included on the left - included on the right.

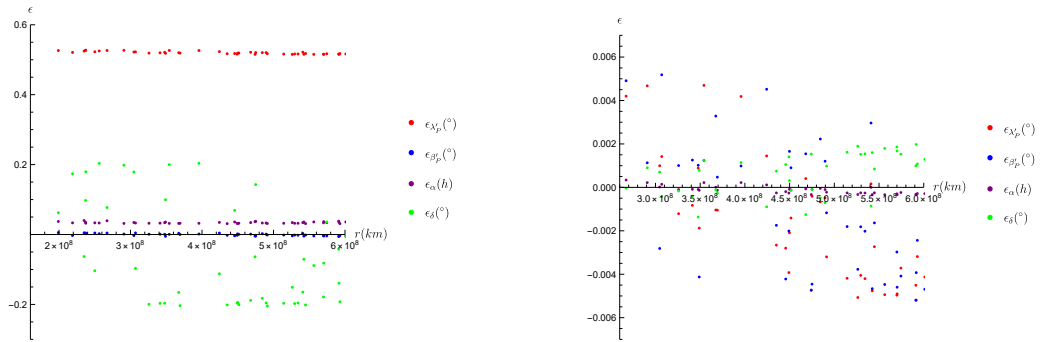


Figure 135: The Distribution of All Errors of Asteroids with Respect to Their Distance From the Spacecraft, Error of the RF is not included on the left - included on the right.

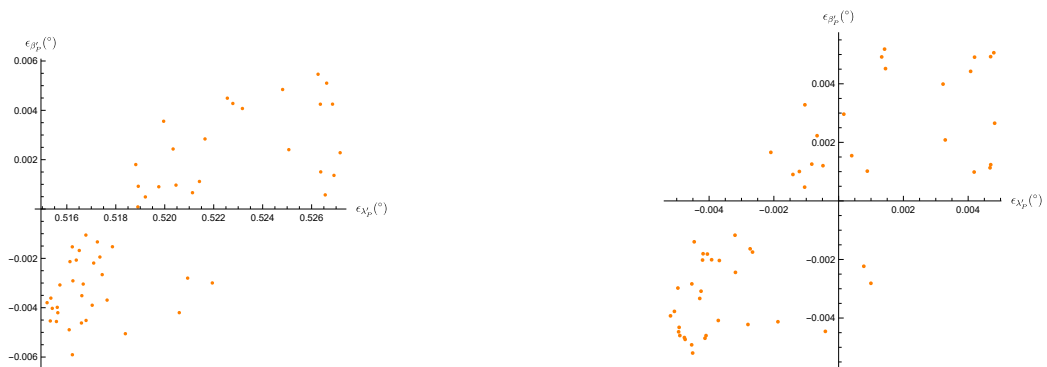


Figure 136: The Error Distribution of Error in  $\lambda'_p$  vs  $\beta'_p$ , Error of the RF is not included on the left - included on the right.

### 5.1.3 Rome

2037 January 13, 03:18:17 UT



Figure 137: 3D Model of the System Created with Mathematica and Its XY Plane

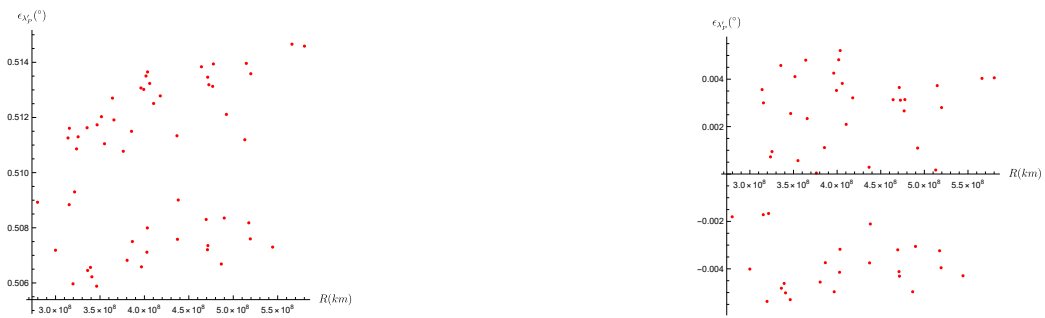


Figure 138: The Distribution of  $\lambda'_p$  Error of Asteroids with Respect to Their Distance From the Sun, Error of the RF is not included on the left - included on the right.



Figure 139: The Distribution of  $\beta'_p$  Error of Asteroids with Respect to Their Distance From the Sun, Error of the RF is not included on the left - included on the right.

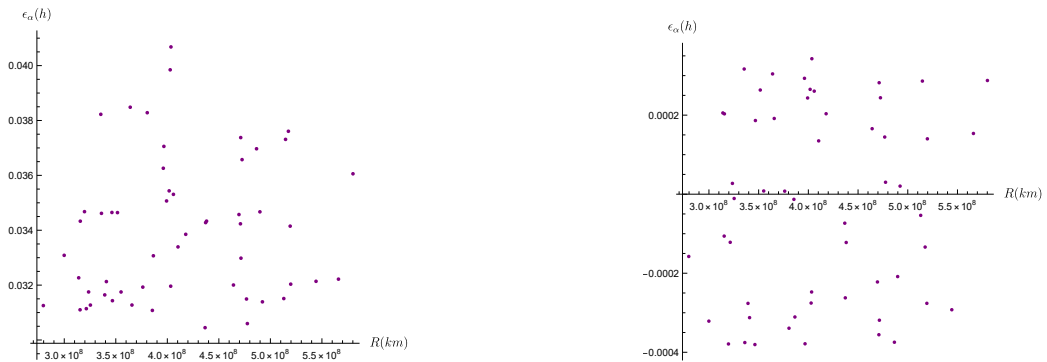


Figure 140: The Distribution of  $\alpha$  Error of Asteroids with Respect to Their Distance From the Sun, Error of the RF is not included on the left - included on the right.

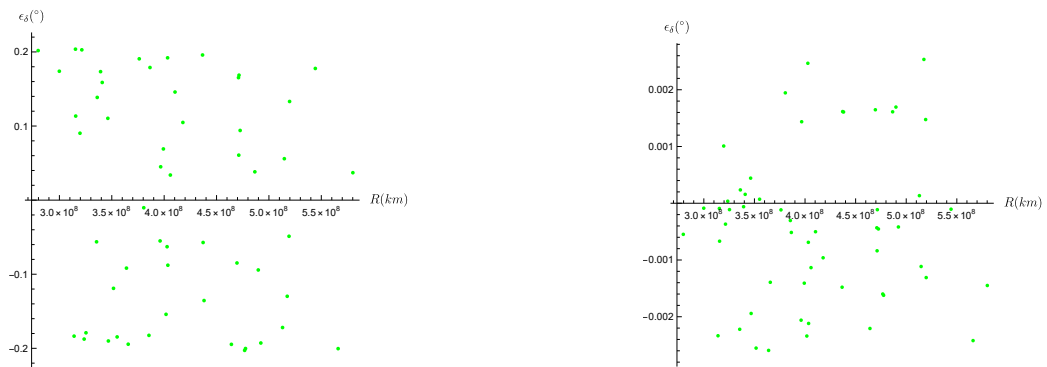


Figure 141: The Distribution of  $\delta$  Error of Asteroids with Respect to Their Distance From the Sun, Error of the RF is not included on the left - included on the right.

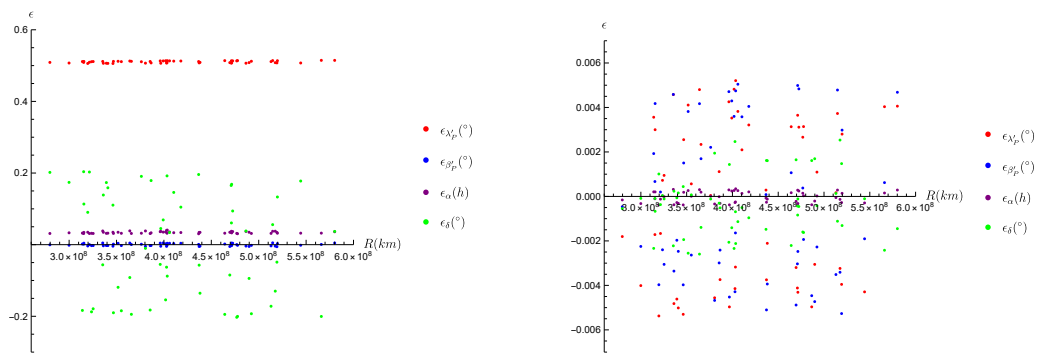


Figure 142: The Distribution of all Errors of Asteroids with Respect to Their Distance From the Sun, Error of the RF is not included on the left - included on the right.

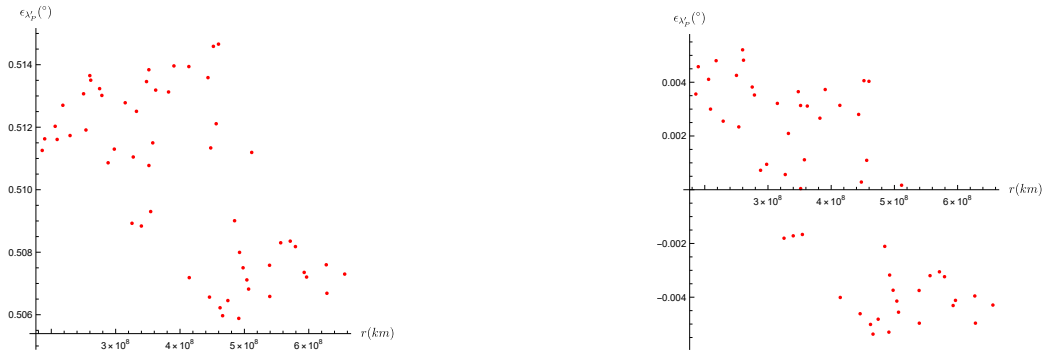


Figure 143: The Error Distribution of  $\lambda'_p$  of Asteroids with Respect to Their Distance From the Earth, Error of the RF is not included on the left - included on the right.

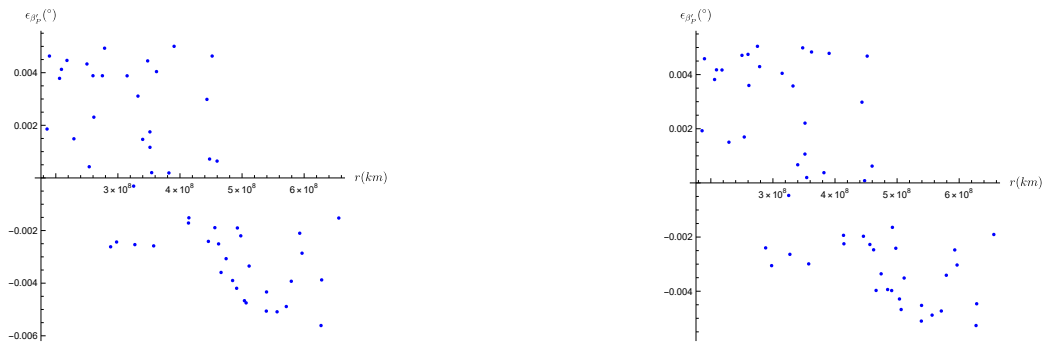


Figure 144: The Error Distribution of  $\beta'_p$  of Asteroids with Respect to Their Distance From the Earth, Error of the RF is not included on the left - included on the right.

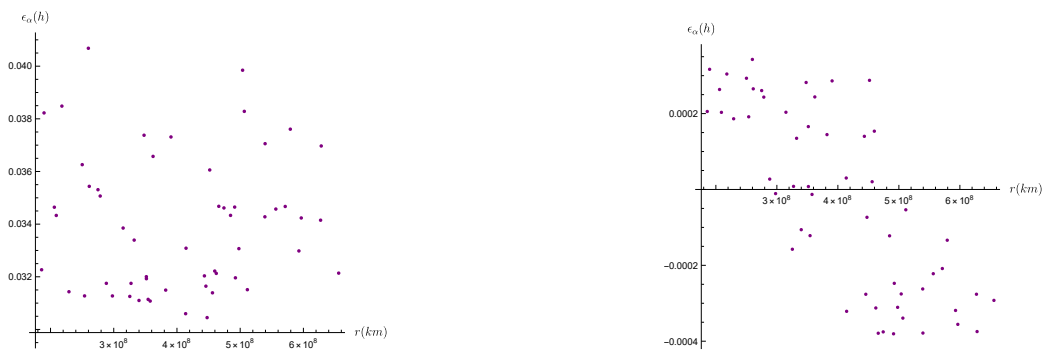


Figure 145: The Error Distribution of  $\alpha$  of Asteroids with Respect to Their Distance From the Earth, Error of the RF is not included on the left - included on the right.

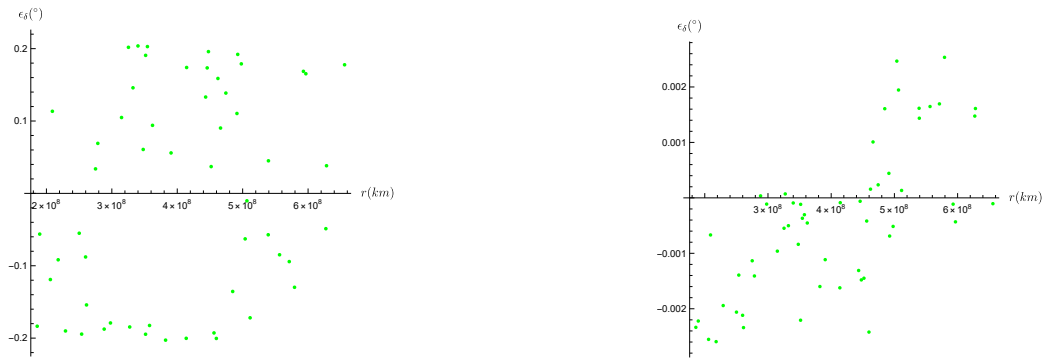


Figure 146: The Error Distribution of  $\delta$  of Asteroids with Respect to Their Distance From the Earth, Error of the RF is not included on the left - included on the right.

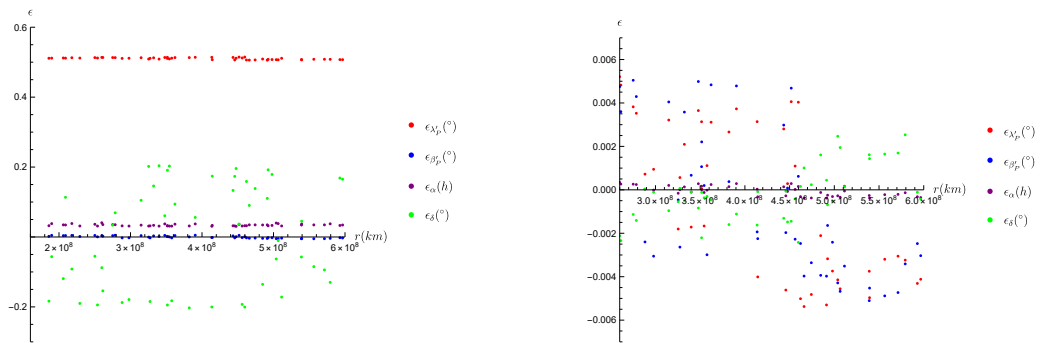


Figure 147: The Distribution of All Errors of Asteroids with Respect to Their Distance From the Earth, Error of the RF is not included on the left - included on the right.

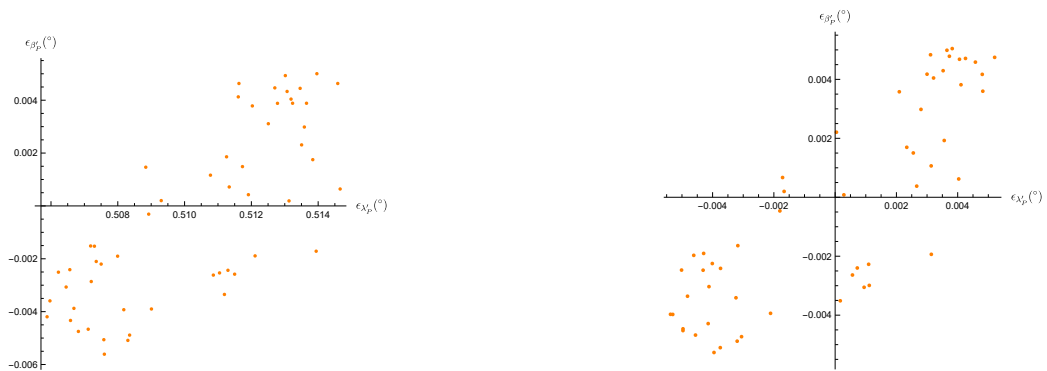


Figure 148: The Error Distribution of  $\lambda'_p$  vs  $\beta'_p$ , Error of the RF is not included on the left - included on the right.

2037 April 13, 03:18:17 UT



Figure 149: 3D Model of the System Created with Mathematica and Its XY Plane



Figure 150: The Distribution of  $\lambda'_p$  Error of Asteroids with Respect to Their Distance From the Sun, Error of the RF is not included on the left - included on the right.

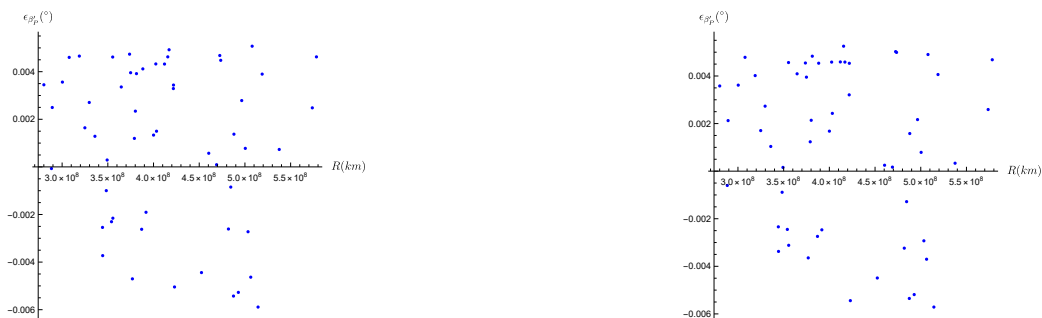


Figure 151: The Distribution of  $\beta'_p$  Error of Asteroids with Respect to Their Distance From the Sun, Error of the RF is not included on the left - included on the right.

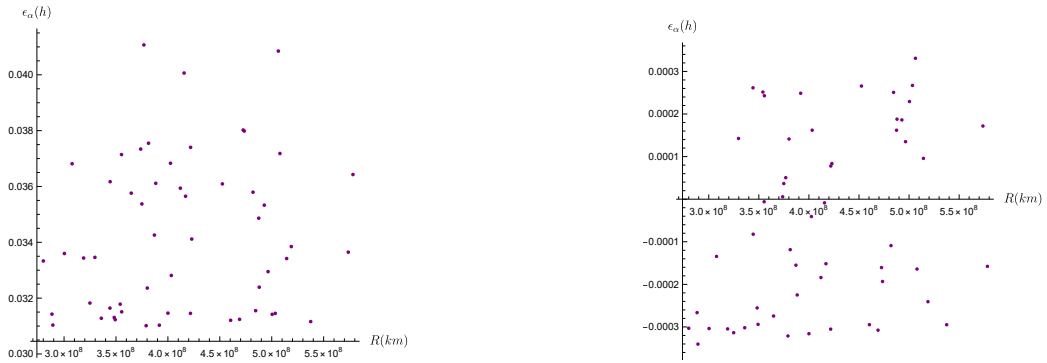


Figure 152: The Distribution of  $\alpha$  Error of Asteroids with Respect to Their Distance From the Sun, Error of the RF is not included on the left - included on the right.

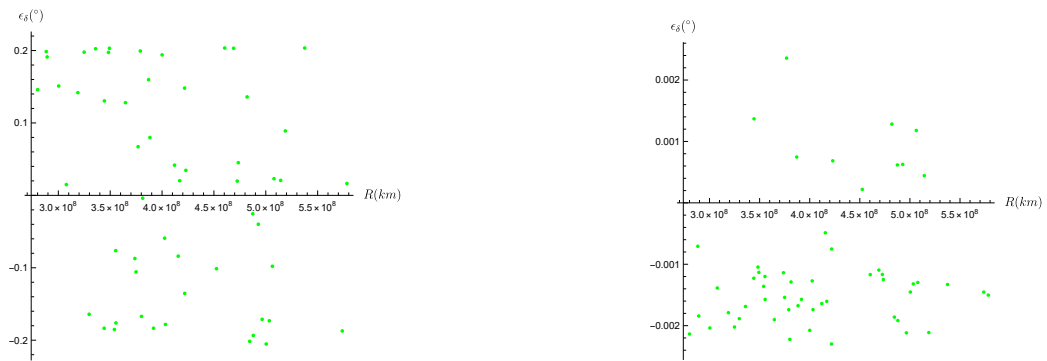


Figure 153: The Distribution of  $\delta$  Error of Asteroids with Respect to Their Distance From the Sun, Error of the RF is not included on the left - included on the right.

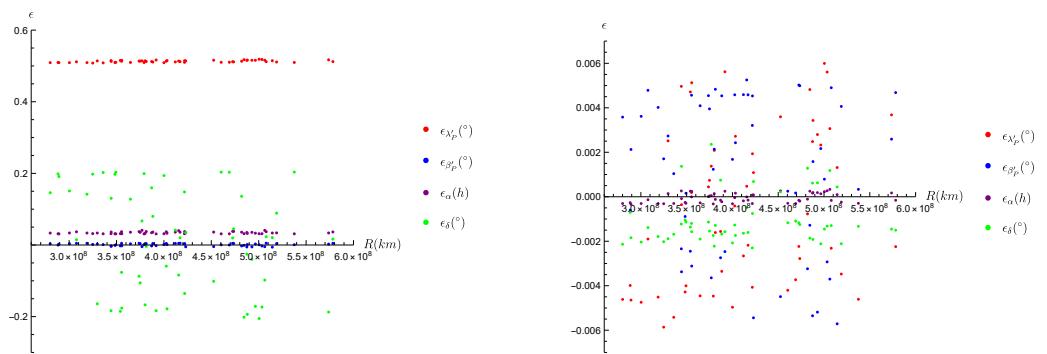


Figure 154: The Distribution of all Errors of Asteroids with Respect to Their Distance From the Sun, Error of the RF is not included on the left - included on the right.



Figure 155: The Error Distribution of  $\lambda'_p$  of Asteroids with Respect to Their Distance From the Spacecraft, Error of the RF is not included on the left - included on the right.



Figure 156: The Error Distribution of  $\beta'_p$  of Asteroids with Respect to Their Distance From the Spacecraft, Error of the RF is not included on the left - included on the right.



Figure 157: The Error Distribution of  $\alpha$  of Asteroids with Respect to Their Distance From the Spacecraft, Error of the RF is not included on the left - included on the right.



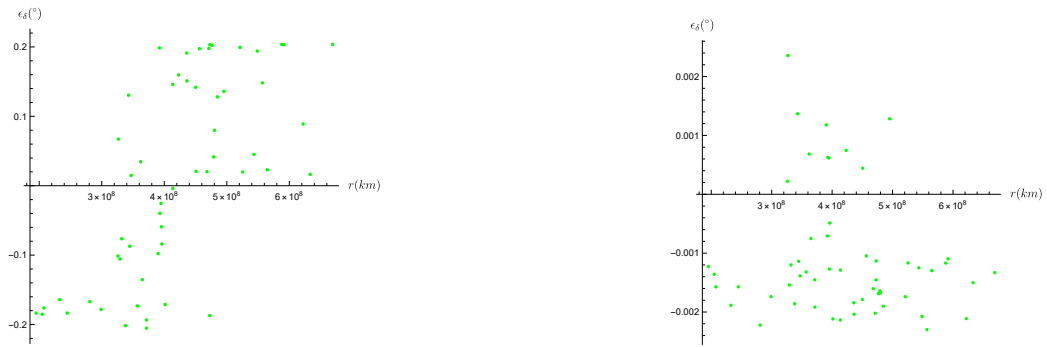


Figure 158: The Error Distribution of  $\delta$  of Asteroids with Respect to Their Distance From the Spacecraft, Error of the RF is not included on the left - included on the right.

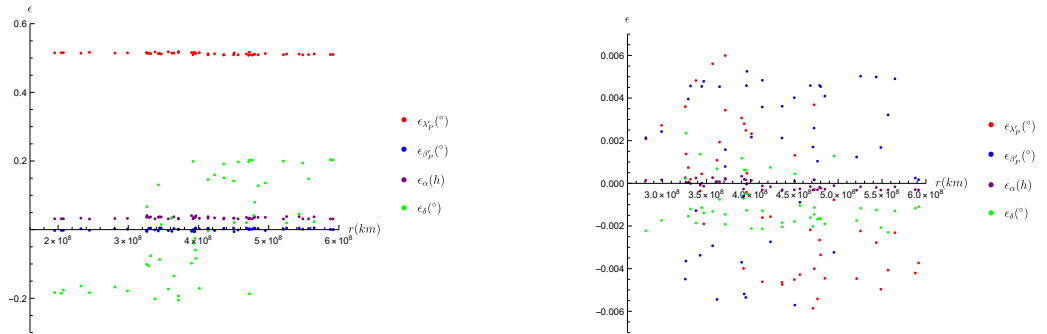


Figure 159: The Distribution of all errors of Asteroids with Respect to Their Distance From the Spacecraft, Error of the RF is not included on the left - included on the right.



Figure 160: The Error Distribution of  $\lambda'_p$  vs  $\beta'_p$ , Error of the RF is not included on the left - included on the right.

2037 July 13, 03:18:17 UT



Figure 161: 3D Model of the System Created with Mathematica and Its XY Plane



Figure 162: The Distribution of  $\lambda'_p$  Error of Asteroids with Respect to Their Distance From the Sun, Error of the RF is not included on the left - included on the right.

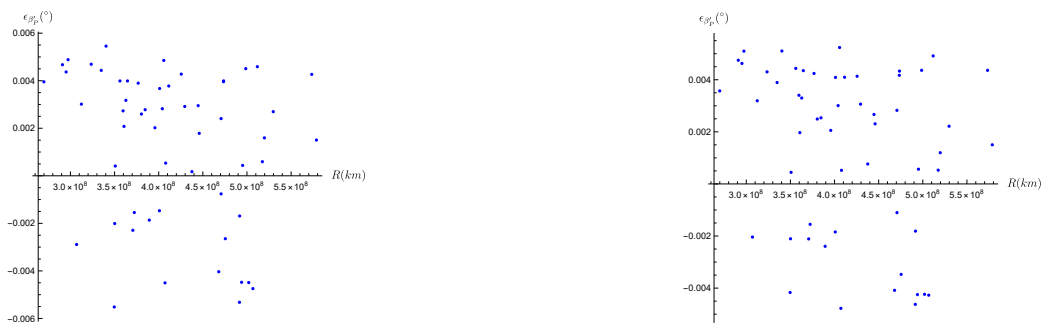


Figure 163: The Distribution of  $\beta'_p$  Error of Asteroids with Respect to Their Distance From the Sun, Error of the RF is not included on the left - included on the right.

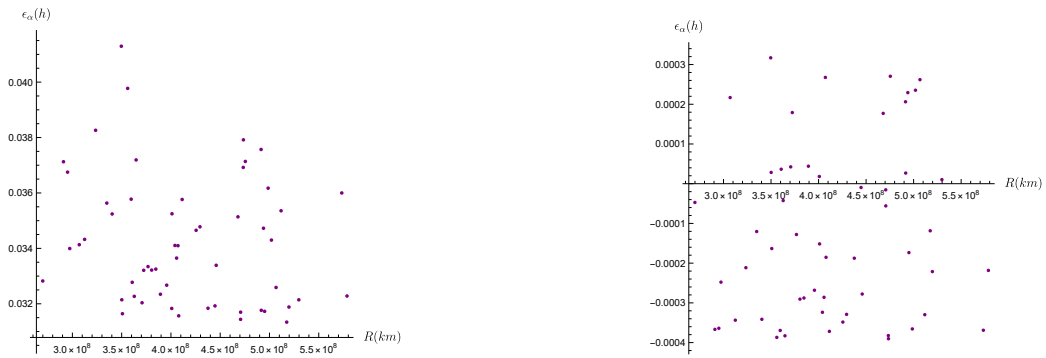


Figure 164: The Distribution of  $\alpha$  Error of Asteroids with Respect to Their Distance From the Sun, Error of the RF is not included on the left - included on the right.

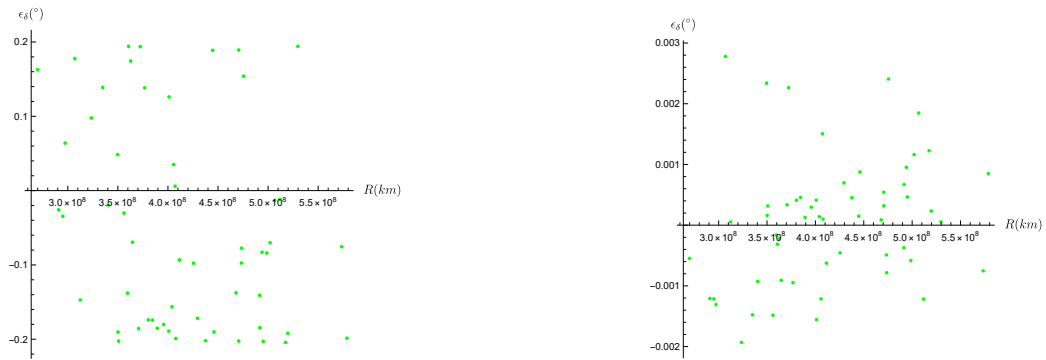


Figure 165: The Distribution of  $\delta$  Error of Asteroids with Respect to Their Distance From the Sun, Error of the RF is not included on the left - included on the right.

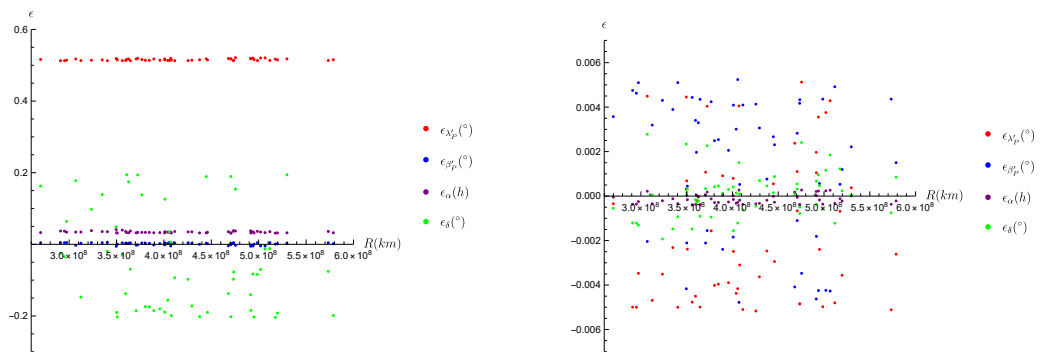


Figure 166: The Distribution of all Errors of Asteroids with Respect to Their Distance From the Sun, Error of the RF is not included on the left - included on the right.

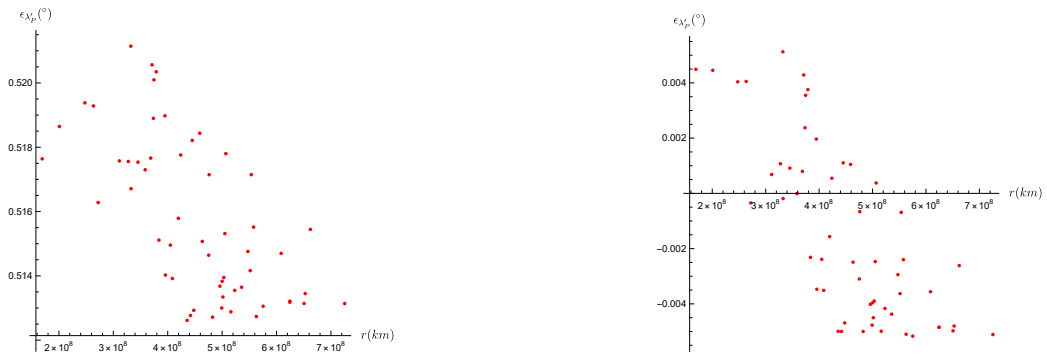


Figure 167: The Error Distribution of  $\lambda'_p$  of Asteroids with Respect to Their Distance From the Spacecraft, Error of the RF is not included on the left - included on the right.

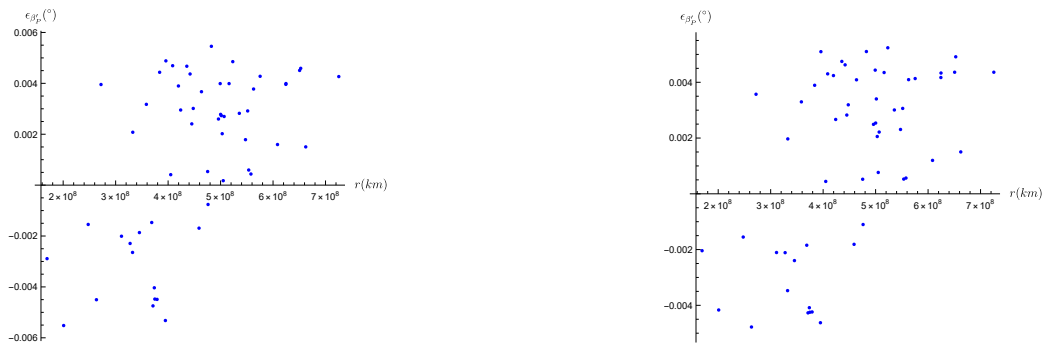


Figure 168: The Error Distribution of  $\beta'_p$  of Asteroids with Respect to Their Distance From the Spacecraft, Error of the RF is not included on the left - included on the right.

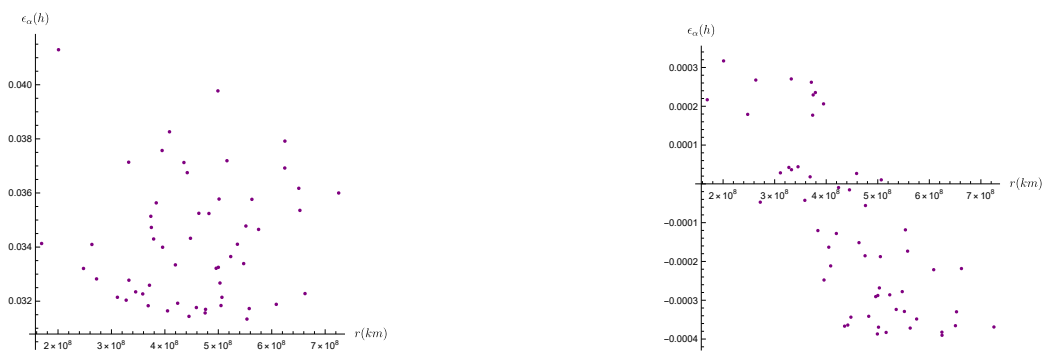


Figure 169: The Error Distribution of  $\alpha$  of Asteroids with Respect to Their Distance From the Spacecraft, Error of the RF is not included on the left - included on the right.

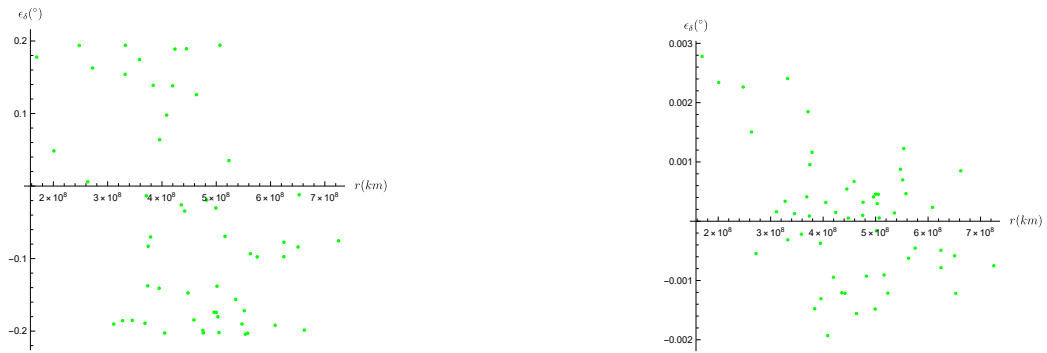


Figure 170: The Error Distribution of  $\delta$  of Asteroids with Respect to Their Distance From the Spacecraft, Error of the RF is not included on the left - included on the right.

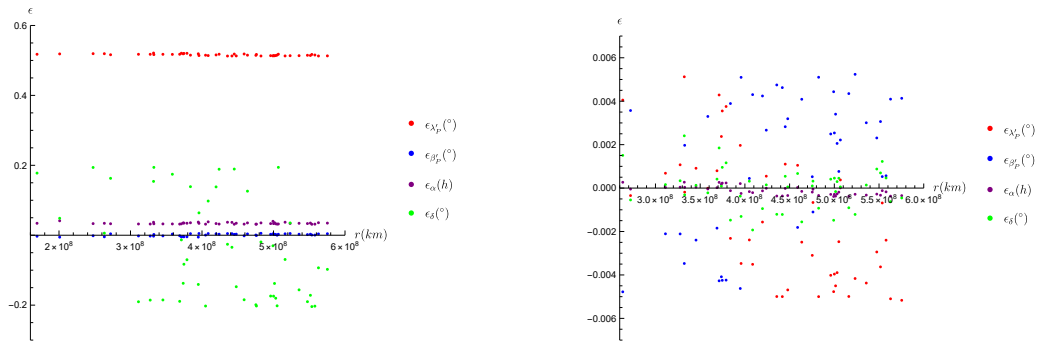


Figure 171: The Distribution of All Errors of Asteroids with Respect to Their Distance From the Spacecraft, Error of the RF is not included on the left - included on the right.

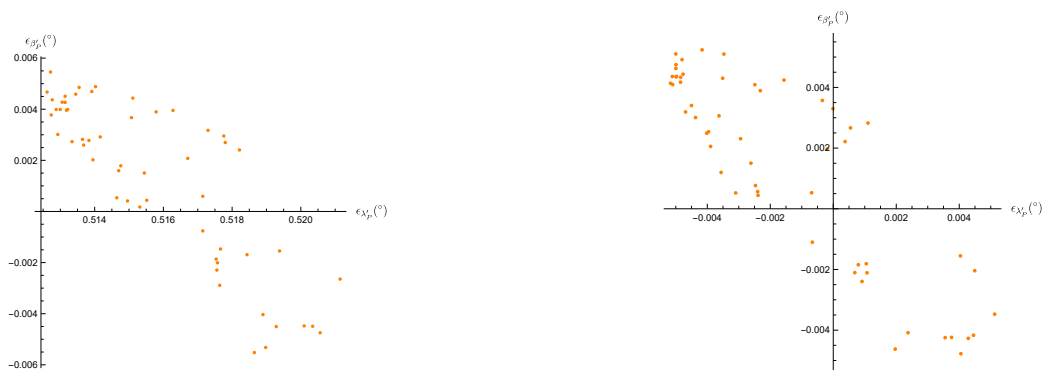


Figure 172: The Error Distribution of  $\lambda'_p$  vs  $\beta'_p$ , Error of the RF is not included on the left - included on the right.

2037 October 13, 03:18:17 UT



Figure 173: 3D Model of the System Created with Mathematica and Its XY Plane



Figure 174: The Distribution of  $\lambda'_p$  Error of Asteroids with Respect to Their Distance From the Sun, Error of the RF is not included on the left - included on the right.

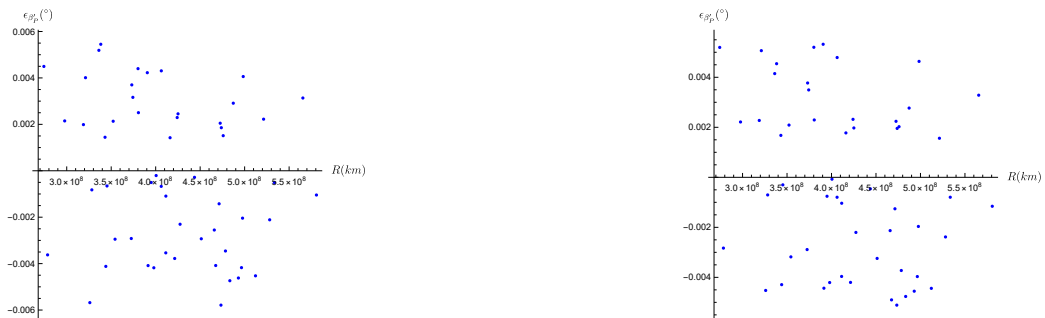


Figure 175: The Distribution of  $\beta'_p$  Error of Asteroids with Respect to Their Distance From the Sun, Error of the RF is not included on the left - included on the right.

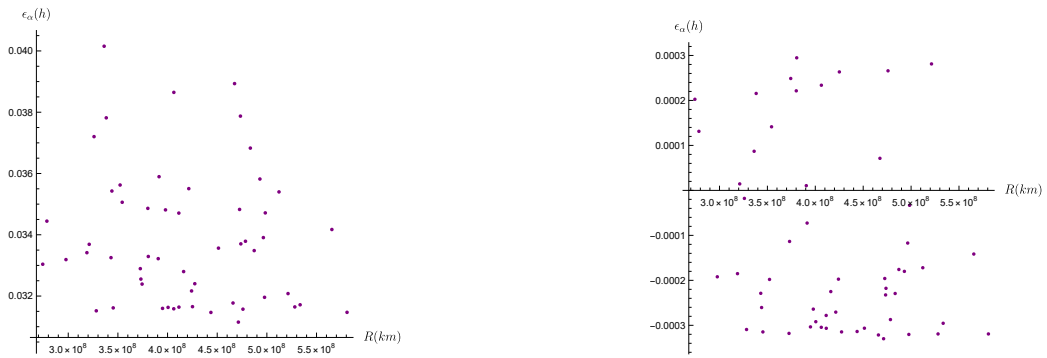


Figure 176: The Distribution of  $\alpha$  Error of Asteroids with Respect to Their Distance From the Sun, Error of the RF is not included on the left - included on the right.

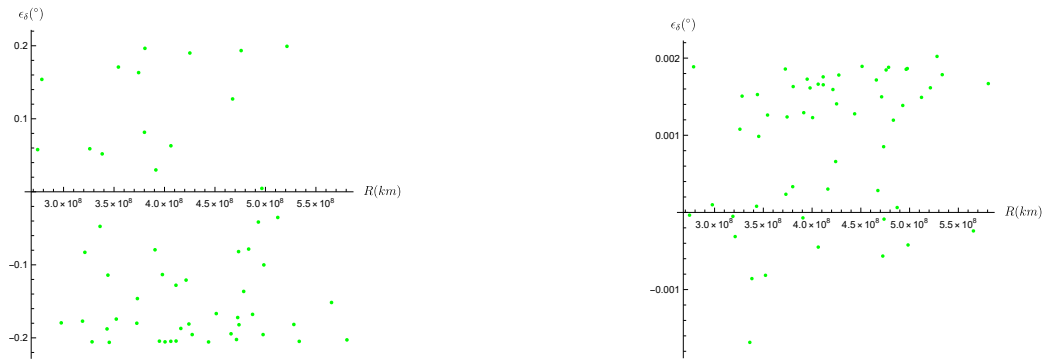


Figure 177: The Distribution of  $\delta$  Error of Asteroids with Respect to Their Distance From the Sun, Error of the RF is not included on the left - included on the right.

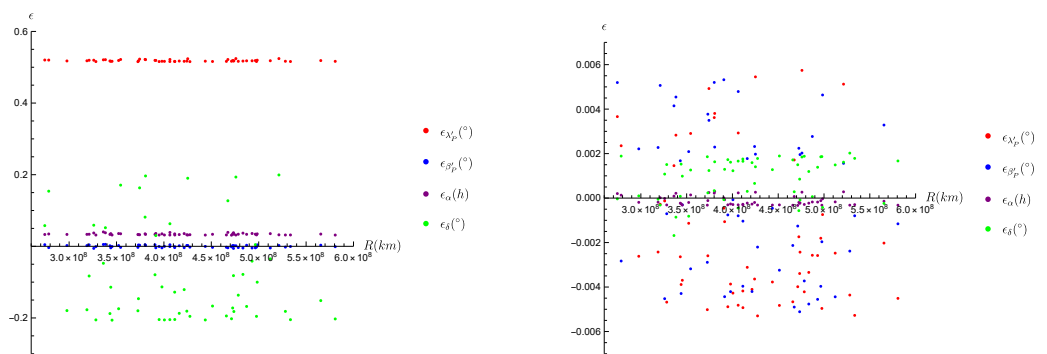


Figure 178: The Distribution of all Errors of Asteroids with Respect to Their Distance From the Sun, Error of the RF is not included on the left - included on the right.

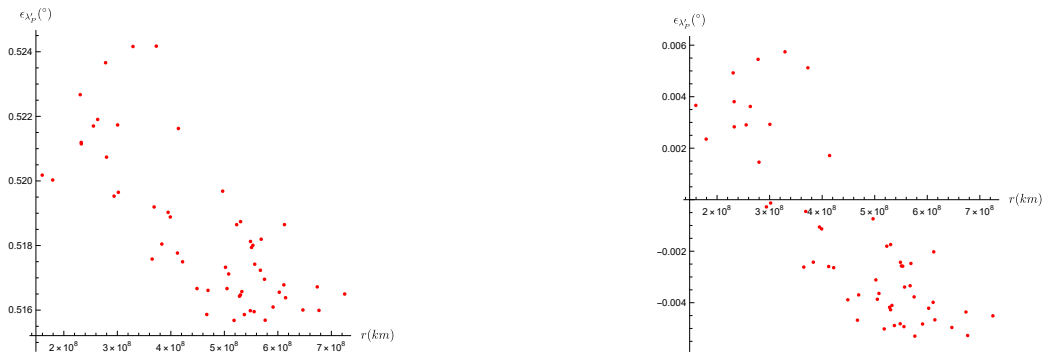


Figure 179: The Error Distribution of Error in  $\lambda'_p$  of Asteroids with Respect to Their Distance From the Spacecraft, Error of the RF is not included on the left - included on the right.



Figure 180: The Distribution of Error in  $\beta'_p$  of Asteroids with Respect to Their Distance From the Spacecraft, Error of the RF is not included on the left - included on the right.

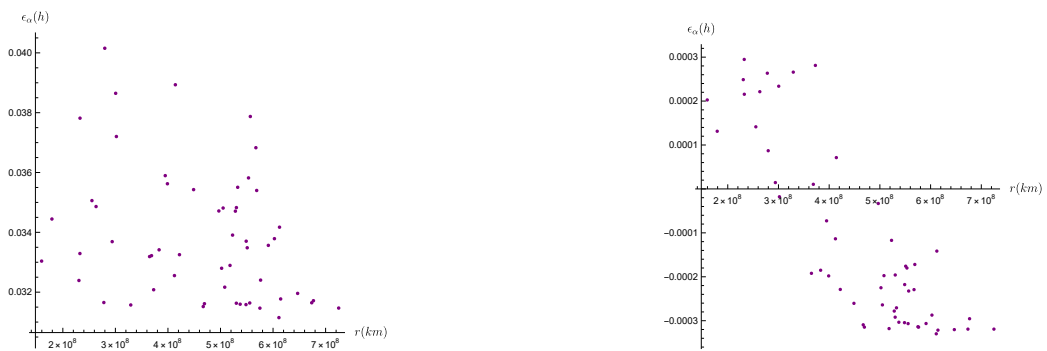


Figure 181: The Distribution of Error in  $\alpha$  of Asteroids with Respect to Their Distance From the Spacecraft, Error of the RF is not included on the left - included on the right.



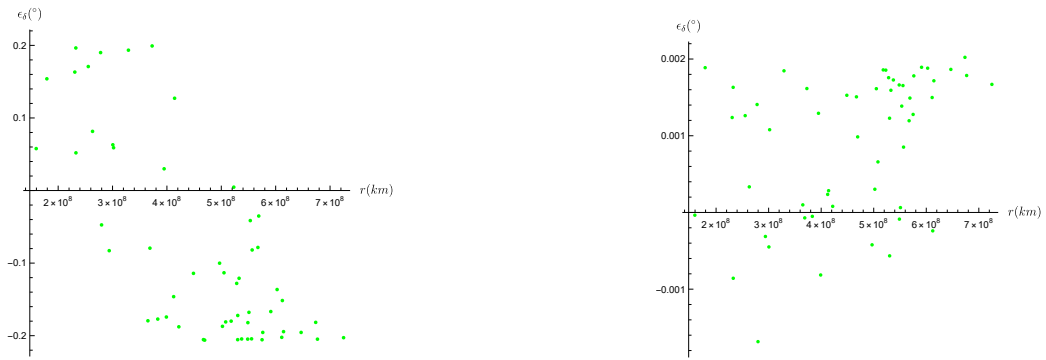


Figure 182: The Distribution of Error in  $\delta$  of Asteroids with Respect to Their Distance From the Spacecraft, Error of the RF is not included on the left - included on the right.

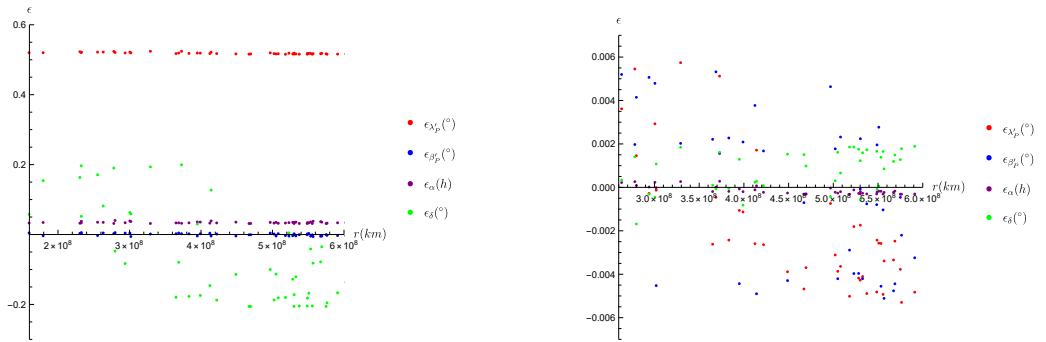


Figure 183: The Distribution of All Errors of Asteroids with Respect to Their Distance From the Spacecraft, Error of the RF is not included on the left - included on the right.

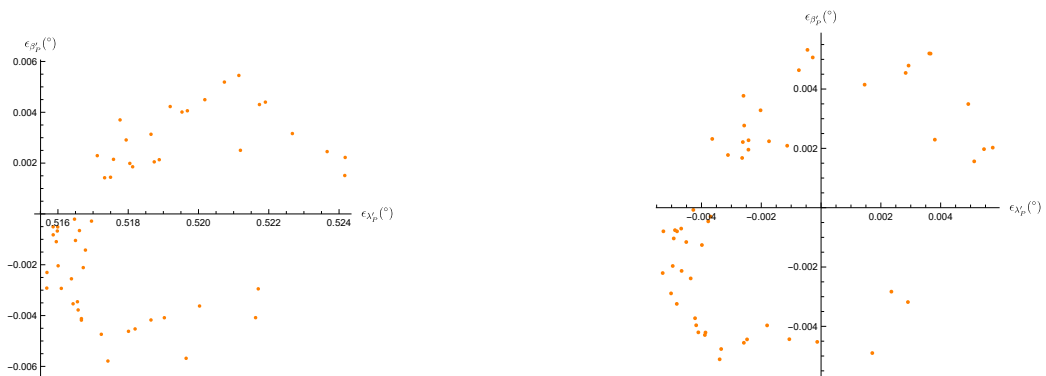


Figure 184: The Error Distribution of  $\lambda'_p$  vs  $\beta'_p$ , Error of the RF is not included on the left - included on the right.

2037 November 13, 03:18:17 UT



Figure 185: 3D Model of the System Created with Mathematica and Its XY Plane



Figure 186: The Distribution of  $\lambda'_p$  Error of Asteroids with Respect to Their Distance From the Sun, Error of the RF is not included on the left - included on the right.

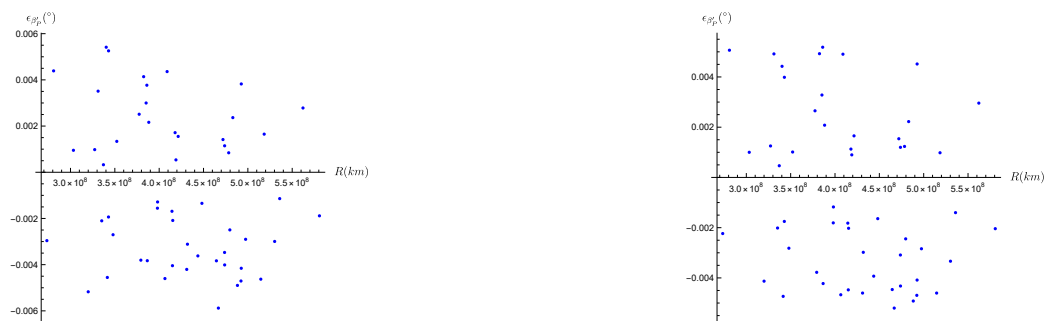


Figure 187: The Distribution of  $\beta'_p$  Error of Asteroids with Respect to Their Distance From the Sun, Error of the RF is not included on the left - included on the right.

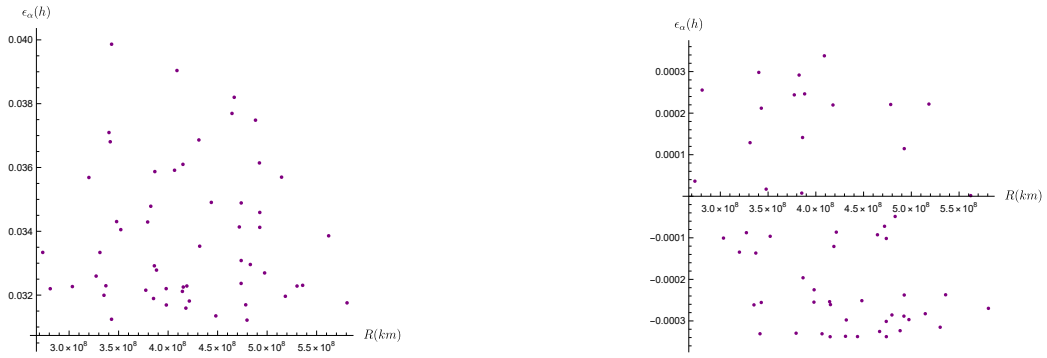


Figure 188: The Distribution of  $\alpha$  Error of Asteroids with Respect to Their Distance From the Sun, Error of the RF is not included on the left - included on the right.

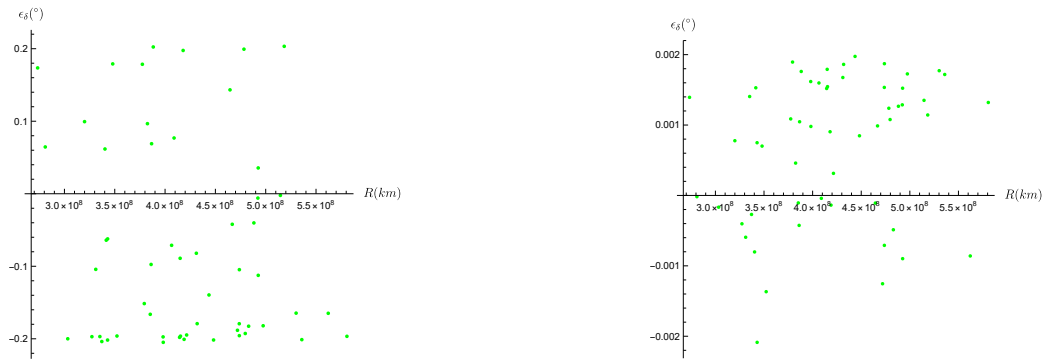


Figure 189: The Distribution of  $\delta$  Error of Asteroids with Respect to Their Distance From the Sun, Error of the RF is not included on the left - included on the right.

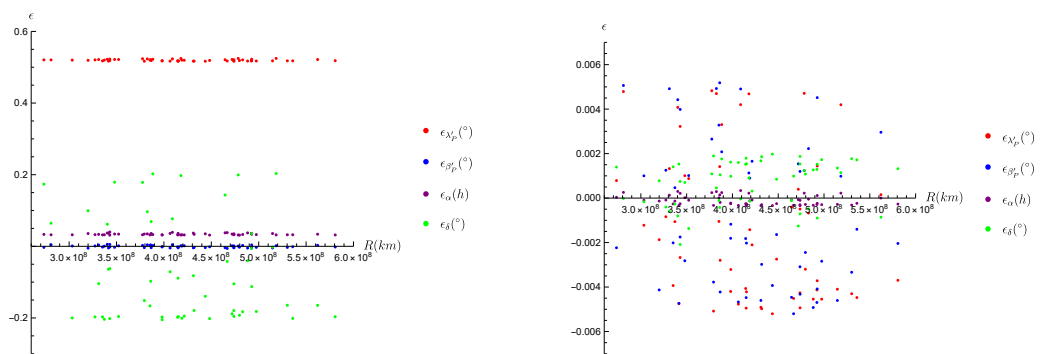


Figure 190: The Distribution of all Errors of Asteroids with Respect to Their Distance From the Sun, Error of the RF is not included on the left - included on the right.

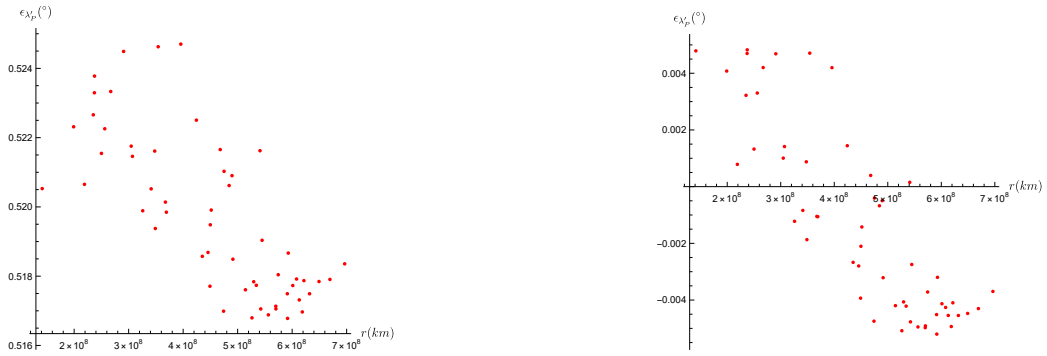


Figure 191: The Error Distribution of  $\lambda'_p$  of Asteroids with Respect to Their Distance From the Spacecraft, Error of the RF is not included on the left - included on the right.

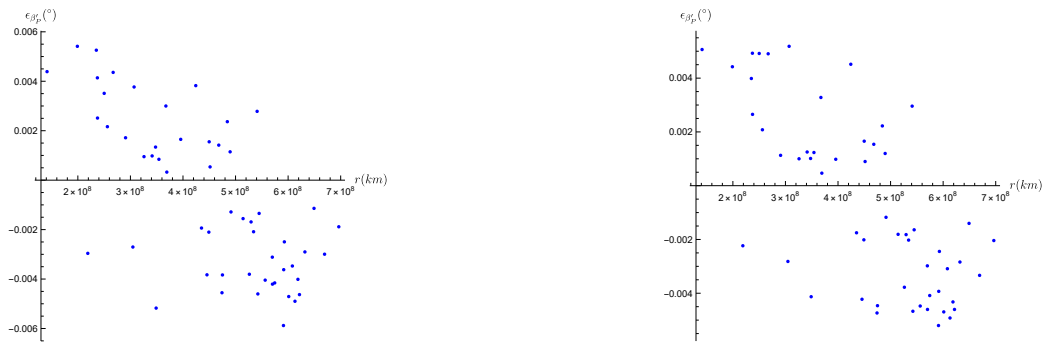


Figure 192: The Distribution of Error in  $\beta'_p$  of Asteroids with Respect to Their Distance From the Spacecraft, Error of the RF is not included on the left - included on the right.

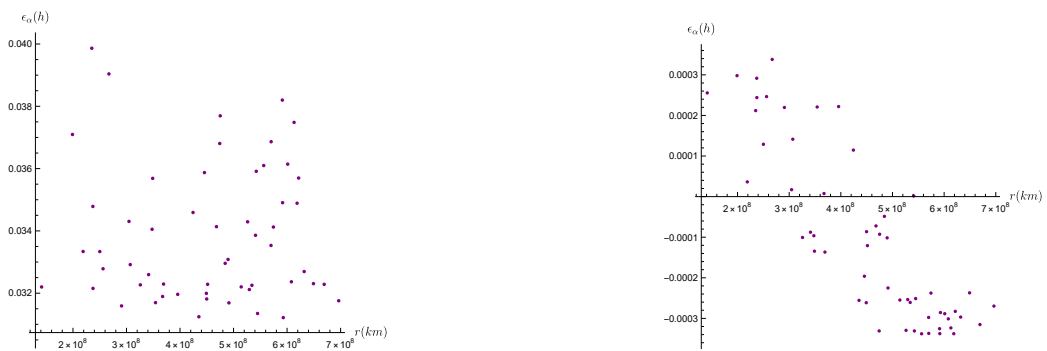


Figure 193: The Distribution of Error in  $\alpha$  of Asteroids with Respect to Their Distance From the Spacecraft, Error of the RF is not included on the left - included on the right.

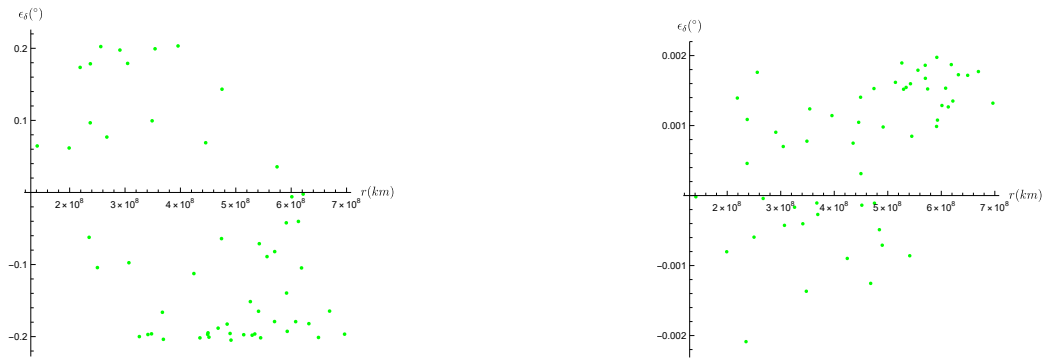


Figure 194: The Distribution of Error in  $\delta$  of Asteroids with Respect to Their Distance From the Spacecraft, Error of the RF is not included on the left - included on the right.

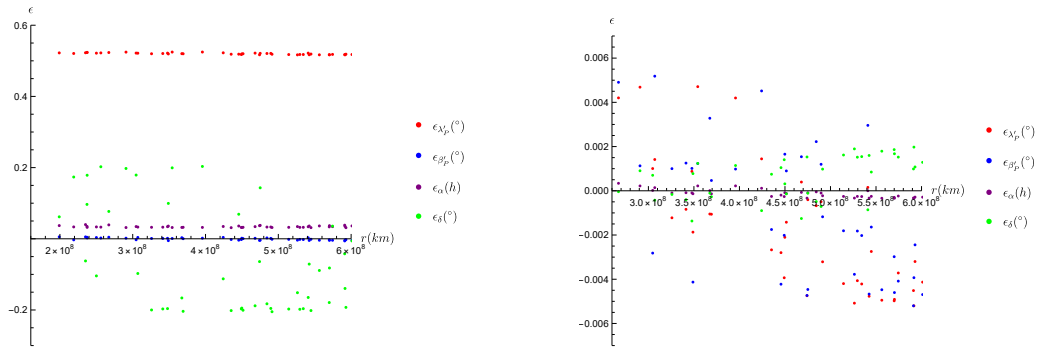


Figure 195: The Distribution of All Errors of Asteroids with Respect to Their Distance From the Spacecraft, Error of the RF is not included on the left - included on the right.

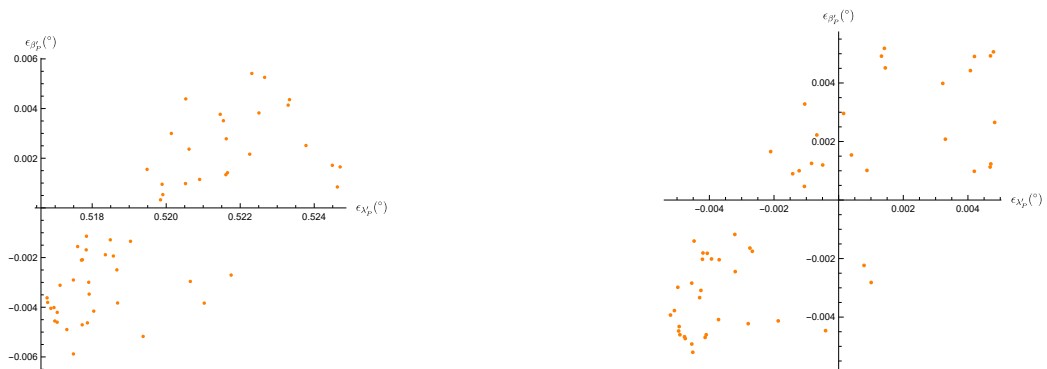


Figure 196: The Error Distribution of  $\lambda'_p$  vs  $\beta'_p$ , Error of the RF is not included on the left - included on the right.

### 5.1.4 Pasadena

2037 January 13, 03:18:17 UT



Figure 197: 3D Model of the System Created with Mathematica and Its XY Plane



Figure 198: The Distribution of Error in  $\lambda'_p$  of Asteroids with Respect to Their Distance From the Sun, Error of the RF is not included on the left - included on the right.



Figure 199: The Distribution of  $\beta'_p$  Error of Asteroids with Respect to Their Distance From the Sun, Error of the RF is not included on the left - included on the right.

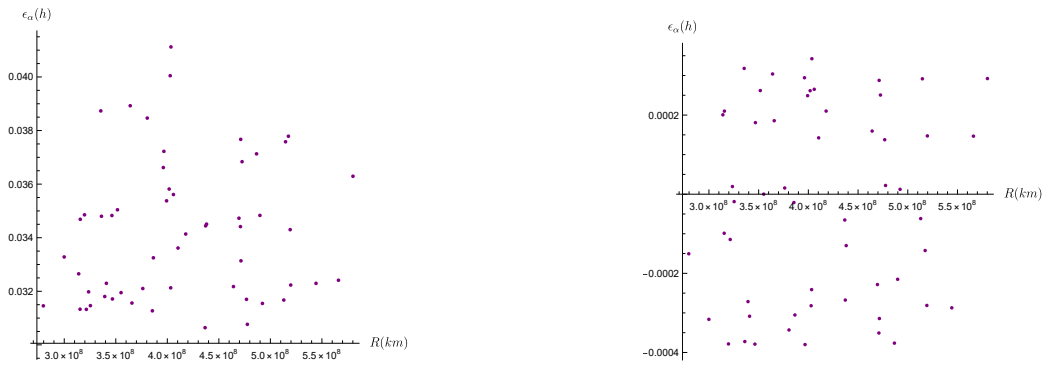


Figure 200: The Distribution of  $\alpha$  Error of Asteroids with Respect to Their Distance From the Sun, Error of the RF is not included on the left - included on the right.

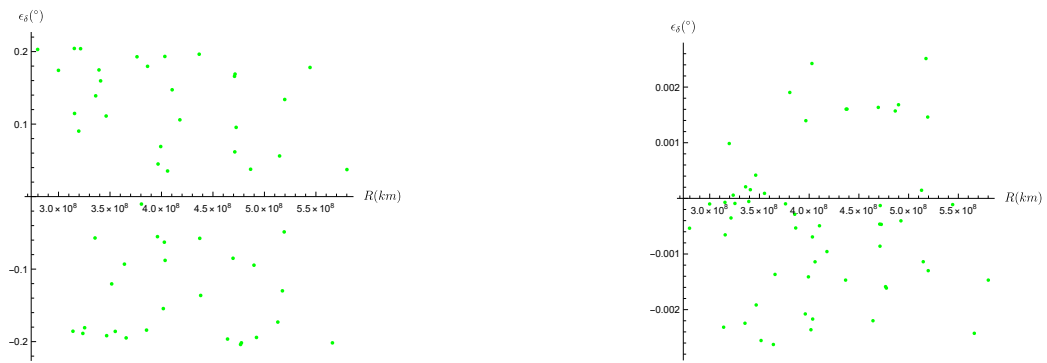


Figure 201: The Distribution of  $\delta$  Error of Asteroids with Respect to Their Distance From the Sun, Error of the RF is not included on the left - included on the right.

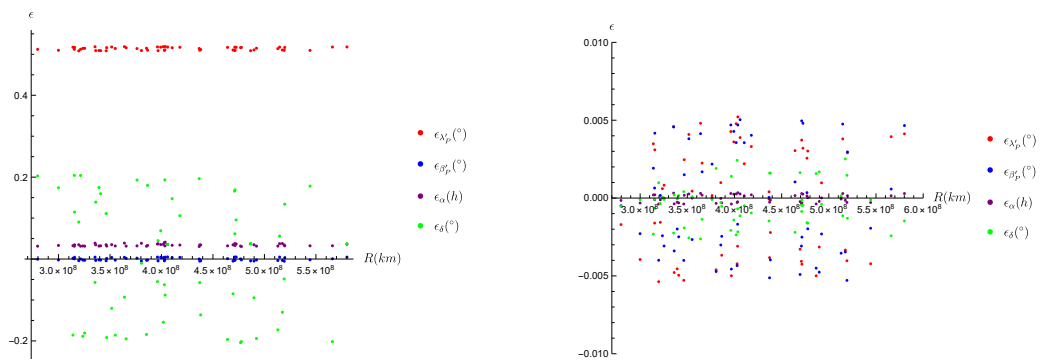


Figure 202: The Distribution of all Errors of Asteroids with Respect to Their Distance From the Sun, Error of the RF is not included on the left - included on the right.

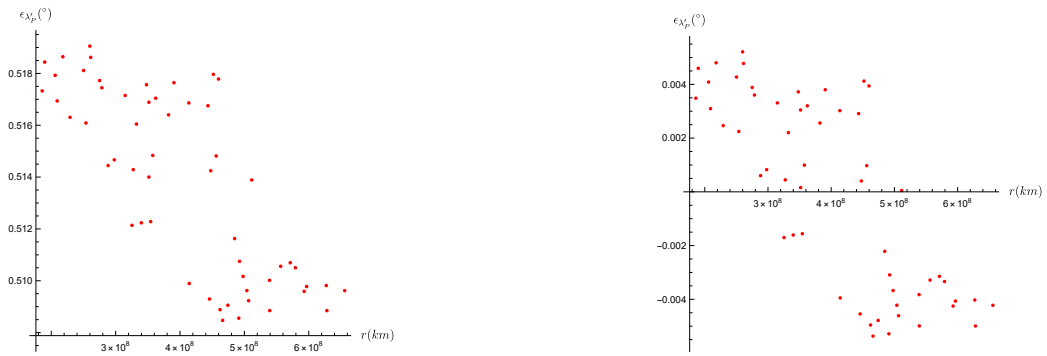


Figure 203: The Error Distribution of Error in  $\lambda'_p$  of Asteroids with Respect to Their Distance From the Earth, Error of the RF is not included on the left - included on the right.

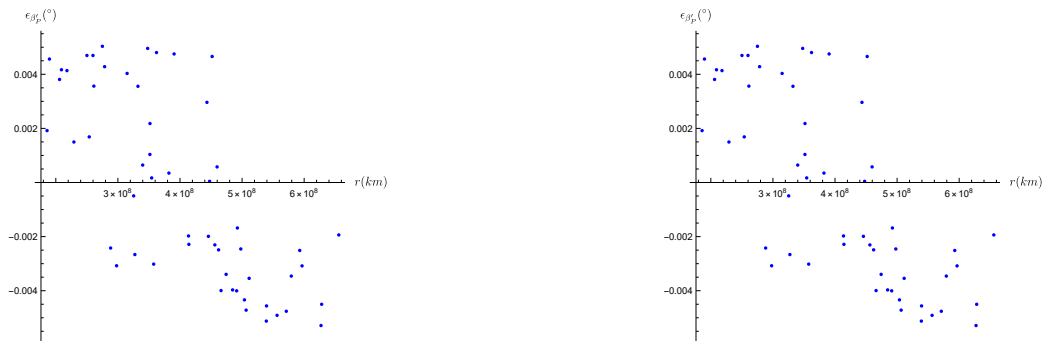


Figure 204: The Error Distribution of  $\beta'_p$  of Asteroids with Respect to Their Distance From the Earth, Error of the RF is not included on the left - included on the right.

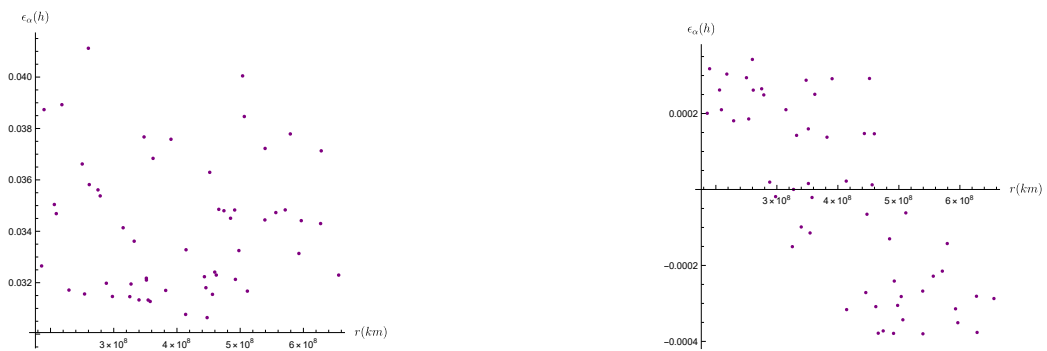


Figure 205: The Error Distribution of  $\alpha$  of Asteroids with Respect to Their Distance From the Earth, Error of the RF is not included on the left - included on the right.



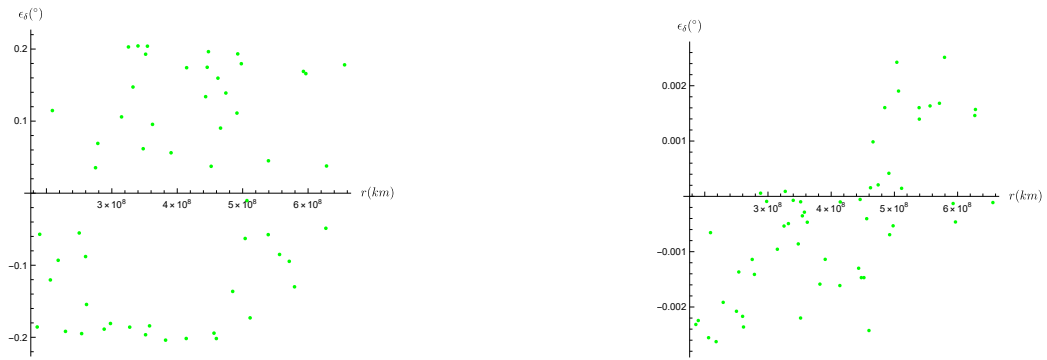


Figure 206: The Error Distribution of  $\delta$  of Asteroids with Respect to Their Distance From the Earth, Error of the RF is not included on the left - included on the right.

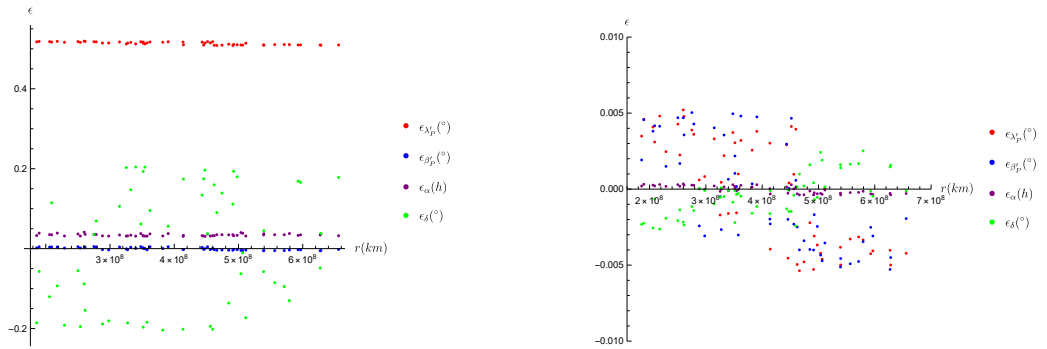


Figure 207: The Distribution of All Errors of Asteroids with Respect to Their Distance From the Earth, Error of the RF is not included on the left - included on the right.

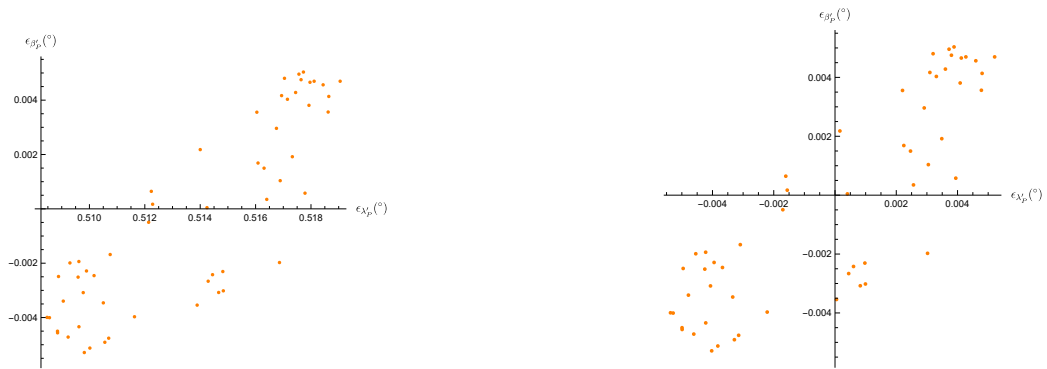


Figure 208: The Error Distribution of Error in  $\lambda'_p$  vs  $\beta'_p$ , Error of the RF is not included on the left - included on the right.

2037 April 13, 03:18:17 UT



Figure 209: 3D Model of the System Created with Mathematica and Its XY Plane



Figure 210: The Distribution of  $\lambda'_p$  Error of Asteroids with Respect to Their Distance From the Sun, Error of the RF is not included on the left - included on the right.

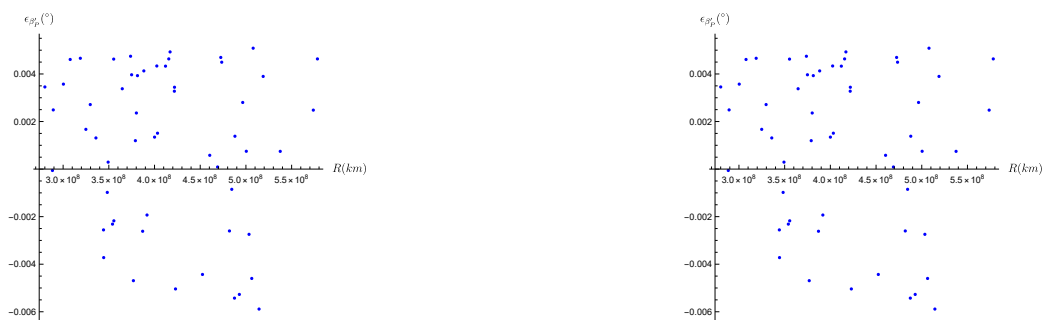


Figure 211: The Distribution of  $\beta'_p$  Error of Asteroids with Respect to Their Distance From the Sun, Error of the RF is not included on the left - included on the right.

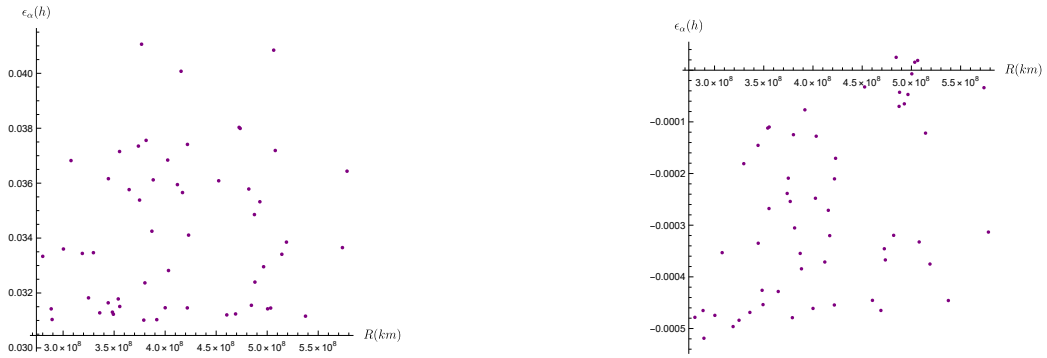


Figure 212: The Distribution of  $\alpha$  Error of Asteroids with Respect to Their Distance From the Sun, Error of the RF is not included on the left - included on the right.

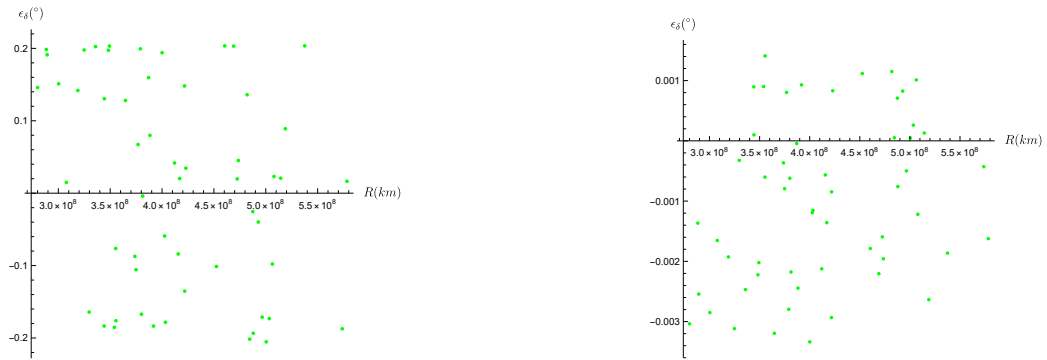


Figure 213: The Distribution of  $\delta$  Error of Asteroids with Respect to Their Distance From the Sun, Error of the RF is not included on the left - included on the right.

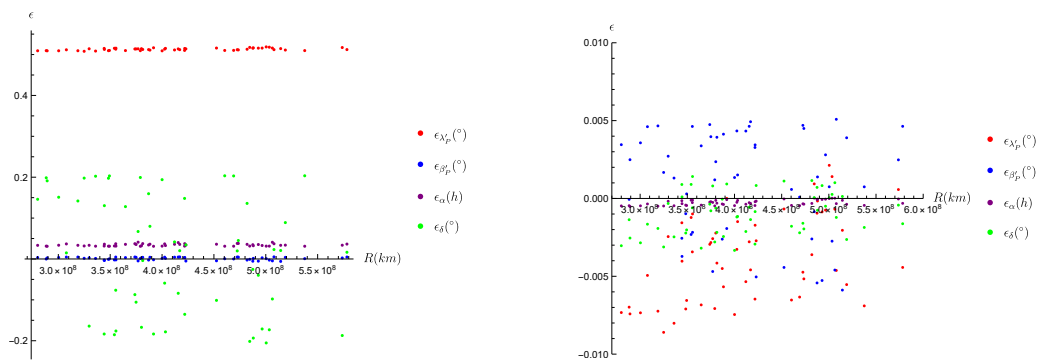


Figure 214: The Distribution of all Errors of Asteroids with Respect to Their Distance From the Sun, Error of the RF is not included on the left - included on the right.



Figure 215: The Error Distribution of  $\lambda'_p$  of Asteroids with Respect to Their Distance From the Spacecraft, Error of the RF is not included on the left - included on the right.



Figure 216: The Error Distribution of  $\beta'_p$  of Asteroids with Respect to Their Distance From the Spacecraft, Error of the RF is not included on the left - included on the right.



Figure 217: The Error Distribution of  $\alpha$  of Asteroids with Respect to Their Distance From the Spacecraft, Error of the RF is not included on the left - included on the right.

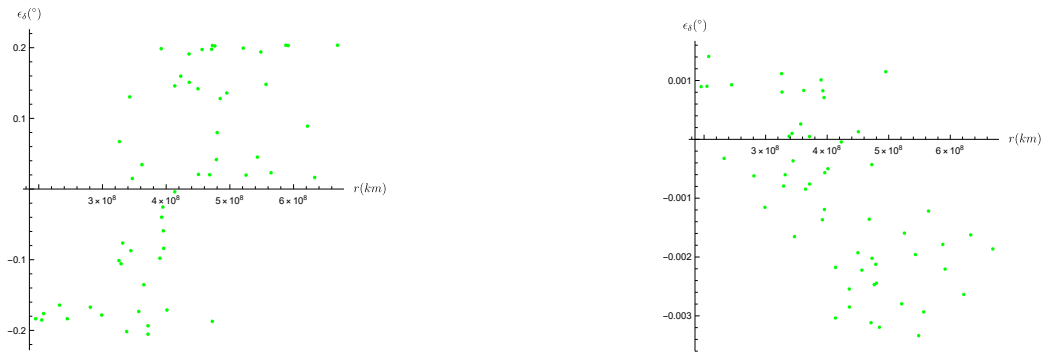


Figure 218: The Error Distribution of  $\delta$  of Asteroids with Respect to Their Distance From the Spacecraft, Error of the RF is not included on the left - included on the right.

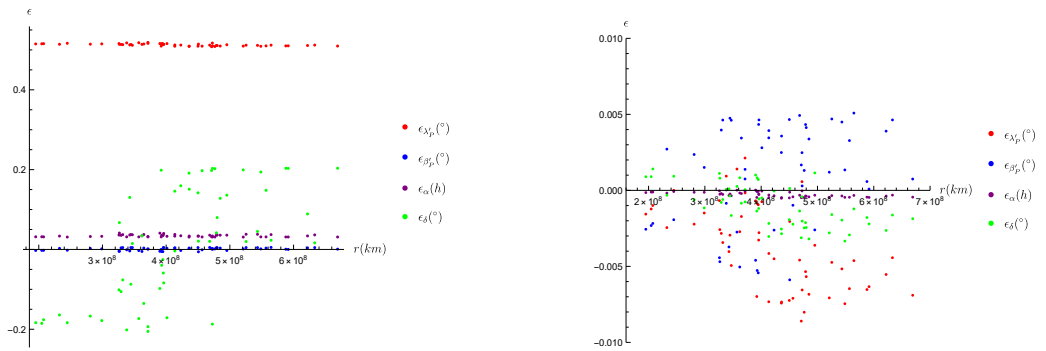


Figure 219: The Distribution of all errors of Asteroids with Respect to Their Distance From the Spacecraft, Error of the RF is not included on the left - included on the right.



Figure 220: The Error Distribution of  $\lambda'_p$  vs  $\beta'_p$ , Error of the RF is not included on the left - included on the right.

2037 July 13, 03:18:17 UT

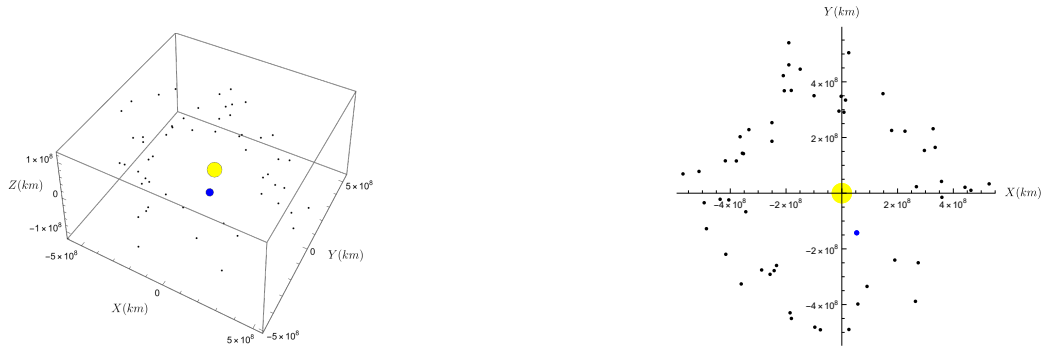


Figure 221: 3D Model of the System Created with Mathematica and Its XY Plane



Figure 222: The Distribution of  $\lambda'_p$  Error of Asteroids with Respect to Their Distance From the Sun, Error of the RF is not included on the left - included on the right.



Figure 223: The Distribution of  $\beta'_p$  Error of Asteroids with Respect to Their Distance From the Sun, Error of the RF is not included on the left - included on the right.

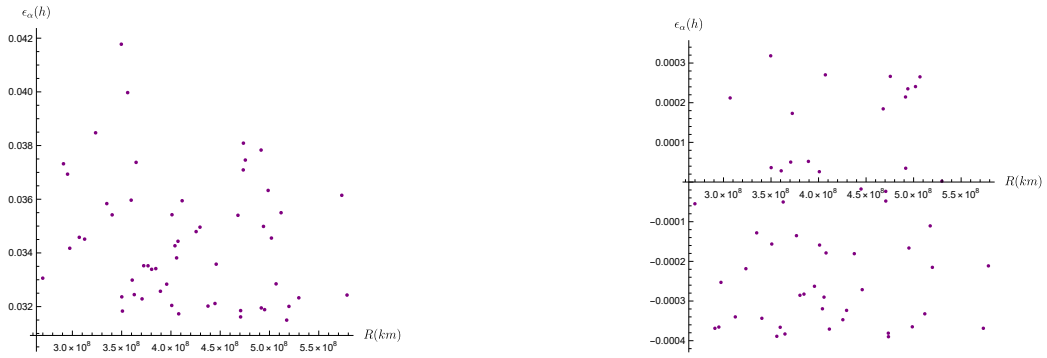


Figure 224: The Distribution of  $\alpha$  Error of Asteroids with Respect to Their Distance From the Sun, Error of the RF is not included on the left - included on the right.

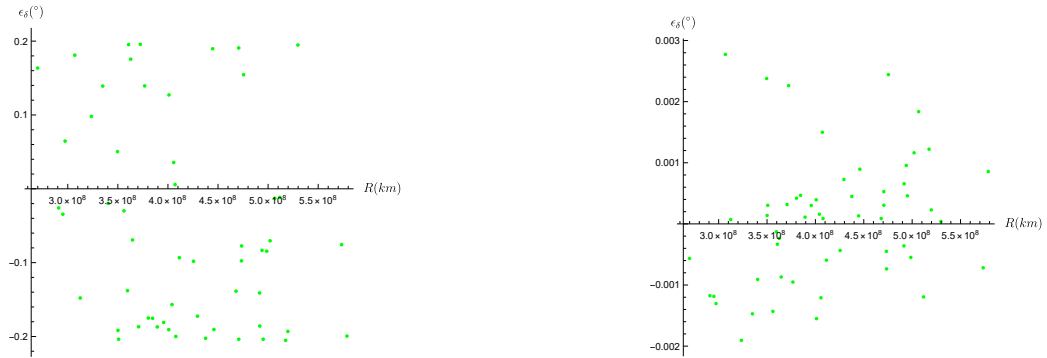


Figure 225: The Distribution of  $\delta$  Error of Asteroids with Respect to Their Distance From the Sun, Error of the RF is not included on the left - included on the right.

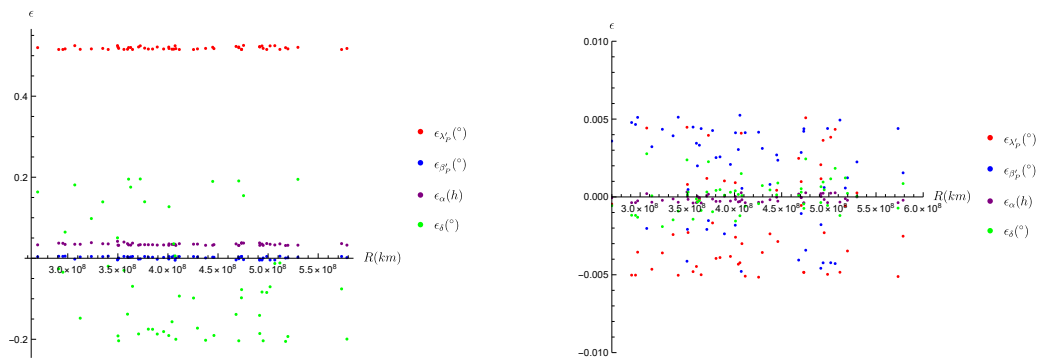


Figure 226: The Distribution of all Errors of Asteroids with Respect to Their Distance From the Sun, Error of the RF is not included on the left - included on the right.



Figure 227: The Error Distribution of  $\lambda'_p$  of Asteroids with Respect to Their Distance From the Spacecraft, Error of the RF is not included on the left - included on the right.

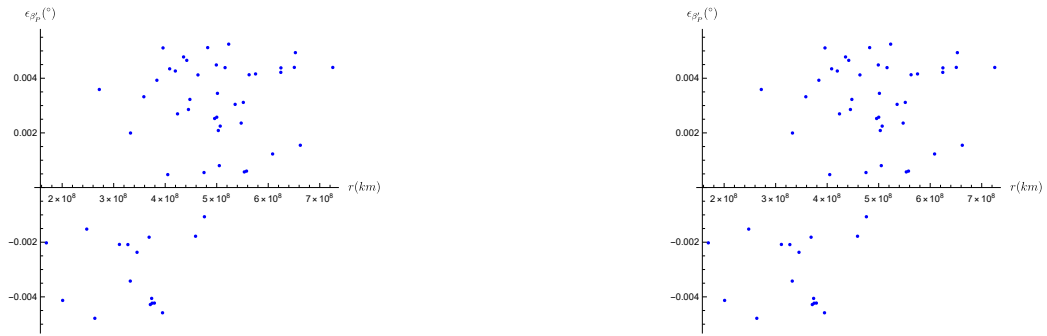


Figure 228: The Error Distribution of  $\beta'_p$  of Asteroids with Respect to Their Distance From the Spacecraft, Error of the RF is not included on the left - included on the right.



Figure 229: The Error Distribution of  $\alpha$  of Asteroids with Respect to Their Distance From the Spacecraft, Error of the RF is not included on the left - included on the right.





Figure 230: The Error Distribution of  $\delta$  of Asteroids with Respect to Their Distance From the Spacecraft, Error of the RF is not included on the left - included on the right.

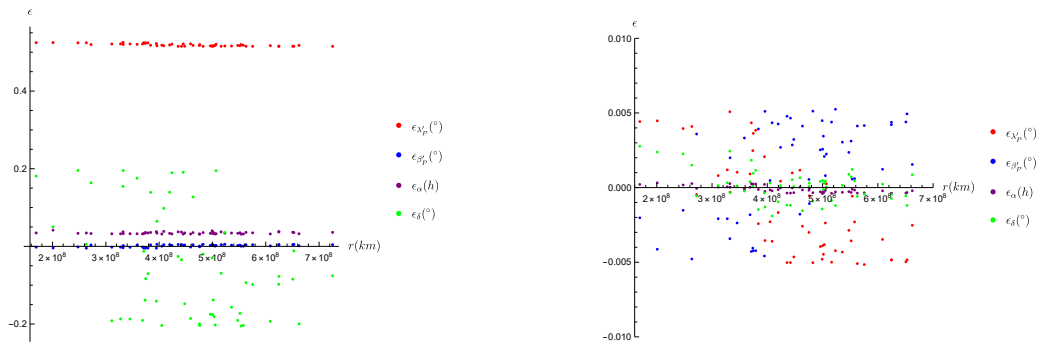


Figure 231: The Distribution of All Errors of Asteroids with Respect to Their Distance From the Spacecraft, Error of the RF is not included on the left - included on the right.

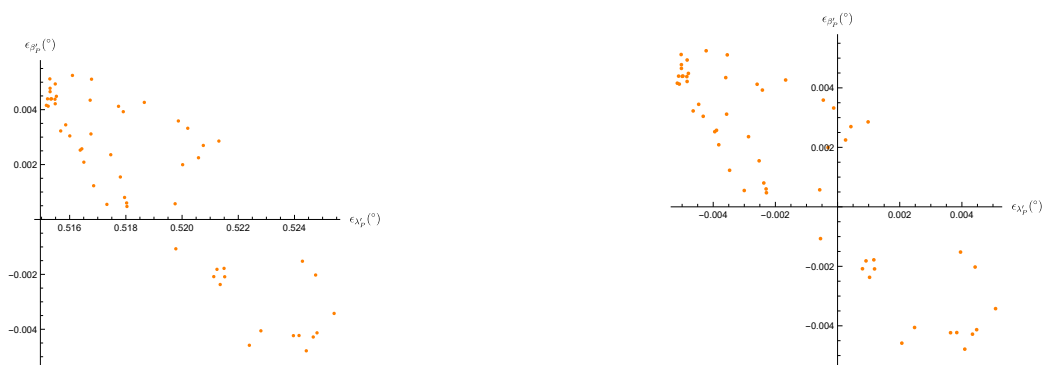


Figure 232: The Error Distribution of  $\lambda'_p$  vs  $\beta'_p$ , Error of the RF is not included on the left - included on the right.

2037 October 13, 03:18:17 UT

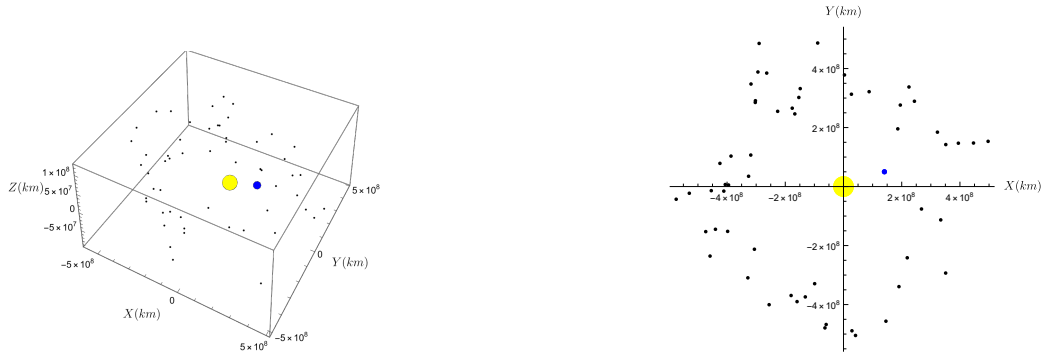


Figure 233: 3D Model of the System Created with Mathematica and Its XY Plane



Figure 234: The Distribution of  $\lambda'_p$  Error of Asteroids with Respect to Their Distance From the Sun, Error of the RF is not included on the left - included on the right.

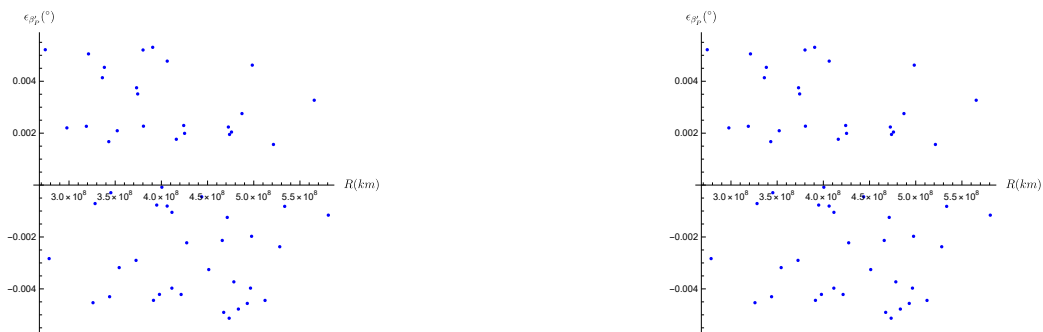


Figure 235: The Distribution of  $\beta'_p$  Error of Asteroids with Respect to Their Distance From the Sun, Error of the RF is not included on the left - included on the right.

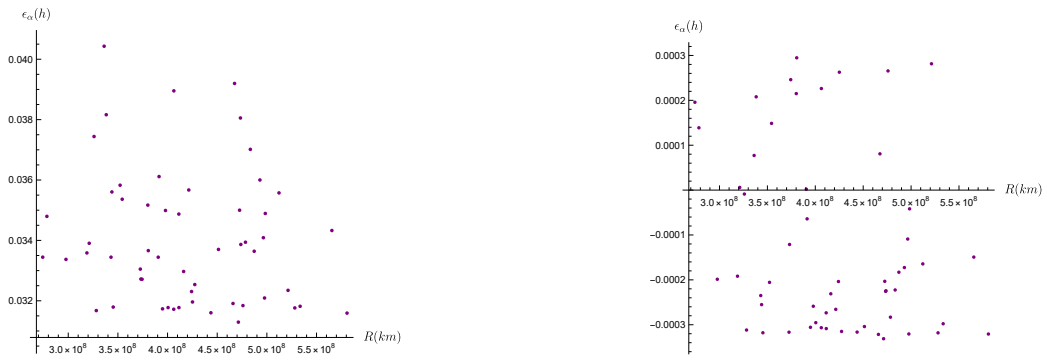


Figure 236: The Distribution of  $\alpha$  Error of Asteroids with Respect to Their Distance From the Sun, Error of the RF is not included on the left - included on the right.

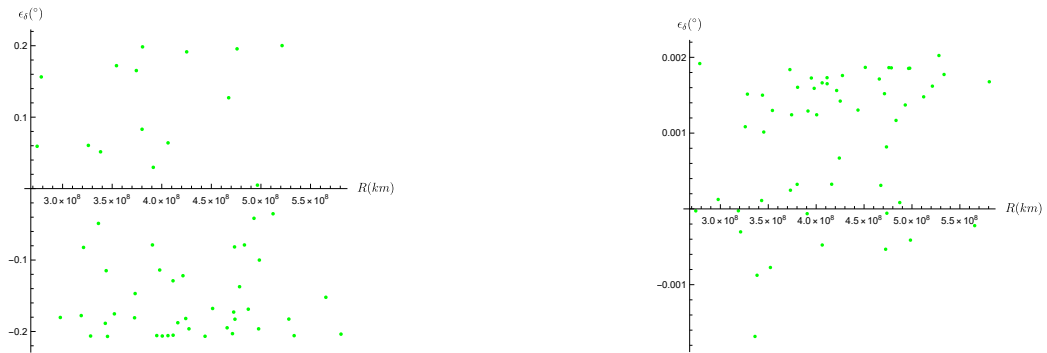


Figure 237: The Distribution of  $\delta$  Error of Asteroids with Respect to Their Distance From the Sun, Error of the RF is not included on the left - included on the right.

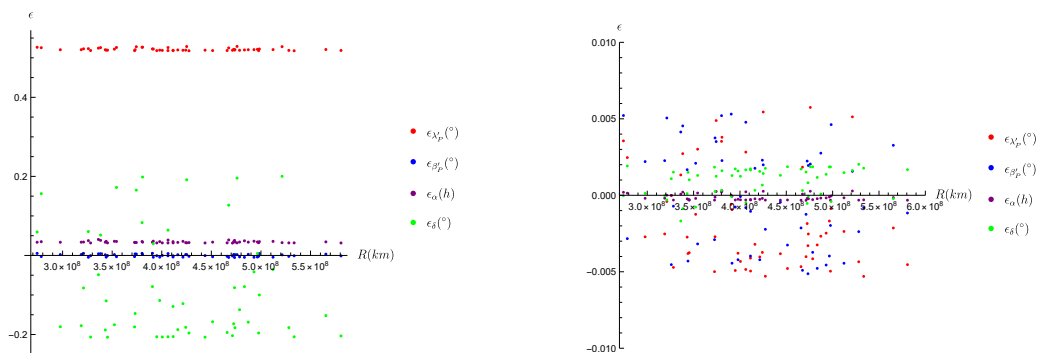


Figure 238: The Distribution of all Errors of Asteroids with Respect to Their Distance From the Sun, Error of the RF is not included on the left - included on the right.

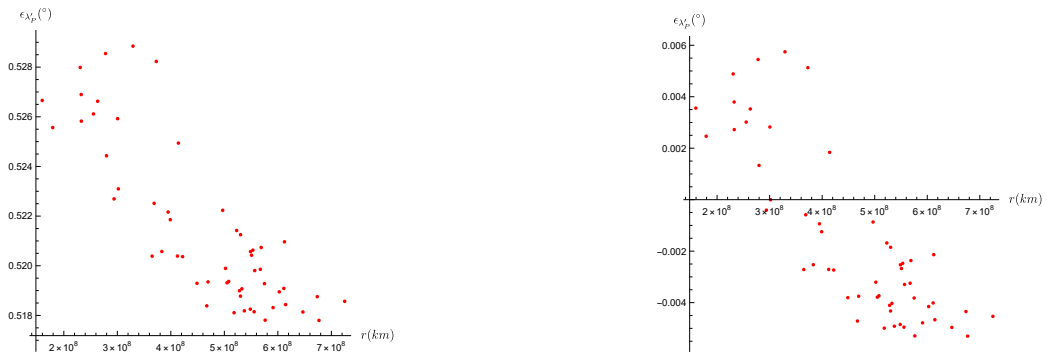


Figure 239: The Error Distribution of  $\lambda'_p$  of Asteroids with Respect to Their Distance From the Spacecraft, Error of the RF is not included on the left - included on the right.

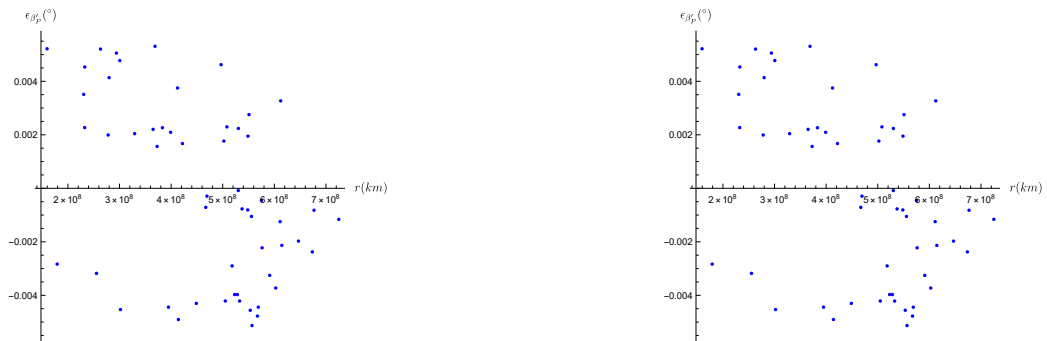


Figure 240: The Distribution of Error in  $\beta'_p$  of Asteroids with Respect to Their Distance From the Spacecraft, Error of the RF is not included on the left - included on the right.

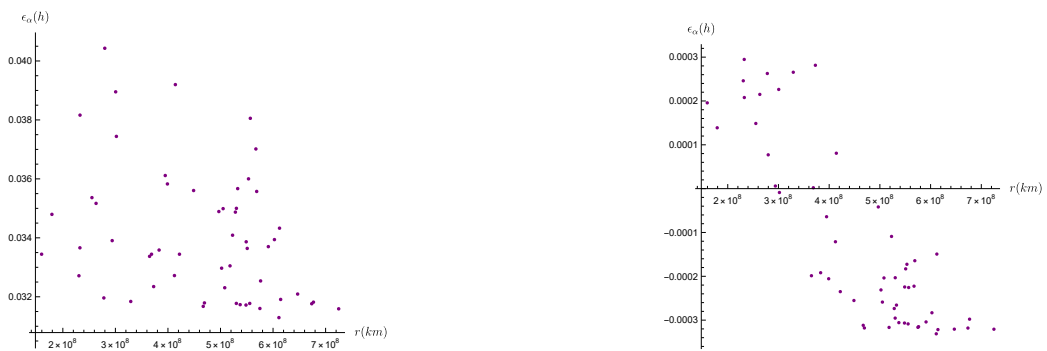


Figure 241: The Distribution of Error in  $\alpha$  of Asteroids with Respect to Their Distance From the Spacecraft, Error of the RF is not included on the left - included on the right.

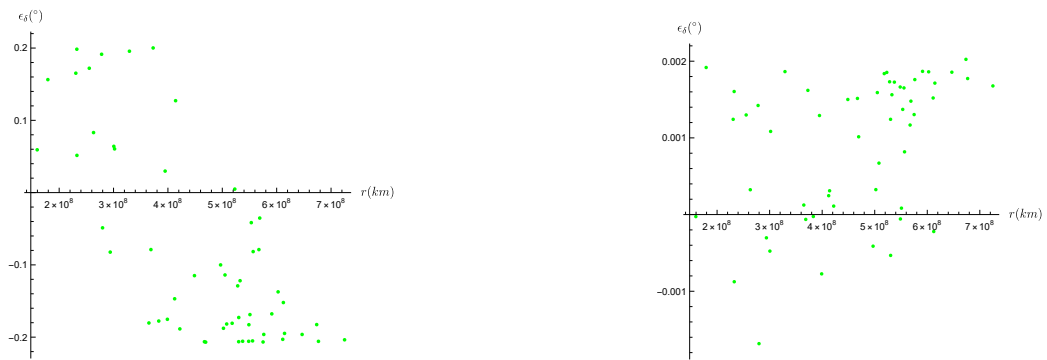


Figure 242: The Distribution of Error in  $\delta$  of Asteroids with Respect to Their Distance From the Spacecraft, Error of the RF is not included on the left - included on the right.

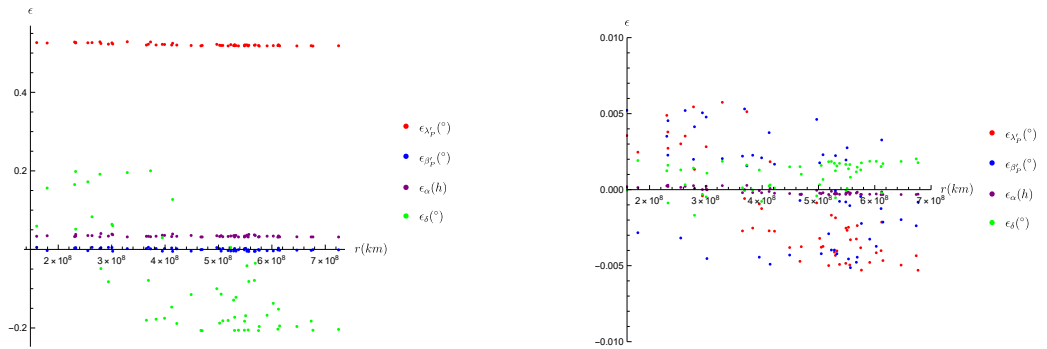


Figure 243: The Distribution of All Errors of Asteroids with Respect to Their Distance From the Spacecraft, Error of the RF is not included on the left - included on the right.

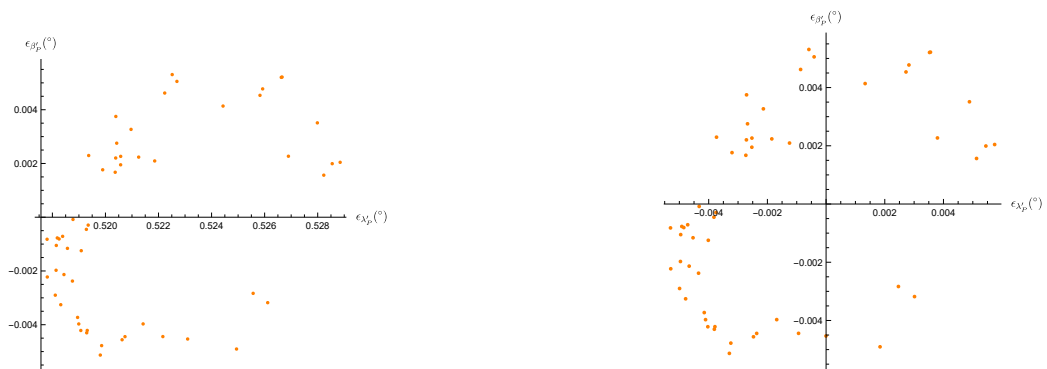


Figure 244: The Error Distribution of  $\lambda'_p$  vs  $\beta'_p$ , Error of the RF is not included on the left - included on the right.

2037 November 13, 03:18:17 UT



Figure 245: 3D Model of the System Created with Mathematica and Its XY Plane



Figure 246: The Distribution of  $\lambda'_p$  Error of Asteroids with Respect to Their Distance From the Sun, Error of the RF is not included on the left - included on the right.

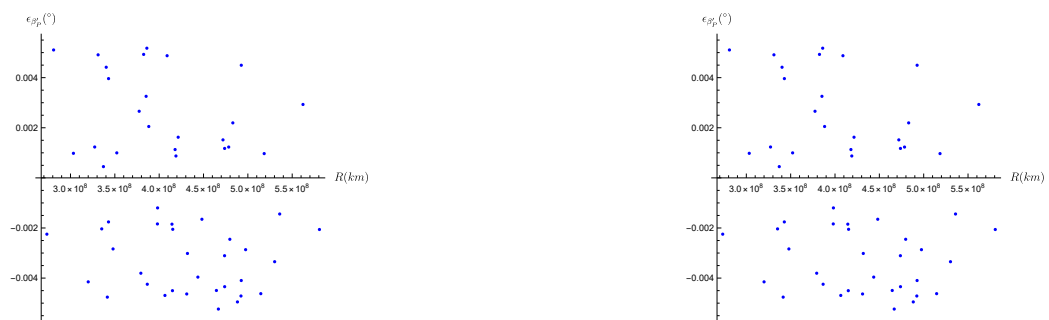


Figure 247: The Distribution of  $\beta'_p$  Error of Asteroids with Respect to Their Distance From the Sun, Error of the RF is not included on the left - included on the right.

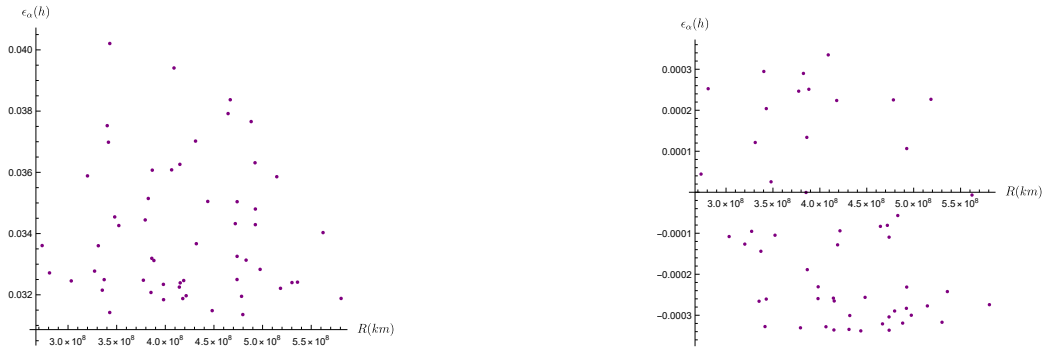


Figure 248: The Distribution of  $\alpha$  Error of Asteroids with Respect to Their Distance From the Sun, Error of the RF is not included on the left - included on the right.

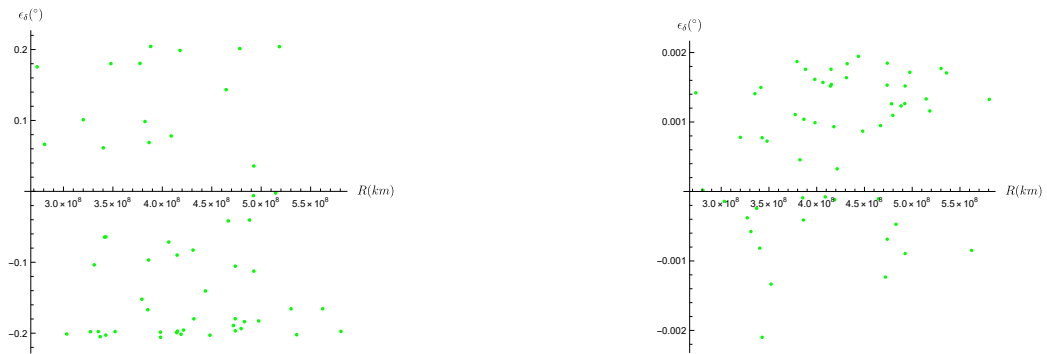


Figure 249: The Distribution of  $\delta$  Error of Asteroids with Respect to Their Distance From the Sun, Error of the RF is not included on the left - included on the right.

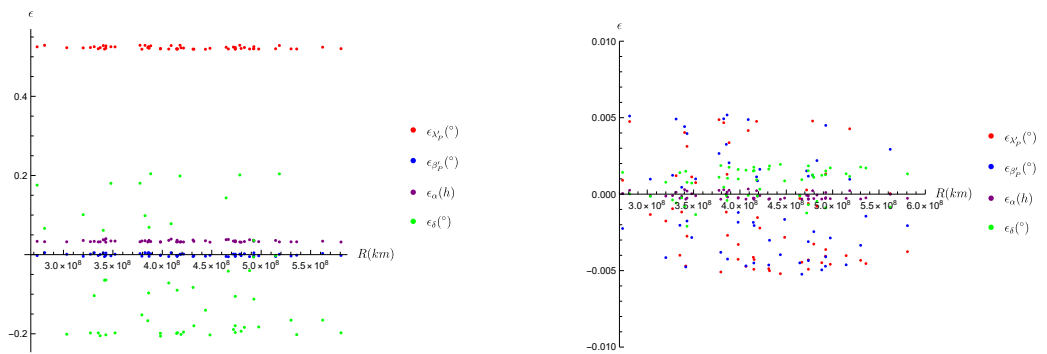


Figure 250: The Distribution of all Errors of Asteroids with Respect to Their Distance From the Sun, Error of the RF is not included on the left - included on the right.

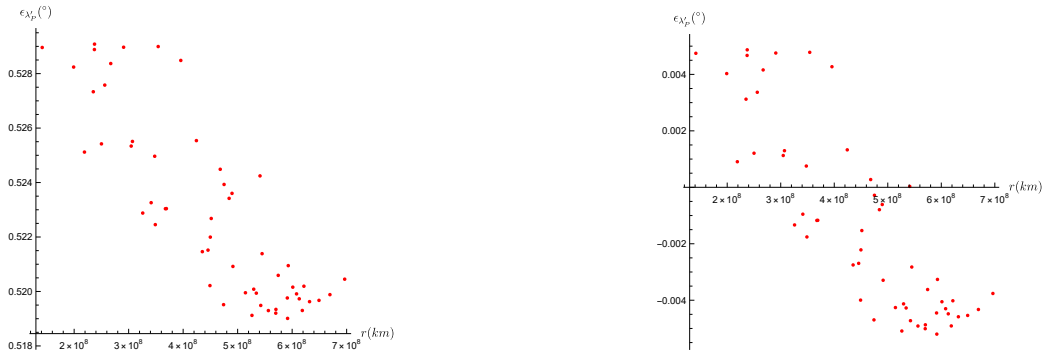


Figure 251: The Error Distribution of  $\lambda'_p$  of Asteroids with Respect to Their Distance From the Spacecraft, Error of the RF is not included on the left - included on the right.

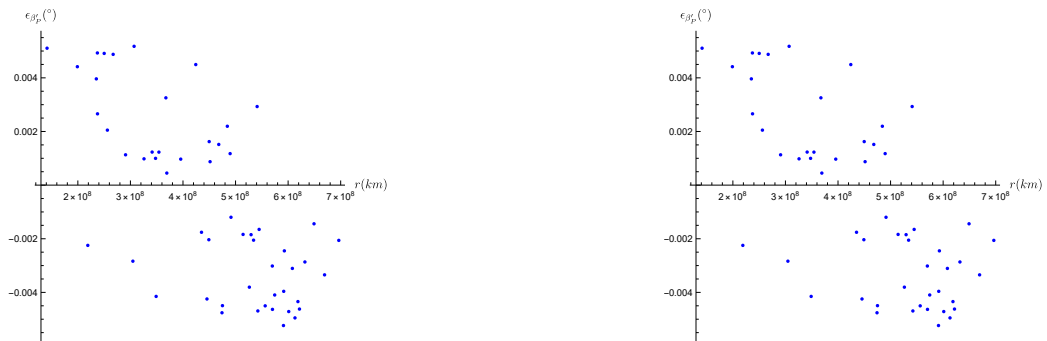


Figure 252: The Distribution of Error in  $\beta'_p$  of Asteroids with Respect to Their Distance From the Spacecraft, Error of the RF is not included on the left - included on the right.

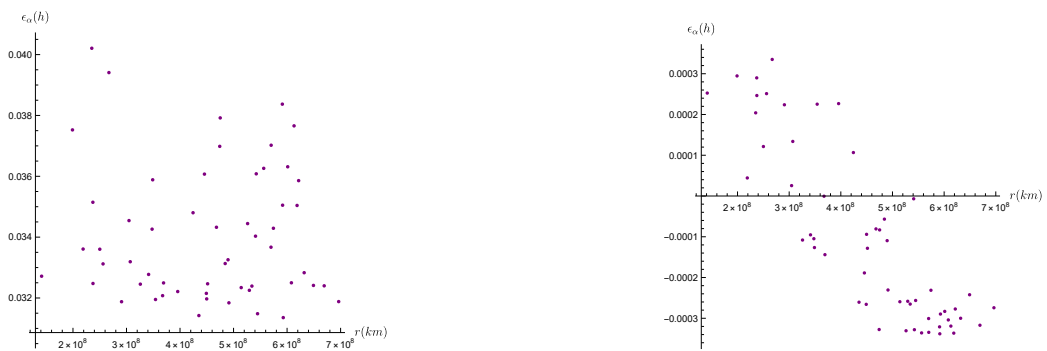


Figure 253: The Distribution of Error in  $\alpha$  of Asteroids with Respect to Their Distance From the Spacecraft, Error of the RF is not included on the left - included on the right.



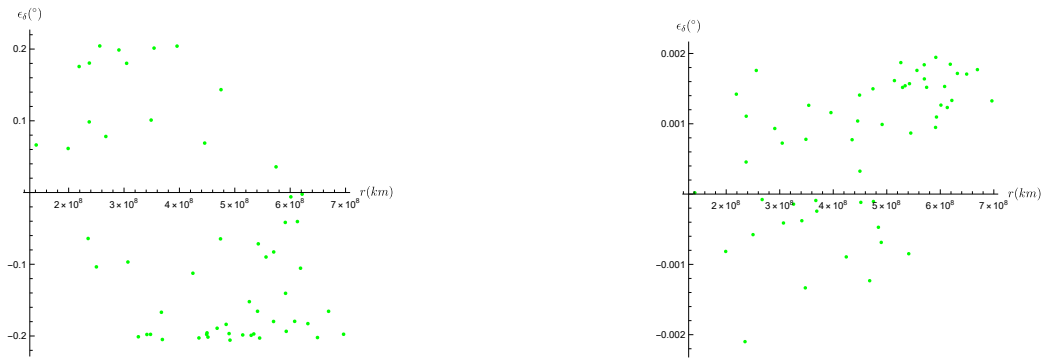


Figure 254: The Distribution of Error in  $\delta$  of Asteroids with Respect to Their Distance From the Spacecraft, Error of the RF is not included on the left - included on the right.

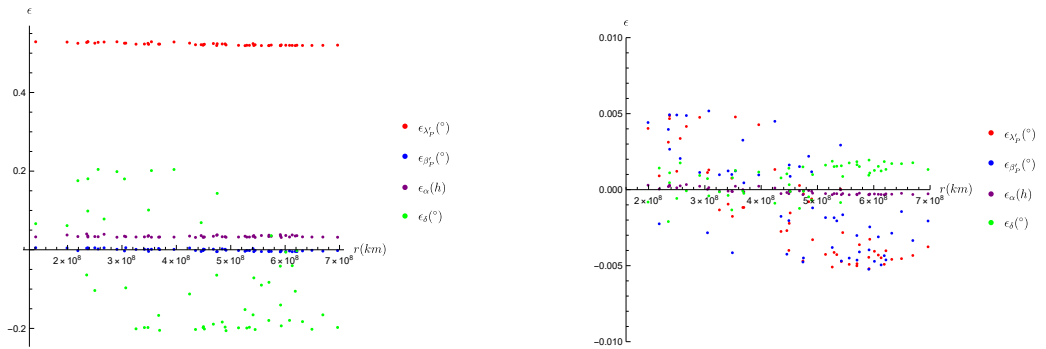


Figure 255: The Distribution of All Errors of Asteroids with Respect to Their Distance From the Spacecraft, Error of the RF is not included on the left - included on the right.

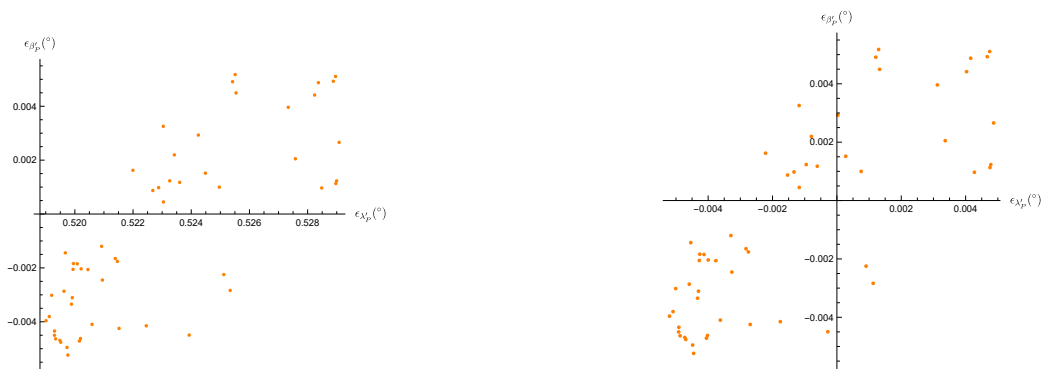


Figure 256: The Distribution of Error in  $\lambda'_p$  vs  $\beta'_p$ , Error of the RF is not included on the left - included on the right.

### 5.1.5 Non-Earth Case: Ceres

In this case the center of the coordinates system is chosen as asteroid 1 Ceres for epoch 2023 June 19, 10:00:00. Hence the number of beacon asteroids are decreased to 54.

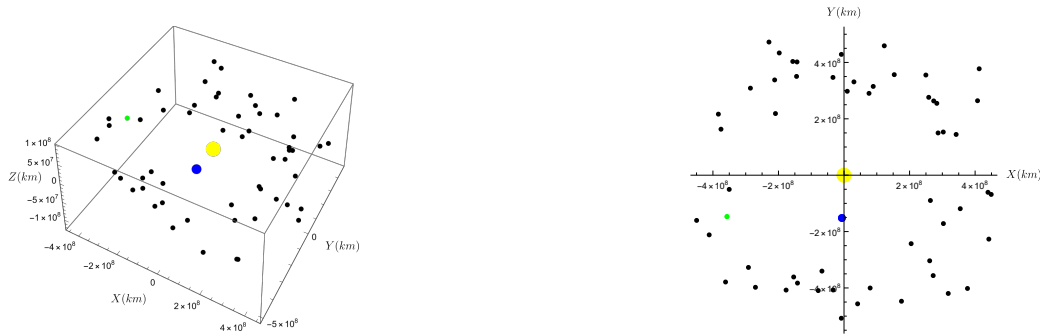


Figure 257: 3D Model of the System Created with Mathematica and Its XY Plane

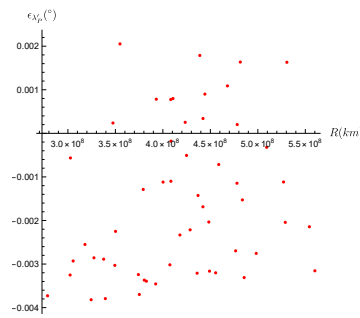


Figure 258: The Distribution of Error in  $\lambda'_p$  of Asteroids with Respect to Their Distance From the Sun.

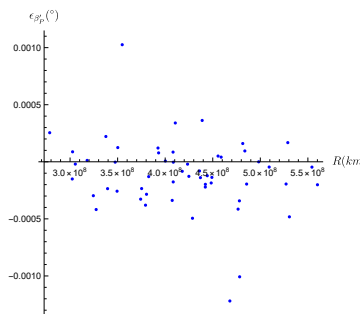


Figure 259: The Distribution of  $\beta'_p$  Error of Asteroids with Respect to Their Distance From the Sun..

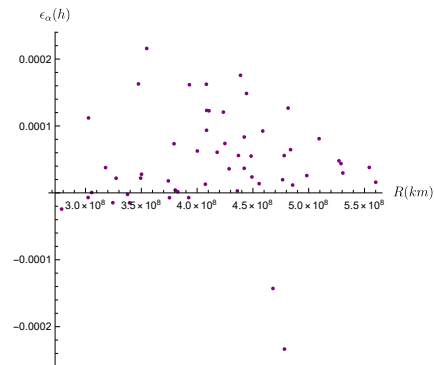


Figure 260: The Distribution of  $\alpha$  Error of Asteroids with Respect to Their Distance From the Sun.

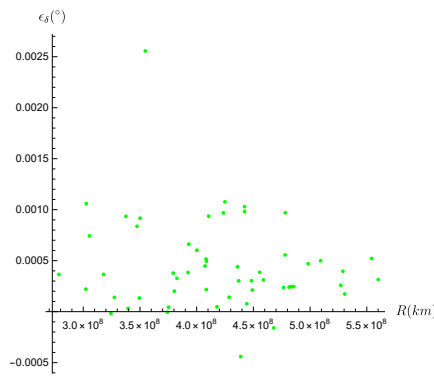


Figure 261: The Distribution in  $\delta$  Asteroids with Respect to Their Distance From the Sun.

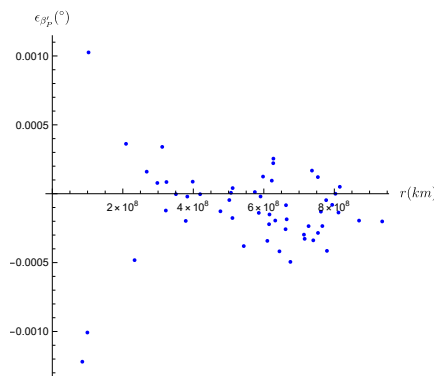


Figure 262: The Error Distribution in  $\beta'_p$  of Asteroids with Respect to Their Distance From the Earth.

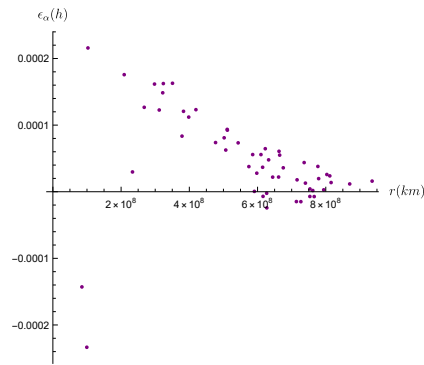


Figure 263: The Error Distribution in  $\alpha$  of Asteroids with Respect to Their Distance From the Earth.

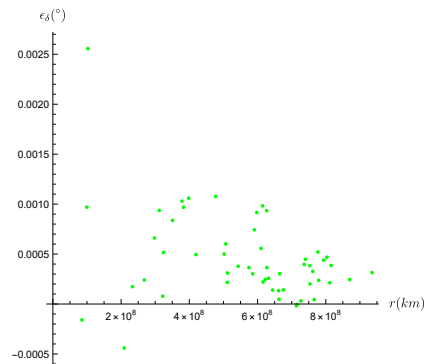


Figure 264: The Error Distribution of  $\delta$  of Asteroids with Respect to Their Distance From the Earth.

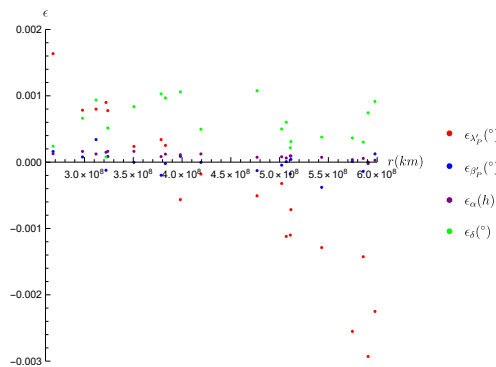


Figure 265: The Distribution of All Errors of Asteroids with Respect to Their Distance From the Earth.

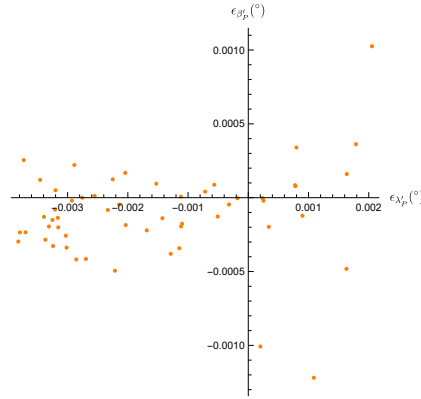


Figure 266: The Error Distribution of  $\lambda'_p$  vs  $\beta'_p$ .

## 5.2 Inverse Problem Results

Inverse Problem can be solved and exemplified. To give an example, the example 5.1.1 can be used. By knowing the topocentric celestial coordinates, the heliocentric cartesian coordinates of the observer can be calculated. To take it easy, we shall use the data we created on the same example which was

$$\alpha = 13.7592 \text{ h},$$

$$\delta = 4.55692^\circ$$

As the topocentric coordinates of the Sun which could be determined via observations will be used to solve the problem, it is possible to use  $\lambda'_S = 23.0246^\circ$  and  $\beta'_S = -0.00474834^\circ$  from the solution of the direct problem.

In inverse problem, the heliocentric cartesian coordinates of the asteroid (1) Ceres are known which is:

$$X_{Ceres} = -3.57411 \times 10^8 \text{ km},$$

$$Y_{Ceres} = -1.48438 \times 10^8 \text{ km},$$

$$Z_{Ceres} = 6.09816 \times 10^8 \text{ km},$$

Hence, the heliocentric ecliptic coordinates of the asteroid is

$$\lambda_P = 202.554^\circ,$$

$$\beta_P = 8.95454^\circ$$

By using equations 33 and 34, the topocentric ecliptic coordinates of the asteroid can be determined.

$$\lambda'_p = 202.725^\circ,$$

$$\beta'_p = 14.4255^\circ.$$

With this data, the distance from the Sun, so the heliocentric cartesian coordinates of the observer can be calculated. (See Sec 4.4)

$$r = 1.49997 \times 10^8 \text{ km},$$

$$X = -1.38048 \times 10^8 \text{ km},$$

$$Y = -5.86679 \times 10^7 \text{ km},$$

$$Z = 12430.9 \text{ km},$$

The error can also be calculated, for (1) Ceres:

$$e_r = 1.49012 \times 10^{-6} \text{ km},$$

$$e_x = -1.37091 \times 10^{-6} \text{ km},$$

$$e_y = -5.36442 \times 10^{-7} \text{ km},$$

$$e_z = 1.21872 \times 10^{-10} \text{ km},$$

The figures below will show the relationship between  $e_r$ ,  $e_x$ ,  $e_y$  and  $e_z$  and other parameters such as topocentric ecliptic coordinates of the asteroid. In those figures, in order to have more accurate results, error is included. (See Sec [4.3.1](#))

## 5.2.1 Uppsala

2037 January 13, 03:18:17 UT

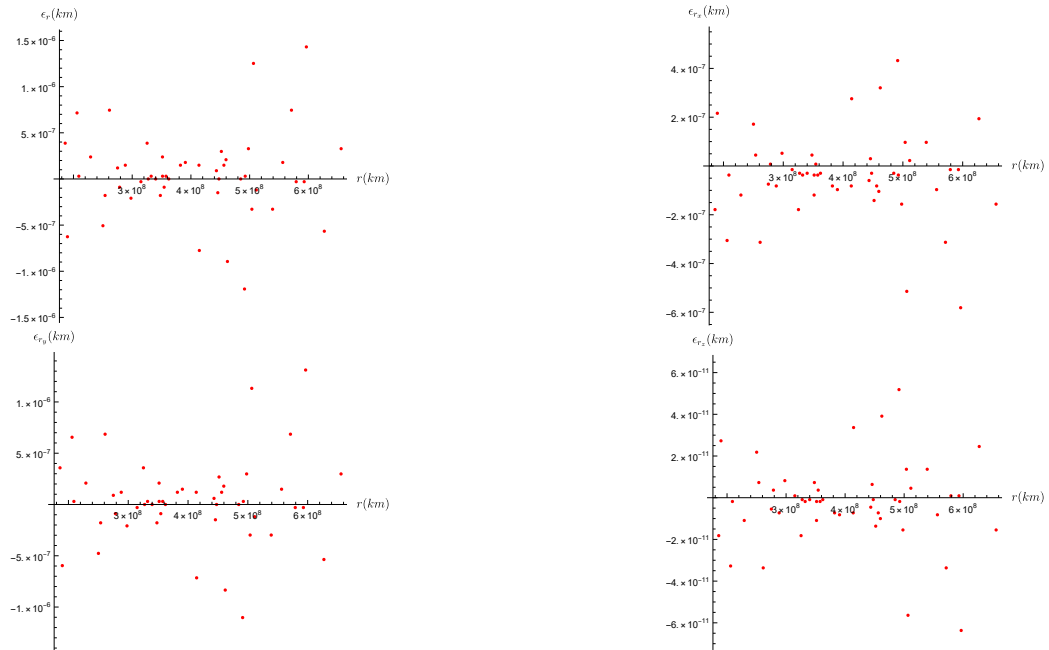


Figure 267: Errors  $e_r$  (Top Left),  $e_x$  (Top Right),  $e_y$  (Bottom Left) and  $e_z$  (Bottom Right) vs The Distance Between Observer and Asteroids

2037 April 13, 03:18:17 UT

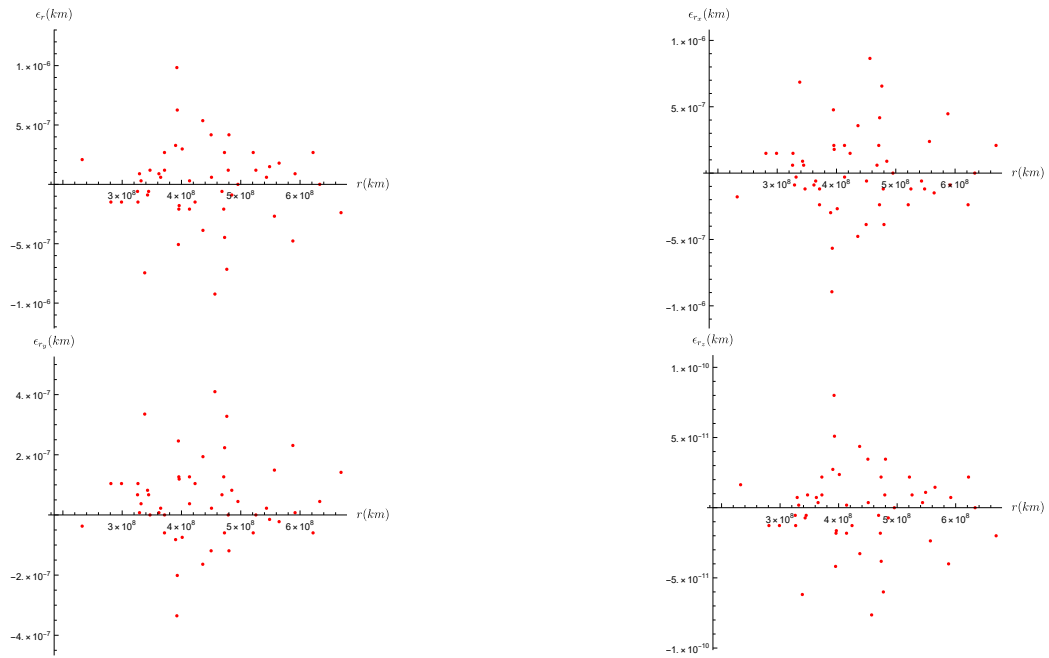


Figure 268: Errors  $e_r$  (Top Left),  $e_x$  (Top Right),  $e_y$  (Bottom Left) and  $e_z$  (Bottom Right) vs The Distance Between Observer and Asteroids



2037 July 13, 03:18:17 UT

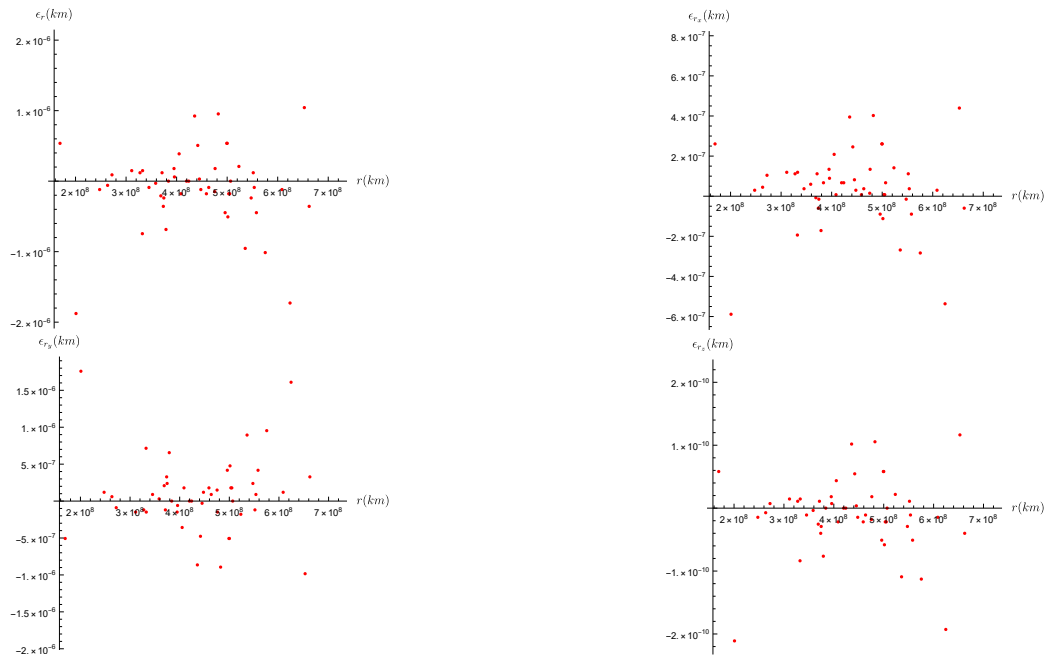


Figure 269: Errors  $e_r$  (Top Left),  $e_x$  (Top Right),  $e_y$  (Bottom Left) and  $e_z$  (Bottom Right) vs The Distance Between Observer and Asteroids

2037 October 13, 03:18:17 UT

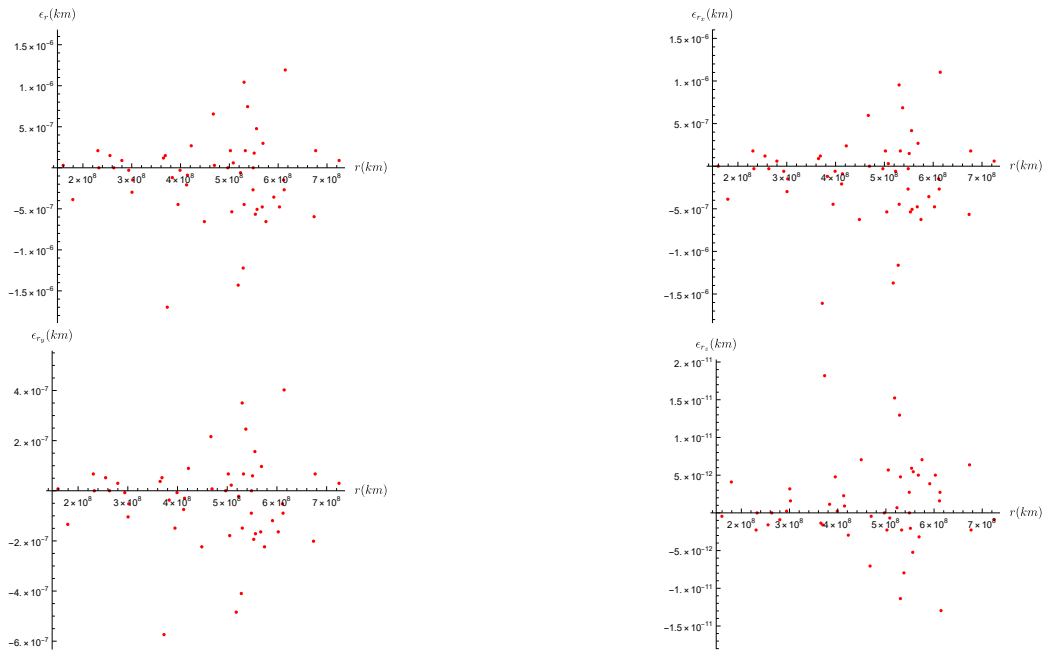


Figure 270: Errors  $e_r$  (Top Left),  $e_x$  (Top Right),  $e_y$  (Bottom Left) and  $e_z$  (Bottom Right) vs The Distance Between Observer and Asteroids

2037 November 13, 03:18:17 UT

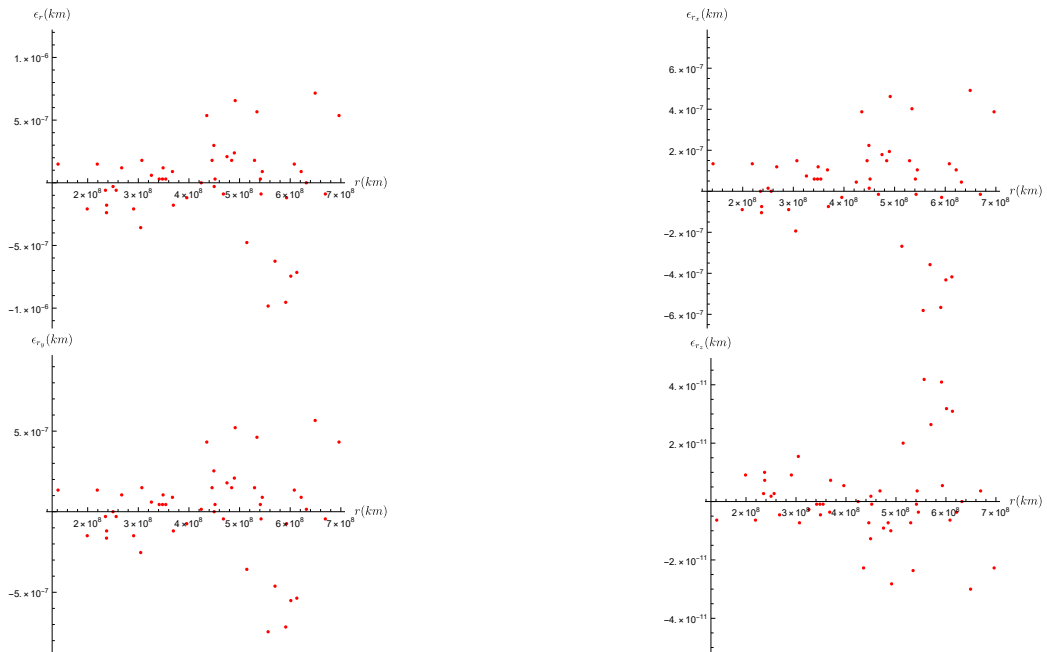


Figure 271: Errors  $e_r$  (Top Left),  $e_x$  (Top Right),  $e_y$  (Bottom Left) and  $e_z$  (Bottom Right) vs The Distance Between Observer and Asteroids

**Topocentric Ecliptic Longitude ( $\lambda'_p$ ) vs Error in The Heliocentric Distance ( $e_r$ )**

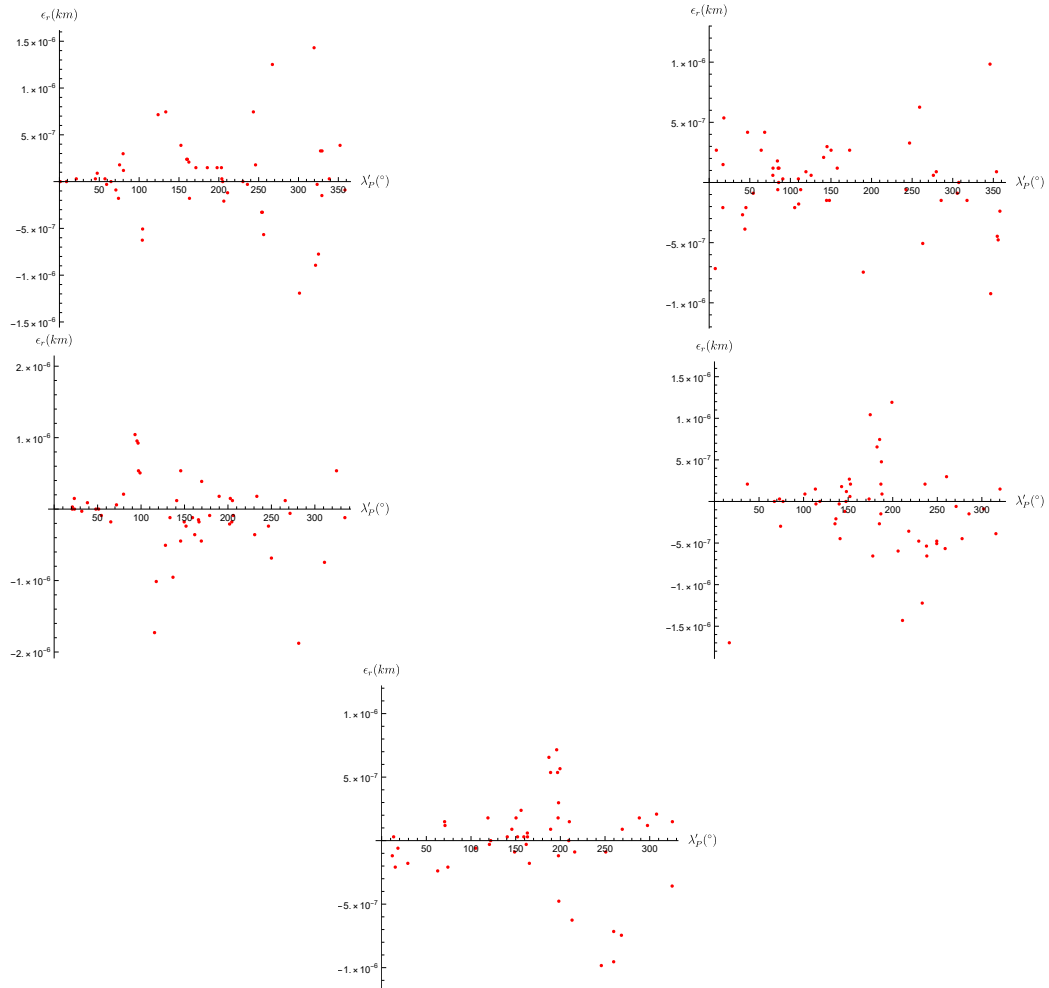


Figure 272: January-2037 (Top Left), April-2037 (Top Right), July-2037 (Middle Left), October-2037 (Middle Right), November-2037 (Bottom)

## 5.2.2 Urla

2037 January 13, 03:18:17 UT

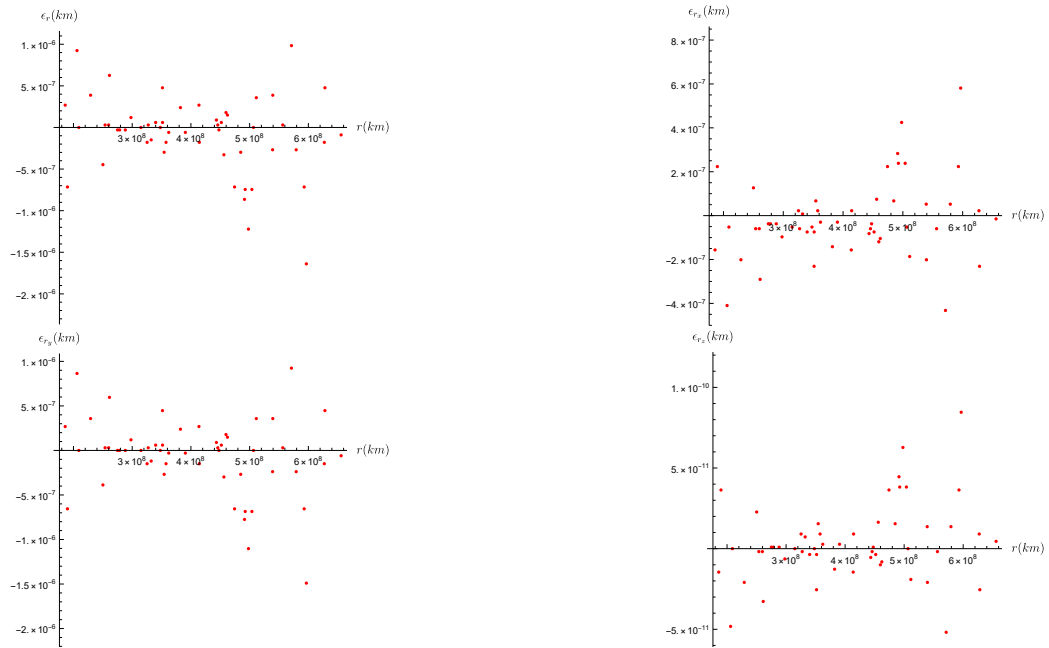


Figure 273: Errors  $e_r$  (Top Left),  $e_x$  (Top Right),  $e_y$  (Bottom Left) and  $e_z$  (Bottom Right) vs The Distance Between Observer and Asteroids

2037 April 13, 03:18:17 UT

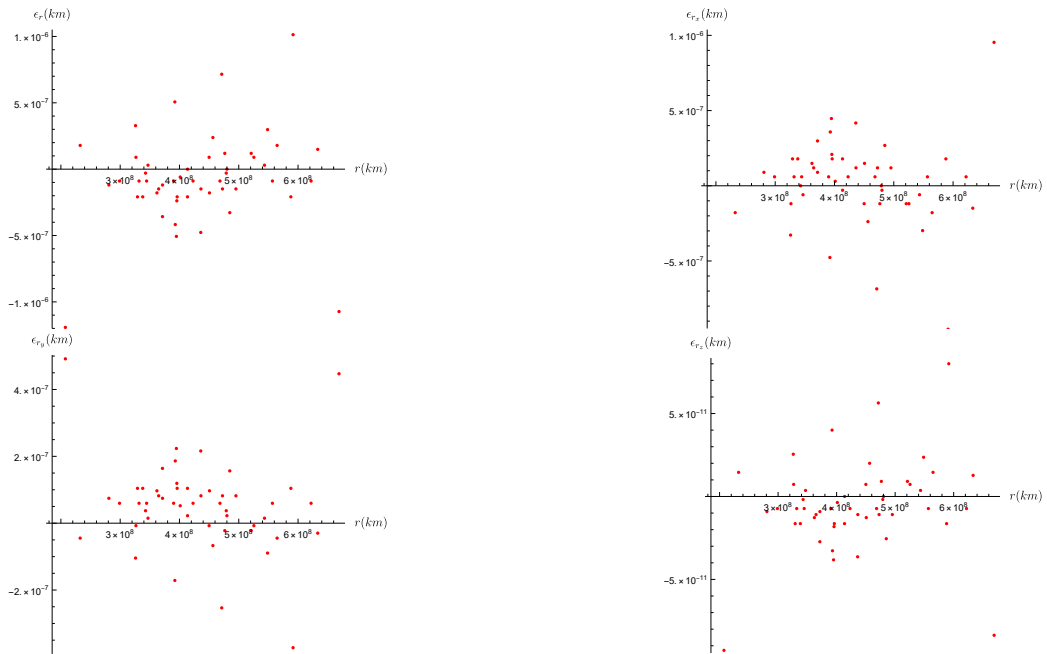


Figure 274: Errors  $e_r$  (Top Left),  $e_x$  (Top Right),  $e_y$  (Bottom Left) and  $e_z$  (Bottom Right) vs The Distance Between Observer and Asteroids

2037 July 13, 03:18:17 UT

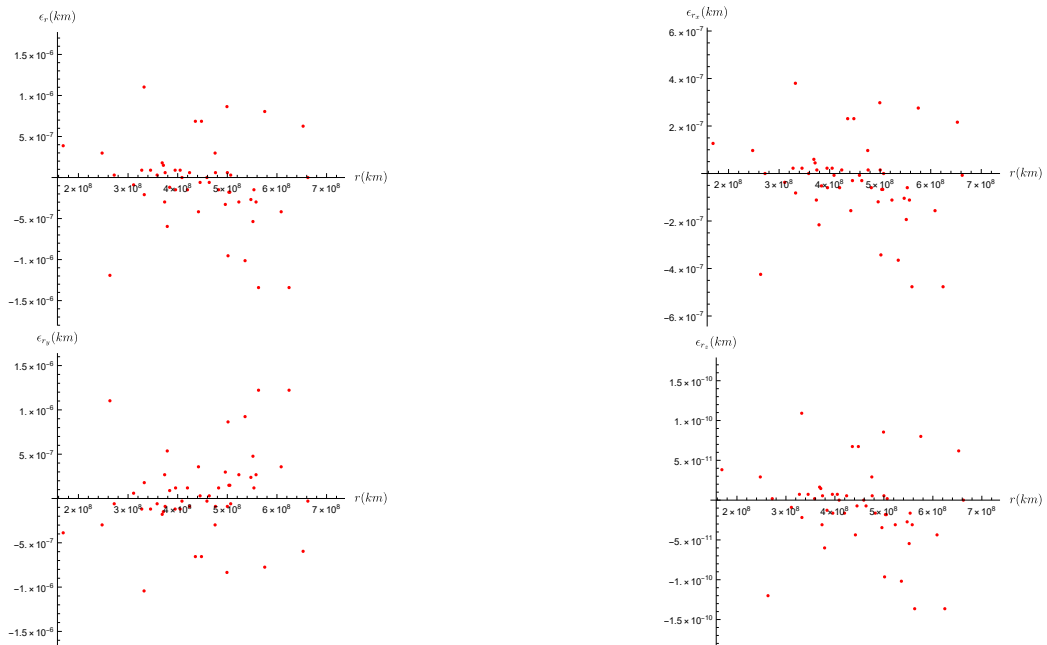


Figure 275: Errors  $e_r$  (Top Left),  $e_x$  (Top Right),  $e_y$  (Bottom Left) and  $e_z$  (Bottom Right) vs The Distance Between Observer and Asteroids

2037 October 13, 03:18:17 UT

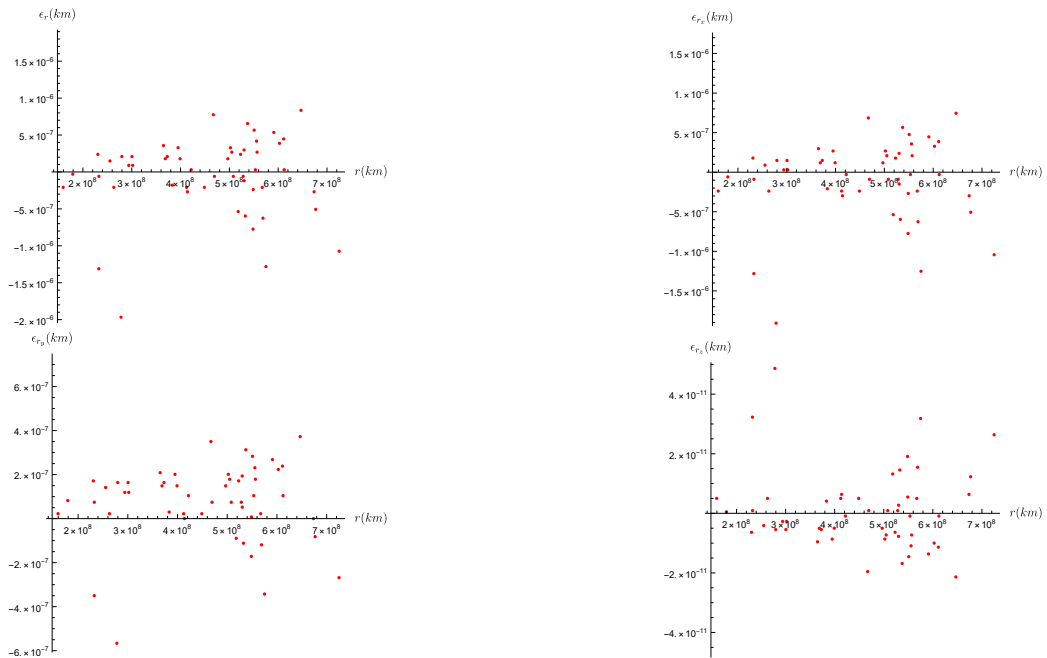


Figure 276: Errors  $e_r$  (Top Left),  $e_x$  (Top Right),  $e_y$  (Bottom Left) and  $e_z$  (Bottom Right) vs The Distance Between Observer and Asteroids



2037 November 13, 03:18:17 UT

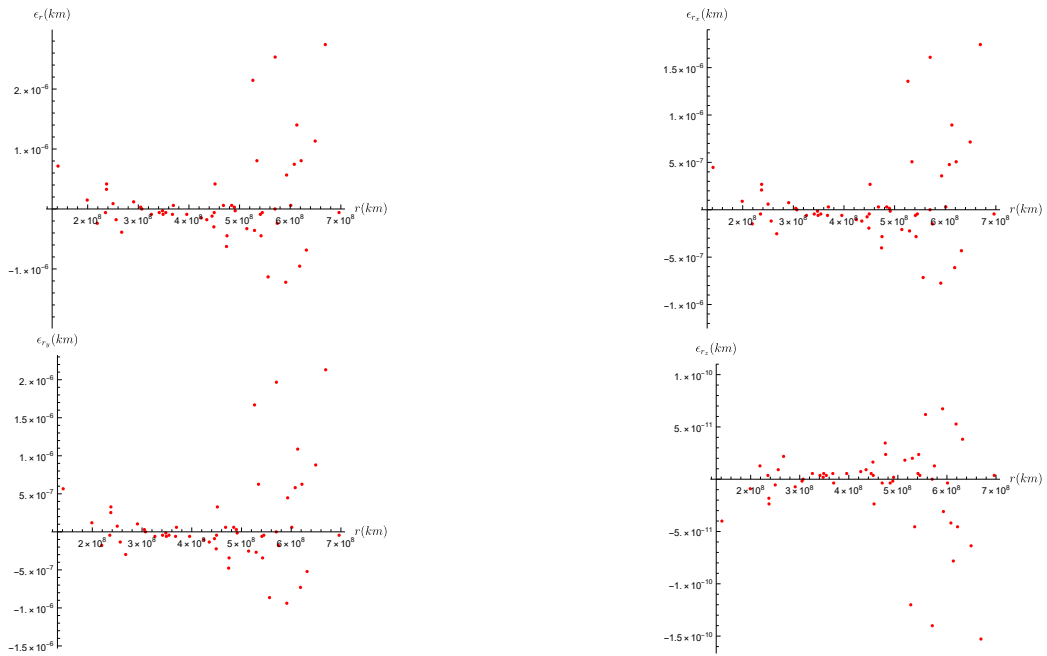


Figure 277: Errors  $e_r$  (Top Left),  $e_x$  (Top Right),  $e_y$  (Bottom Left) and  $e_z$  (Bottom Right) vs The Distance Between Observer and Asteroids

**Topocentric Ecliptic Longitude ( $\lambda'_p$ ) vs Error in The Heliocentric Distance ( $e_r$ )**

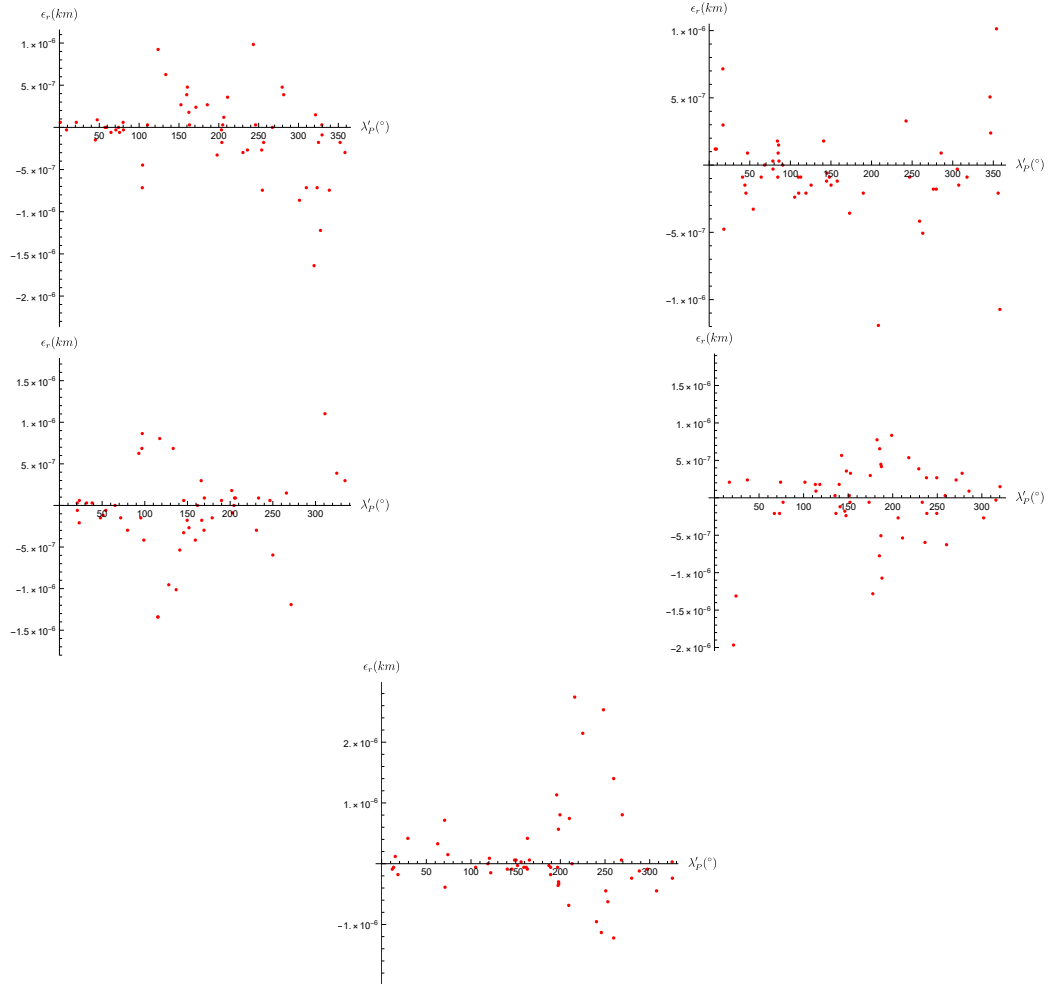


Figure 278: January-2037 (Top Left), April-2037 (Top Right), July-2037 (Middle Left), October-2037 (Middle Right), November-2037 (Bottom)

### 5.2.3 Rome

2037 January 13, 03:18:17 UT

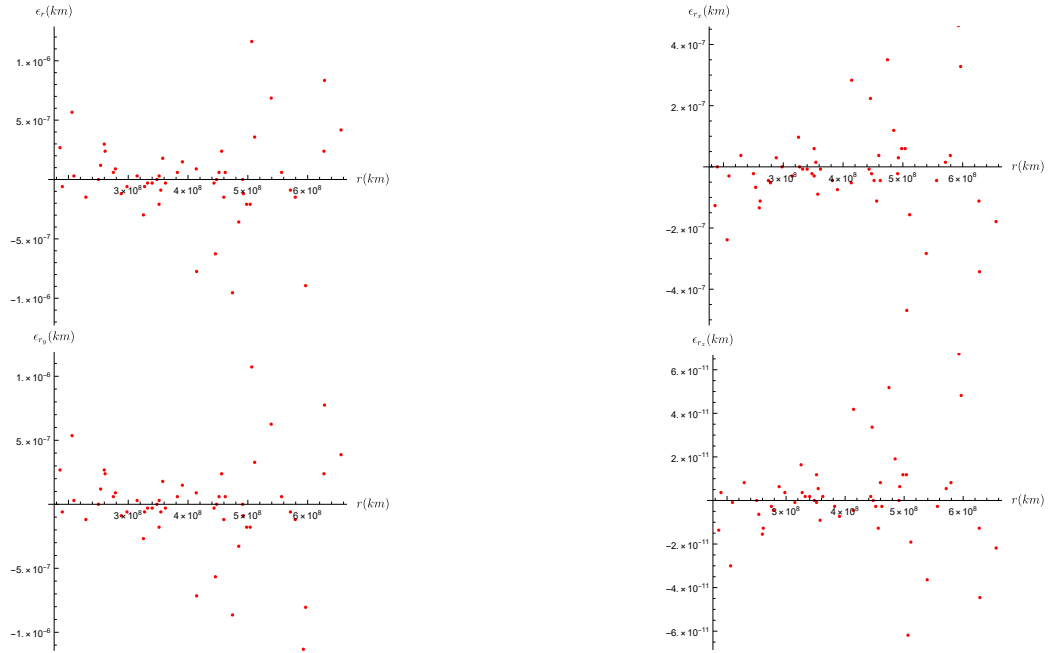


Figure 279: Errors  $e_r$  (Top Left),  $e_x$  (Top Right),  $e_y$  (Bottom Left) and  $e_z$  (Bottom Right) vs The Distance Between Observer and Asteroids

2037 April 13, 03:18:17 UT

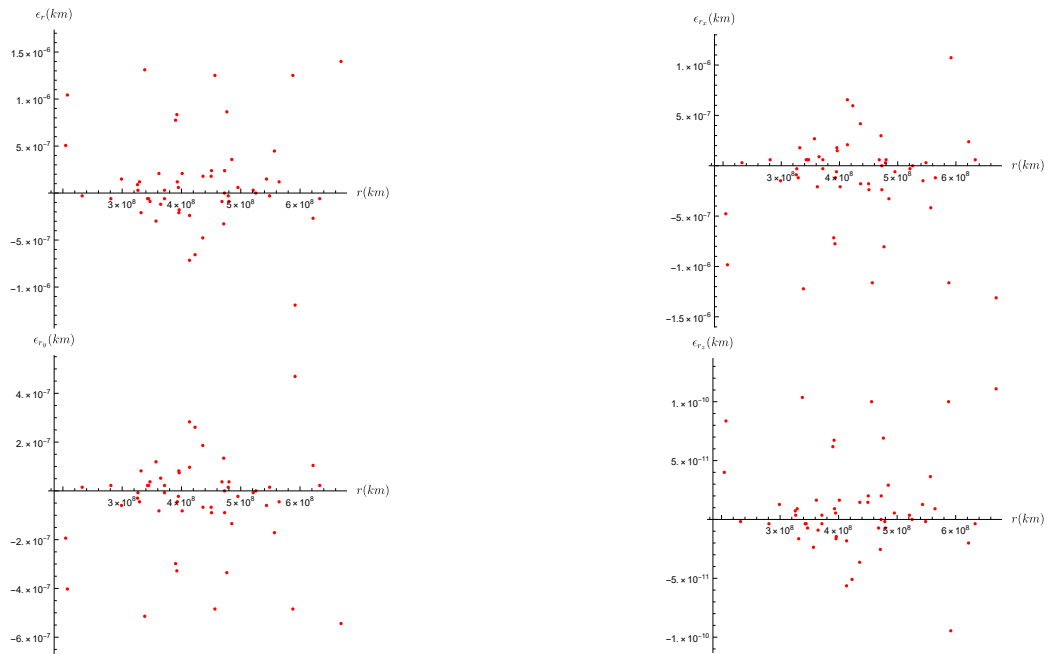


Figure 280: Errors  $e_r$  (Top Left),  $e_x$  (Top Right),  $e_y$  (Bottom Left) and  $e_z$  (Bottom Right) vs The Distance Between Observer and Asteroids

2037 July 13, 03:18:17 UT

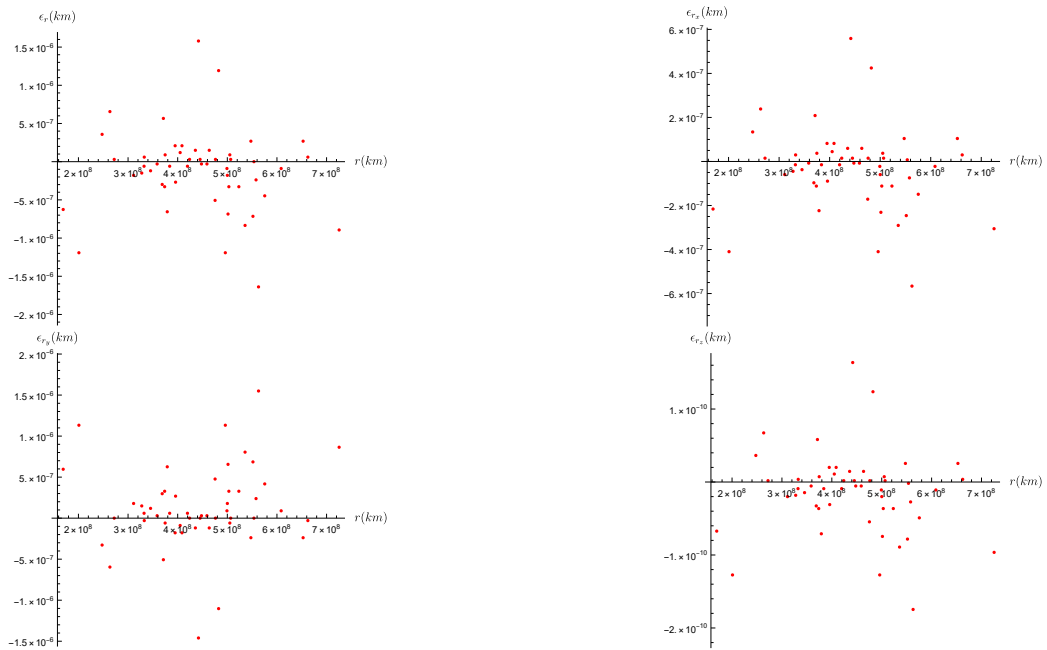


Figure 281: Errors  $e_r$  (Top Left),  $e_x$  (Top Right),  $e_y$  (Bottom Left) and  $e_z$  (Bottom Right) vs The Distance Between Observer and Asteroids

2037 October 13, 03:18:17 UT

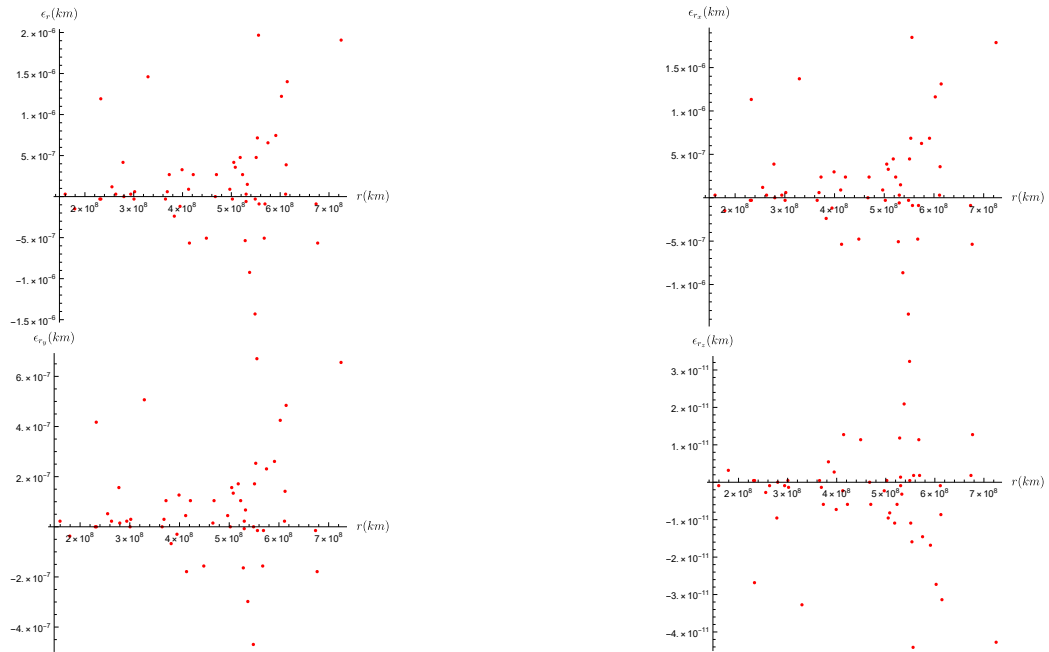


Figure 282: Errors  $e_r$  (Top Left),  $e_x$  (Top Right),  $e_y$  (Bottom Left) and  $e_z$  (Bottom Right) vs The Distance Between Observer and Asteroids

2037 November 13, 03:18:17 UT

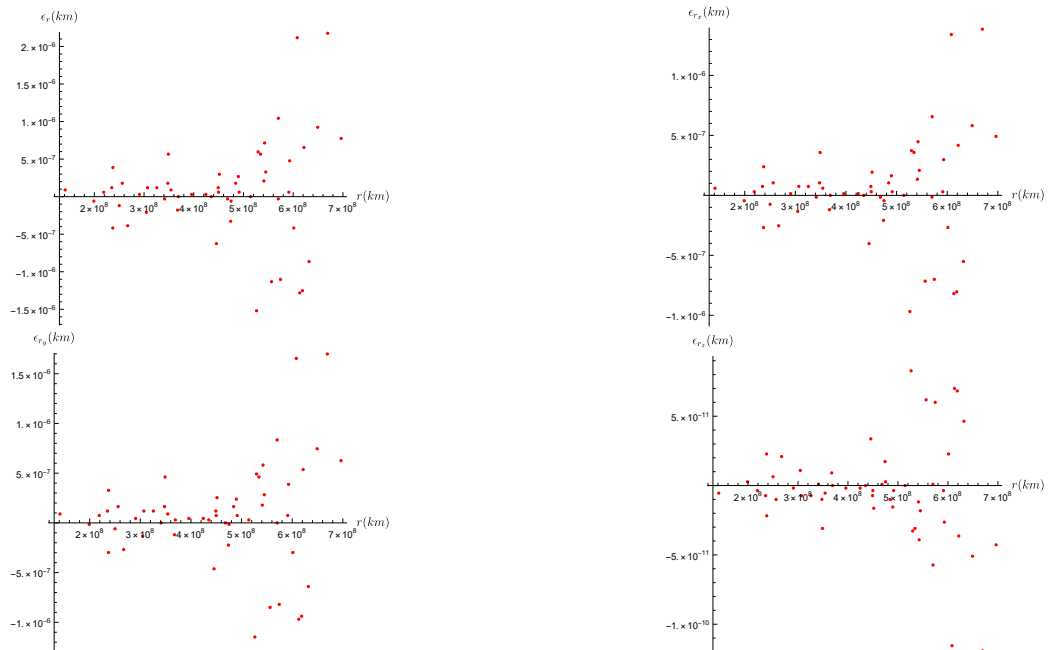


Figure 283: Errors  $e_r$  (Top Left),  $e_x$  (Top Right),  $e_y$  (Bottom Left) and  $e_z$  (Bottom Right) vs The Distance Between Observer and Asteroids

## Topocentric Ecliptic Longitude ( $\lambda'_p$ ) vs Error in The Heliocentric Distance ( $e_r$ )

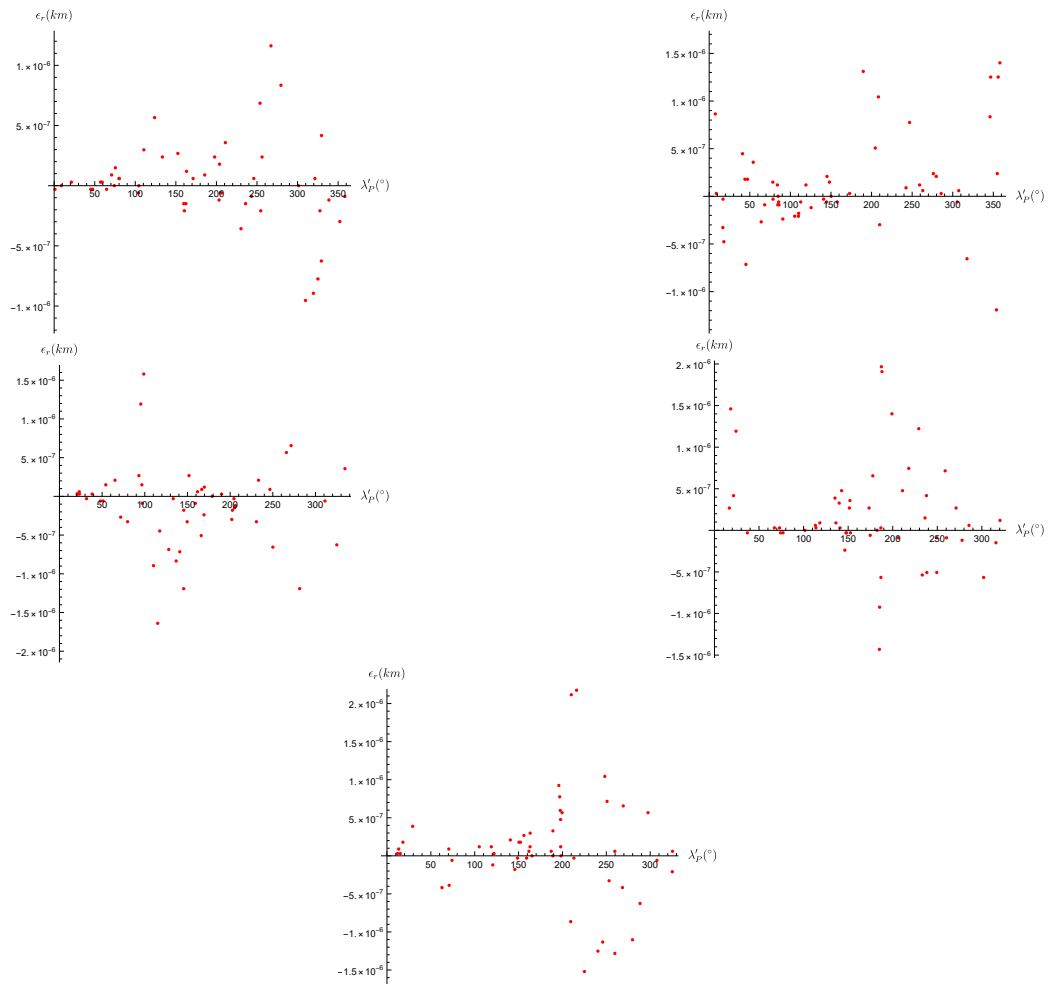


Figure 284: January-2037 (Top Left), April-2037 (Top Right), July-2037 (Middle Left), October-2037 (Middle Right), November-2037 (Bottom)



## 5.2.4 Pasadena

2037 January 13, 03:18:17 UT

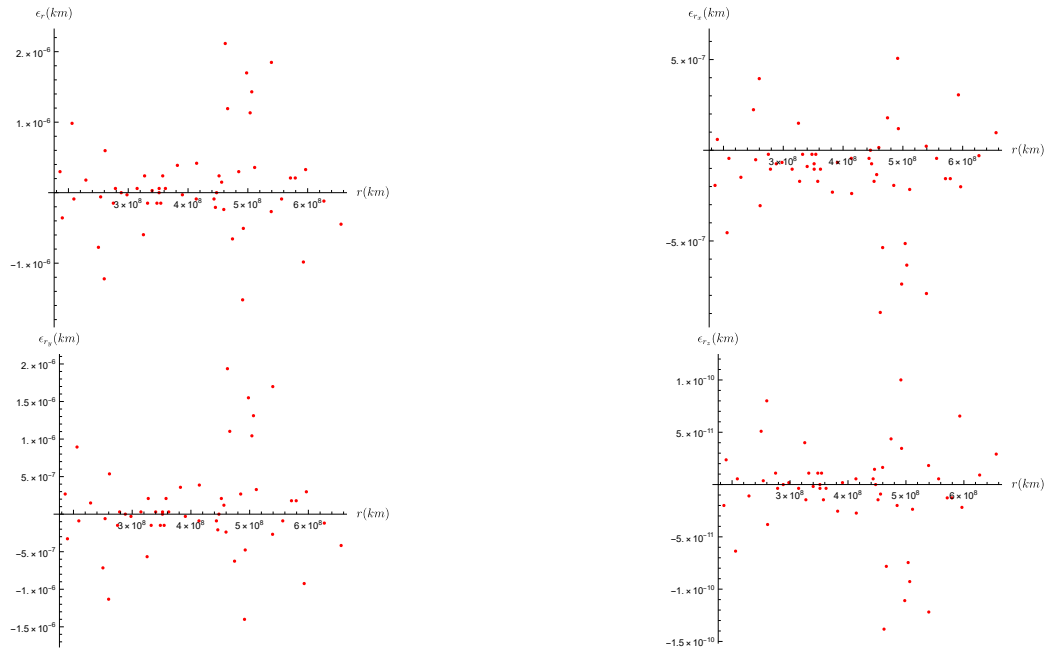


Figure 285: Errors  $e_r$  (Top Left),  $e_x$  (Top Right),  $e_y$  (Bottom Left) and  $e_z$  (Bottom Right) vs The Distance Between Observer and Asteroids

2037 April 13, 03:18:17 UT

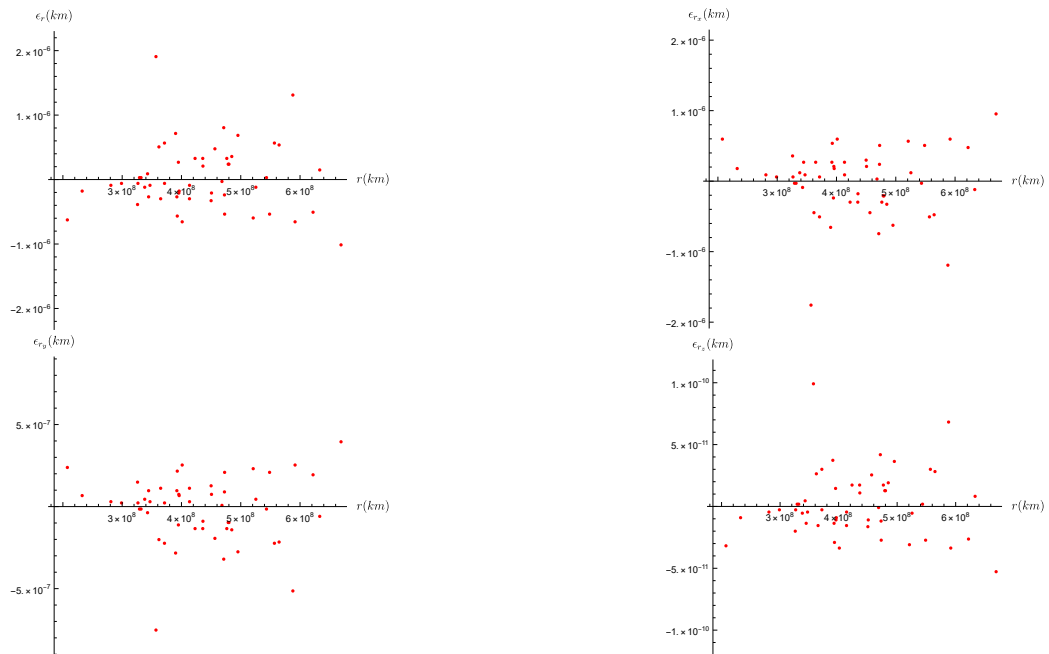


Figure 286: Errors  $e_r$  (Top Left),  $e_x$  (Top Right),  $e_y$  (Bottom Left) and  $e_z$  (Bottom Right) vs The Distance Between Observer and Asteroids

2037 July 13, 03:18:17 UT

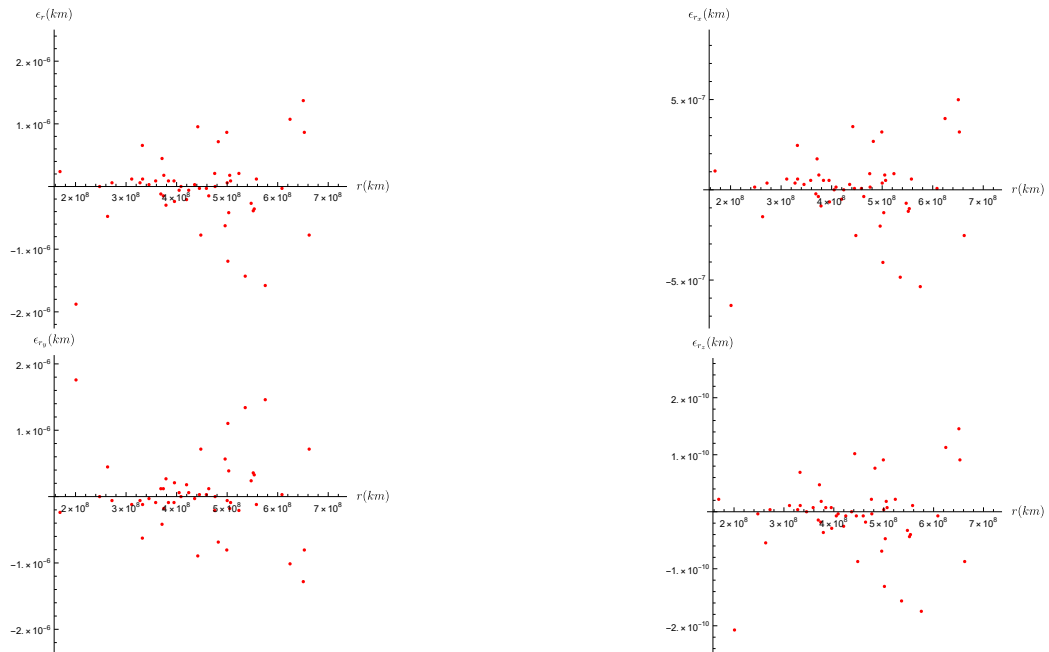


Figure 287: Errors  $e_r$  (Top Left),  $e_x$  (Top Right),  $e_y$  (Bottom Left) and  $e_z$  (Bottom Right) vs The Distance Between Observer and Asteroids

2037 October 13, 03:18:17 UT

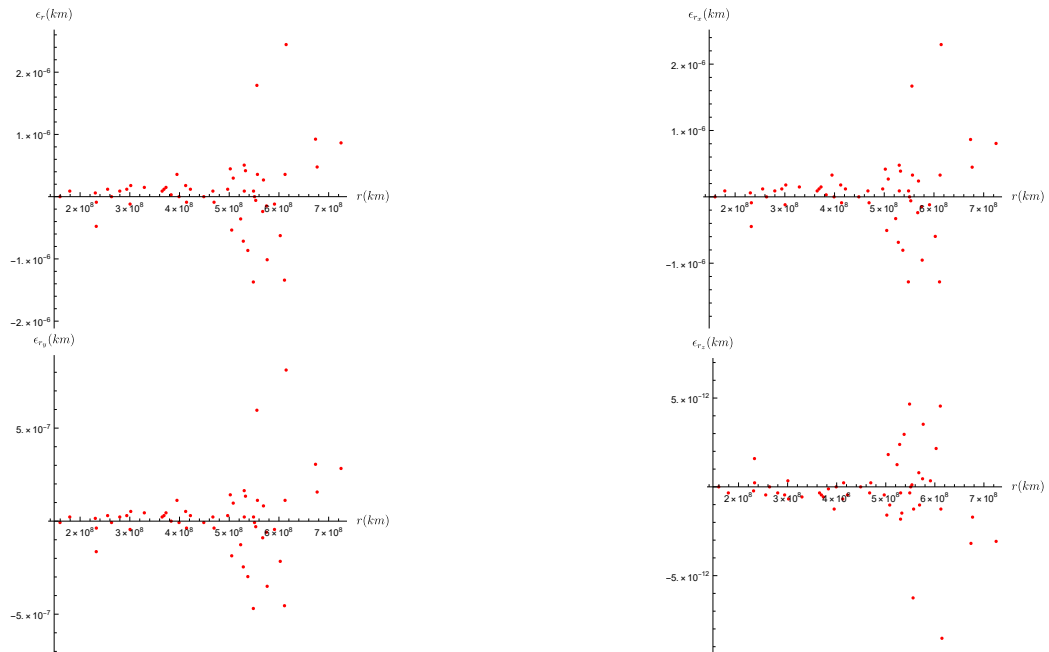


Figure 288: Errors  $e_r$  (Top Left),  $e_x$  (Top Right),  $e_y$  (Bottom Left) and  $e_z$  (Bottom Right) vs The Distance Between Observer and Asteroids

2037 November 13, 03:18:17 UT

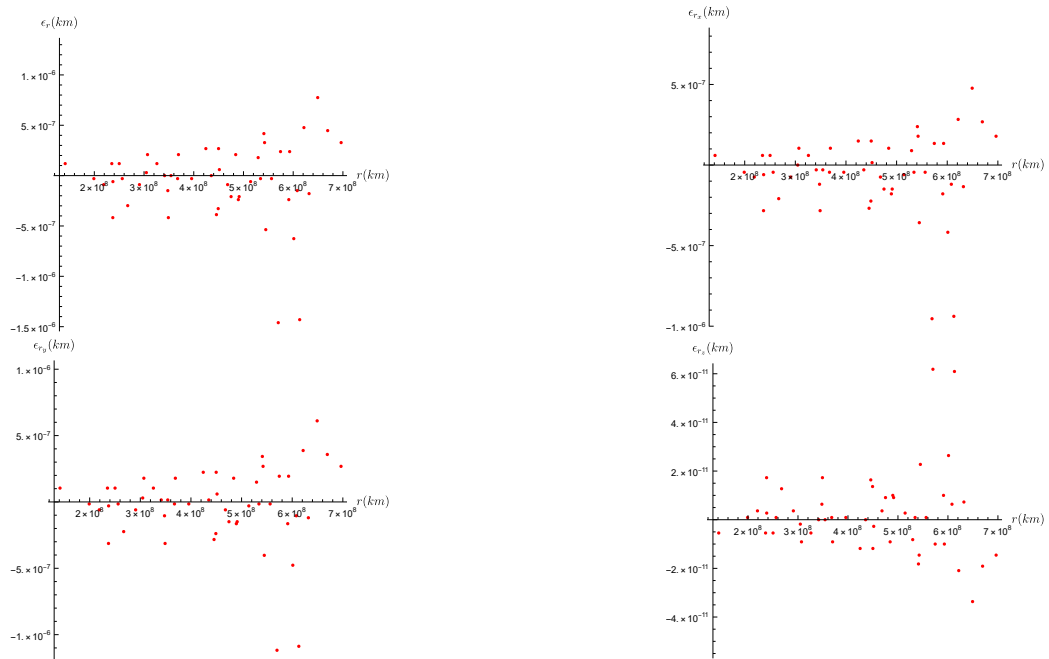


Figure 289: Errors  $e_r$  (Top Left),  $e_x$  (Top Right),  $e_y$  (Bottom Left) and  $e_z$  (Bottom Right) vs The Distance Between Observer and Asteroids

## Topocentric Ecliptic Longitude ( $\lambda'_p$ ) vs Error in The Heliocentric Distance ( $e_r$ )

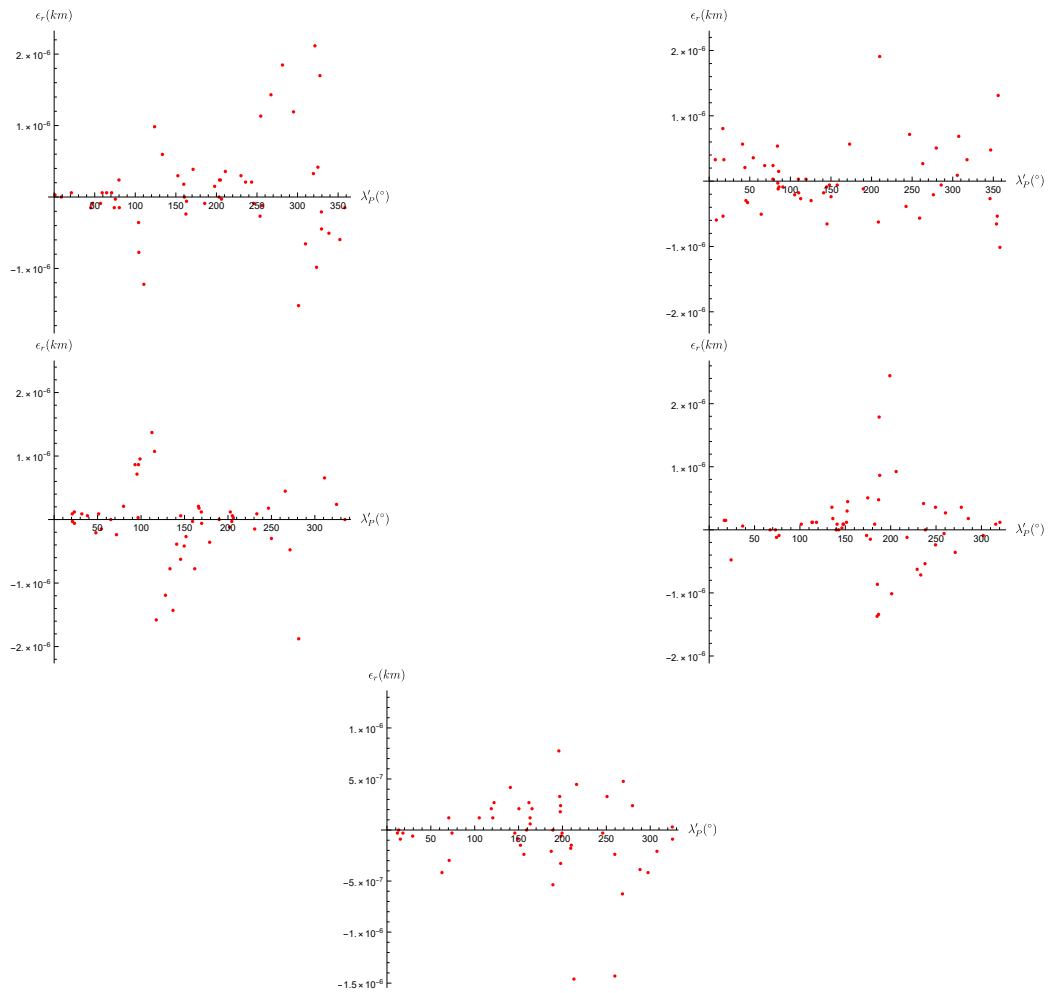


Figure 290: January-2037 (Top Left), April-2037 (Top Right), July-2037 (Middle Left), October-2037 (Middle Right), November-2037 (Bottom)

### 5.2.5 Non-Earth Observer: Ceres

After studying on Earth cases, it is needed to perform tests on another body such as an asteroid. Ceres is chosen in this way because it is one of the oldest known asteroids and Horizons has its data. However, there is a limitation on Horizons side that Horizons does not accept all asteroids as the coordinate system center. It can do it for 1 Ceres. Hence, Ceres is chosen.

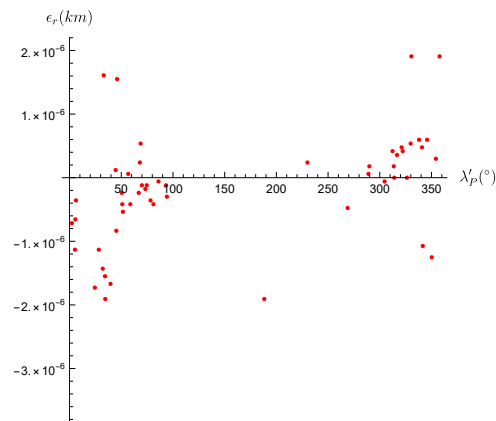


Figure 291:  $\lambda'_P$  vs  $e_r$

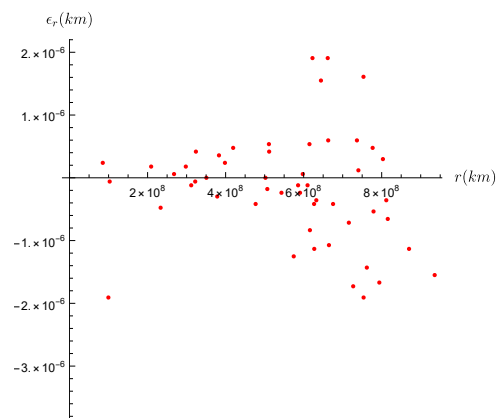


Figure 292: The Distance Between Ceres and Other Asteroids vs  $e_r$

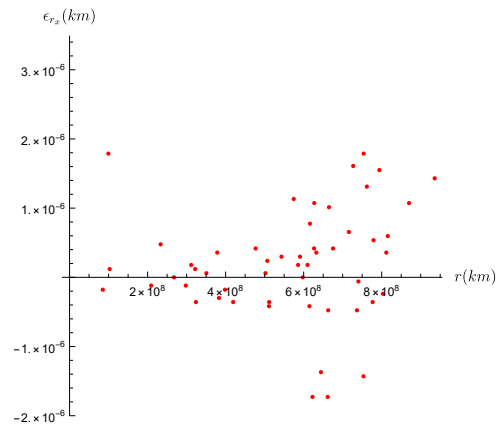


Figure 293: The Distance Between Ceres and Other Asteroids vs  $e_{r,x}$

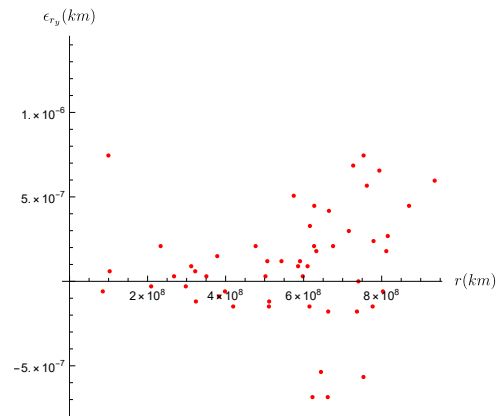


Figure 294: The Distance Between Ceres and Other Asteroids vs  $e_{r,y}$

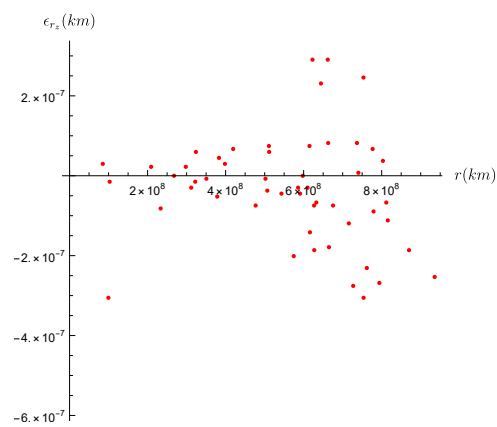


Figure 295: The Distance Between Ceres and Other Asteroids vs  $e_{r,z}$



### 5.3 Change in Error with Time

The figures below show how the error because of the different reference frames that the Sun and the Earth uses with time. To see how it changes with the location of the observer. All tests are done for the year of 2037.

#### Uppsala

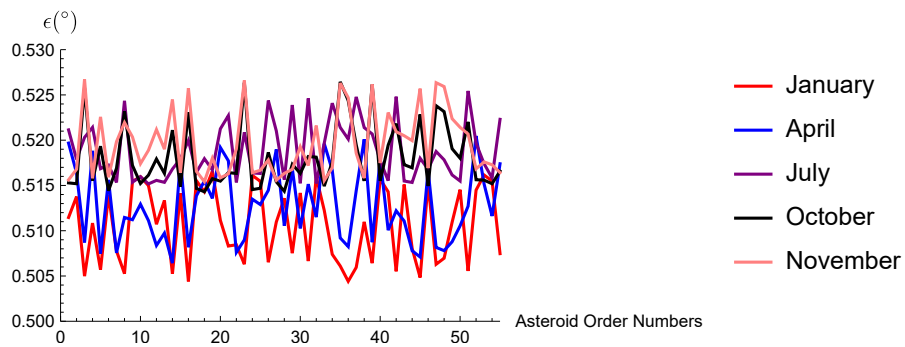


Figure 296: Change of Error for Different Asteroids

#### Rome

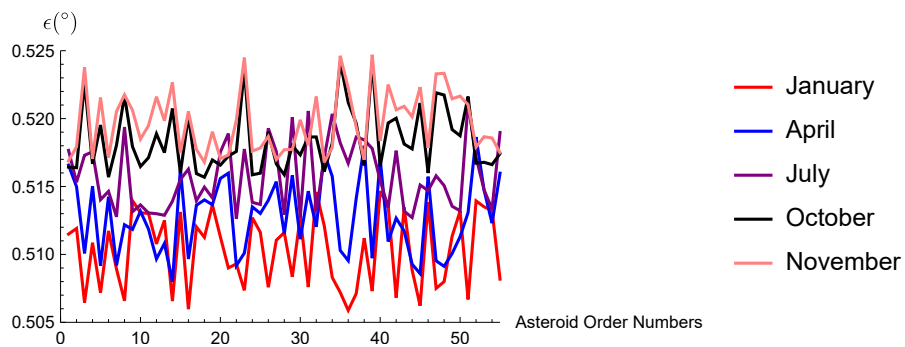


Figure 297: Change of Error for Different Asteroids

## Pasadena

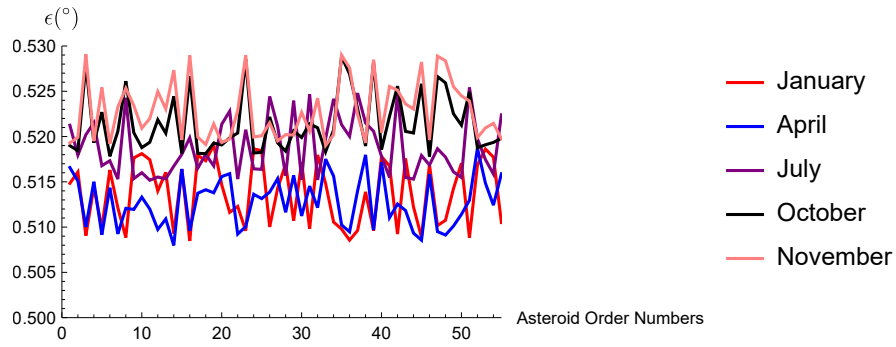


Figure 298: Change of Error for Different Asteroids

## Urla

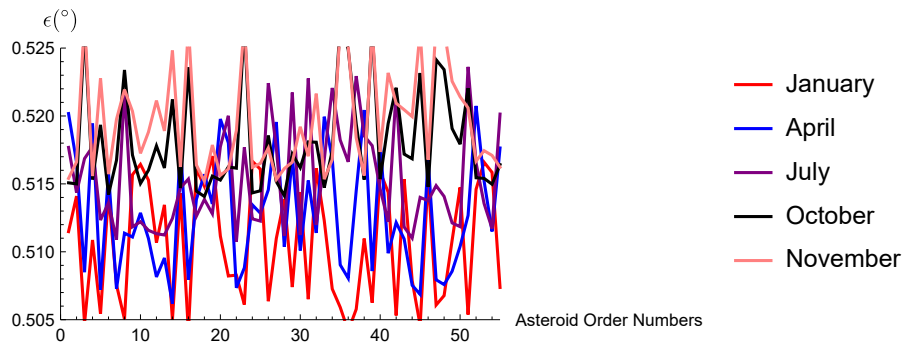


Figure 299: Change of Error for Different Asteroids

## 5.4 AstroGrav Results:

In AstroGrav, the simulation was on the chosen epoch to see the positions of the asteroids, the spacecraft and of course, the Sun. By using AstroGrav, it is possible to see if our assumptions and approach is correct or not. So, one of the simulations was done to see the first step of solution of the Direct Problem and another one is to see the solution of the Inverse Problem. Here is one example to those simulations whose epoch is 2037 April 13 , 03:18:17 UT.

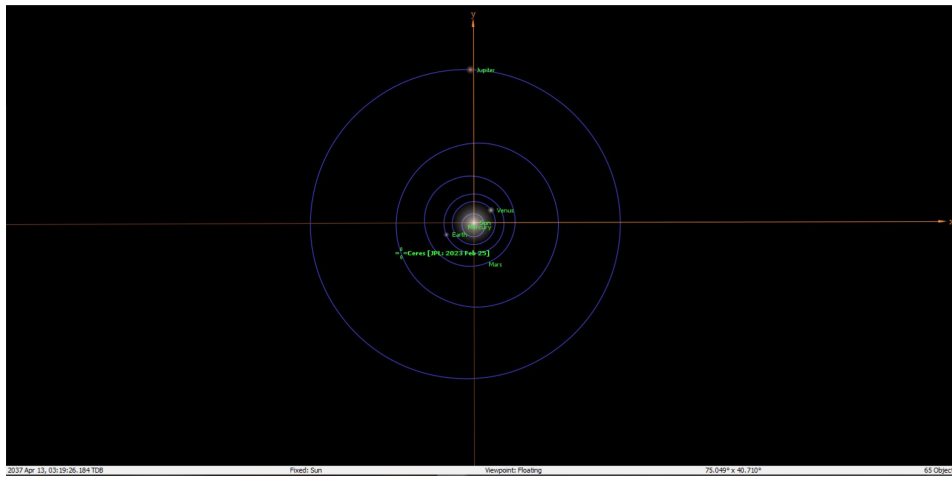


Figure 300: Orbits of the Components of The Solar System and Ceres is chosen as beacon

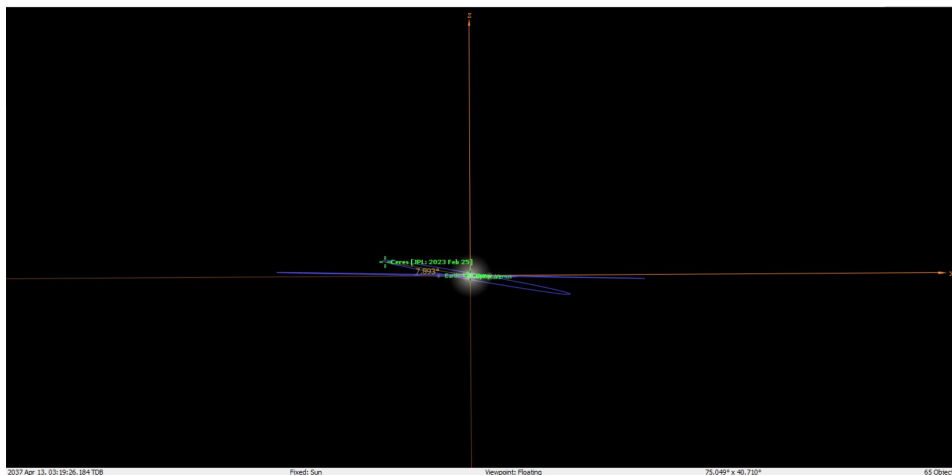


Figure 301: Orbits of the Components of The Solar System and Ceres is chosen as beacon

In AstroGrav, the heliocentric ecliptic coordinates of the Ceres is given as  $\lambda_P = 202^\circ 15' 37.9''$  and  $\beta_P = 14^\circ 25' 30.96''$ . However, unfortunately, AstroGrav cannot give topocentric coordinates of the asteroid. Then it is needed to move to Stellarium.

## 5.5 Stellarium Results:

On the contrary of AstroGrav, in Stellarium the topocentric coordinates of the asteroid can be observed. With those tests, it is obvious to see that Stellarium shows two different ecliptic coordinates.

- J2000 Ecliptic,
- on-date Ecliptic

Those systems were already discussed above. See 4.3.1. The picture of Ceres which is taken from the Earth via Stellarium is below.



Figure 302: Uppsala to 1 Ceres

Notice that the difference between  $\lambda'_{P,J2000}$  and  $\lambda'_{P,on-date}$  is  $0.5177^\circ$  which gives the error calculated in section 4.3.1.

Now, observe the Earth from Ceres.

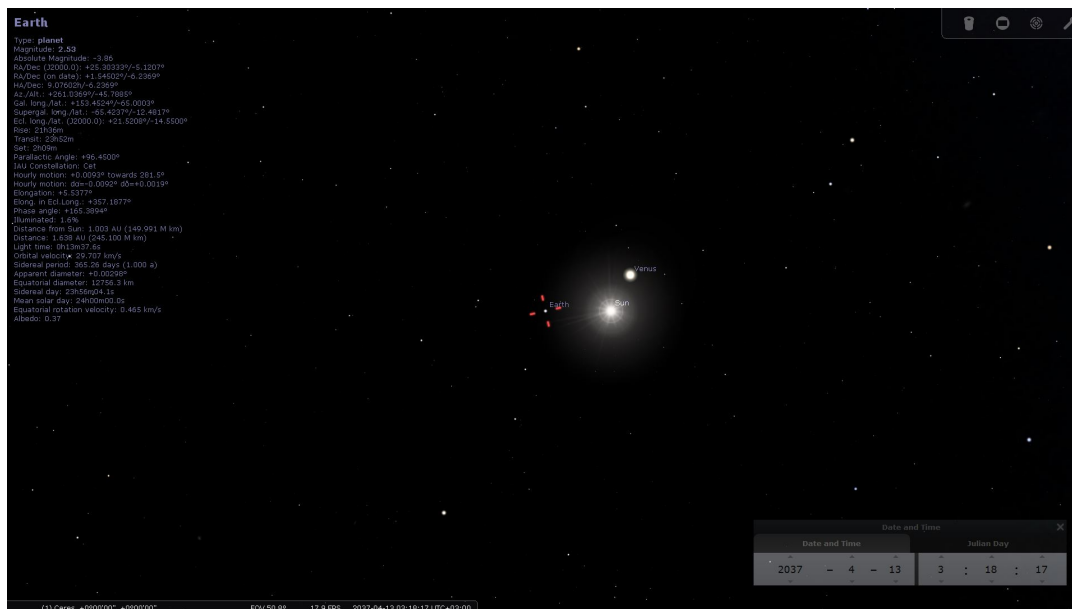


Figure 303: 1 Ceres to the Earth

In this case  $\lambda'_{P,J2000} = 21.5208^\circ$ . Please notice that the light aberration is also included in Stellarium. With those two approaches, Earth to Ceres and Ceres to Earth, it could be said that there is only  $0.003^\circ$  of error between the topocentric longitudes which is acceptable.

## 6 Discussion on the Results

### 6.1 Direct Problem Results' Analysis

#### Errors vs Distance From The Sun

Results given in section (5) are presented as figures on the left having no error adjustment happening in Horizon's with their corresponding calibrated figures on the right. Right off the bat, as the calculations were ran, it was discovered that R vs Errors figure had a very noticable systematical error present. At this point, our team was not aware of the reason behind these systematical errors, thus weren't able to achieve the figures on the right. This result was the first clue to investigate and find the reference system error in section 4.3.2 (4.3.2). As discussed in that section, non-earth observer locations were forced to print J2000 Inertial Reference Frame while Earth Observers were given the Reference Frame of the date. This phenomenon was very difficult to spot as said error gradually increases from 0 to  $0.53^\circ$  as the dates move from the year 2000 to 2037. While very subtle, this change is even visible within the year 2037 if enough attention is paid. Red dots, which represent  $\epsilon_{\lambda_p}$  very subtly increase from January to November for all locations. While this phenomenon is present on all locations, let us take Pasadena for an example. On Figure 78, January of 2037,  $\epsilon_{\lambda_p}$  is contained within the range of  $[0.508, 0.520]$  Degrees, fascinatingly, this range increases to  $[0.518, 0.530]$  Degrees on November of 2037. Once our team spotted this phenomenon, a calibration step was added which measured the difference of the J2000 Reference Frame and On-Date Reference Frame and using this difference of error as a subtraction on the data, Right hand side figures were achieved. Please note that while errors keep increasing as time passes, this patch allowed all five months to contain  $\epsilon_{\lambda_p}$  within  $\pm 0.005$  Degrees instead. Checking for different locations, same result can be obtained for all locations as well.

#### Errors vs Distance From The Earth

When r vs  $\epsilon$  charts are taken into account, four different results are to be examined. These are,  $\epsilon_{\lambda_p}$ ,  $\epsilon_{\beta_p}$ ,  $\epsilon_{\alpha_p}$ , and  $\epsilon_{\delta_p}$ .

$\epsilon_{\lambda_p}$ , which is legended in red color, it can be noted that error decreases as the distance increases with the observer on the figure on the left hand side. On the right figure, value of  $\epsilon_{\lambda_p}$  decreases according to the distance, but after a certain distance, error increases in a negative direction.

$\epsilon_{\beta_p}$ , legended in blue color is on the left figure, error decelerates as the distance between them increases. However, after a certain distance is passed,  $\epsilon_{\beta_p}$  moves in

a negative direction. Similar trend can be seen on the right hand side figure, which takes Reference Frame difference error into account.

When we examine  $\epsilon_{\alpha'_p}$  values, legended in purple, it can be noted that dots are randomly distributed on the left side, but on the right hand side figure, similar pattern as the other figures can be seen.

The  $\epsilon_{\delta'_p}$ , legended in green, is randomly scattered on the left figure. In other words, increasing the distance does not have much of an effect on the clutter. On the right side however, we see that it is progressing by showing an increase from the negative direction to the positive direction first. There is an inverse relationship when compared to other figures.

## 6.2 Inverse Problem Results' Analysis

In the inverse problem, accurate results are get from calculations. In this part, we will analyse the relationship between the error in the location of the spacecraft (Earth-Observers)  $\epsilon_r$  and  $r_{VP}$  which is the distance between the observer and the asteroid.

It can be seen that as the time passes, the error graph shifts to the negative side with almost same error values and then comes back to its original position.



## 7 Conclusion

The history of space exploration should continue in the future with new developments in the space sector and connected sectors. As optical navigation is one of them, it was decided to develop an autonomous optical navigation system which will use a CCD on-board camera by the reference of previous research. With the developments in the autonomous technology in the near future, it looks possible for us to develop it.

By explaining the methods that are used which are mainly called as the Direct and Inverse Problem and performing their tests, it is seen that the errors are much less than the expected (Lower than  $0.001^\circ$  especially for the longitude.) with higher accuracy without losses on the system. Those errors could be about the relativistic motions of the bodies with respect to each other. However, as the accuracy of the calculation of the position via inverse problem is high as in millimetric scale and above.

Although there are some limitations of this system to make the process easier such as not including the special relativistic effects, radiation pressure and other astrophysical properties of the bodies, with those numbers of accuracies for different cases, it is ready to be used on a real space mission.

## 8 Appendix

### Horizons

Horizons App : <https://ssd.jpl.nasa.gov/horizons/app.html#/>  
Horizons Manual : <https://ssd.jpl.nasa.gov/horizons/manual.html>

### AstroGrav

The detailed explanation for AstroGrav can be found in <http://www.astrograv.co.uk/> and also “AstroGrav.jex” in the attachments.

### Stellarium

You can download Stellarium for free and see its documentation on its page: <https://stellarium.org/>

### Asteroid List

See the file named “List-of-asteroids.csv” and <https://mp3c.oca.eu/best-values-search/>

### Sample Jupyter Notebook

It can be found in the additional files on Zenodo. A sample dataset which will be used to run Jupyter Notebook is included in the attachments, too.

### MaTeX[10]

During creation of the figures which are imported to this report, MaTeX was used to generate the legends of the plots in LaTeX. MaTeX can be expressed as a LaTeX for Mathematica. In the attachments there is a Jupyter Notebook called “fabrizio-pinto-maTeX-Test-from-Orhun-Sivasli-v1.ipynb” which tests MaTeX.

**Acknowledgements:**The instructions provided below are valid for recent versions of Mathematica. Thanks are due to our supervisor, Fabrizio Pinto, for experimenting with and sharing the downgrade instructions needed by users of earlier versions , particularly Mathematica 11.3 on Windows 8.

## Installation of MaTeX

Created by This was originally sent to me by student Orhun Sivak (8 July 2023) to whom thanks are due.  
Downgraded by Fabrizio Pinto for use with Mathematica 11.3

```
In [1]: (*This approach fails because of the Mathematica early version number*)
ResourceFunction["MaTeXInstall"][]

This version of '1' will no longer be supported for use with the Wolfram Cloud beginning '2'. '3'. This version
of Mathematica will no longer be supported for use with the Wolfram Cloud beginning Sun 3 Oct 2023. Please Ryp
eLink to please your license, https://store.wolfram.com/view/app/mathematica-upgrade?license=12183-7012] or Ryp
eLink to contact us, https://www.wolfram.com/contact-us?description=12183-7012?will-not-linger+has+registered+forma
+with+the+Wolfram+Cloud+beginning+Sun+3+Oct+2023+00:30:00+3A00.].
'1.1' channel: near InitialSubscribingContext failed: SEC_ERROR_BAD_SIGNATURE (0a009032c) - This error usually
occurs when a fatal SSL/TLS alert is received (e.g. handshake failed). More detail may be available in the Win
dows system event log.

Out[1]: $Failed[]

The approach below is from:
https://github.com/zhovav/MaTeX#revision-history

In [4]: (*possibly useless but start here*)
Needs["PacletManager`"]

In [17]: (*possibly useless*)
PacletFind["MaTeX"]

Out[17]: Paclet[MaTeX, 1.7.9, <>]

In [28]: (*there is a typo at Github*)
PacletInformation["MaTeX"]

Out[28]: Name -> MaTeX, Version -> 1.7.9, BuildNumber -> ,
Qualifier -> , MinFrameworkVersion -> 18.0, SystemID -> All,
Description -> Create LaTeX-typed labels within Mathematica.,
Category -> {Creator -> Cookies Hovot <shovav@gmail.com>,
Publisher -> , Support -> , Internal -> False, Location -> C:\Users\hp
pc\AppData\Roaming\Mathematica\Paclets\Repository\MaTeX-1.7.9,
Context -> {MaTeX`}, Enabled -> True, Loading -> Manual

In [7]: updateMaTeX[] :=
Module[{json, download, target,
Check}
, json = Import["https://api.github.com/repos/zhovav/MaTeX/releases/latest", "JSON"];
Download = Lookup[First@Lookup[json, "assets", {}], "browser_download_url"];
target = FileNameJoin[{CreateDirectory[], "MaTeX.paclet"}];
If[!Exists@target,
PrintTemporary[Labelled[ProgressIndicator[Appearance -> "Necklace"], "Downloading...", Right],
Print["Downloading..."];
];
URLSave[download, target];
Return[Failed];
];
If[FileExistsQ[target], PacletManager`PacletInstall[target], $Failed]
];

In [8]: updateMaTeX[]

Out[8]: Paclet[MaTeX, 1.7.9, <>]

In [9]: <<MaTeX`

The path to pdflatex is not configured.
Please configure pdflatex using ConfigureMaTeX["pdflatex" -> "path to\
> pdflatex executable..."]
The path to Ghostscript is not configured.
Please configure Ghostscript using ConfigureMaTeX["ghostscript" -> "path to\
> gs executable..."]
Hyperlink[Click here: paclet:MaTeX/tutorial/ConfiguringMaTeX]
> for documentation on configuring MaTeX.

In [18]: ConfigureMaTeX["pdflatex" -> "C:/Users/hp pc/AppData/Local/Programs/MiKTeX 2.9/miktex/bin/x64/pdflatex.exe", "Ch
Ghostscript -> "C:/Program Files/gs/gs10.02.2/bin/gstscript.exe"]

Out[18]:

In [11]: <<MaTeX`

In [12]: MaTeX["x^2"]

Out[12]: x^2

In [13]: MaTeX["R_["mag]"]

Out[13]: R_["mag]

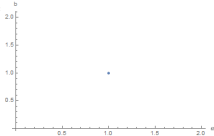
In [14]: MaTeX["m_["R_["mag]"]"]

Out[14]: m_["R_["mag]

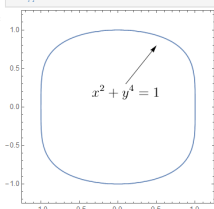
In [15]: MaTeX["m_["\lambda_["R]"]"]

Out[15]: m_["\lambda_["R]

In [16]: ListPlot[{{1,1}}, AxesLabel -> {MaTeX["x"], MaTeX["y"]}

Out[16]:


In [21]: texStyle = {FontFamily -> "Latin Modern Roman", FontSize -> 12};
ContourPlot[x^2 + y^4 == 1, {x, -1.2, 1.2}, {y, -1.2, 1.2},
BaseStyle -> texStyle,
EgStyle -> {
Arrow[{{0.1, 0.3}, {0.5, 0.8}}],
Text[MaTeX["x^2 + y^4 == 1"], Magnification -> 2], {0.1, 0.3}, Scaled[0.5, 1]}]
];

Out[21]:

```

## References

- [1] A. Roy, *Orbital Motion Fourth Edition* (2005). doi:<https://doi.org/10.1201/9780367806620>.
- [2] J. E. Riedel, S. Bhaskaran, S. Desai, D. Hand, B. Kennedy, T. McElrath, M. Ryne, *Autonomous Optical Navigation(AutoNav) DS 1 Technology Validation Report, Deep Space 1 technology validation reports(A 01-26126 06-12)*, Pasadena, CA, Jet Propulsion Laboratory(JPL Publication 00-10) (2000).
- [3] J. Meeus, *Astronomical Algorithms (2nd)* (William-Bell, Inc., Richmond, 1998).
- [4] F. Pinto, *Elements of optical navigation* (2022, August 29). doi:[10.5281/zenodo.7032245](https://doi.org/10.5281/zenodo.7032245).
- [5] H. Karaaliler, Y. Akan, D. L. Demirbağ, I. Macit, *Autonomous optical and inertial navigation of solar-sail propelled CubeSat class spacecraft during targeting missions to asteroids and minor moons*. (2022, August 29). doi:[10.5281/zenodo.7032367](https://doi.org/10.5281/zenodo.7032367).
- [6] E. Sahr, E. Lessac-chenen, J. Pelgrift, D. Nelson, C. Adam, D. Stanbridge, *POST-LAUNCH CHARACTERIZATION AND CALIBRATION OF THE OPTICAL NAVIGATION INSTRUMENTS FOR NASA ' S LUCY MISSION* (October) (2022) 10–12.  
URL <https://seal.ae.gatech.edu/sites/default/files/2022-10/SIW22-03.pdf>
- [7] M. Vertregt, *Orientation in Space*, JBIS - Journal of the British Interplanetary Society 15 (1956) 324–338.
- [8] D. Wang, M. Li, *Spacecraft Autonomous Navigation Technologies Based on Multi-source Information Fusion*, Springer.  
URL <https://link.springer.com/book/10.1007/978-981-15-4879-6>
- [9] N. L. Team, *The l'lorri instrument - lucy mission* (2023, May 24).  
URL <http://lucy.swri.edu/instruments/LLORRI.html>
- [10] S. Horvát, *Matex* (Aug. 2022). doi:[10.5281/zenodo.7050091](https://doi.org/10.5281/zenodo.7050091).